1-1-2003

Evaluation of bridges strengthened or newly constructed with innovative materials

Yoon-Si Lee
Iowa State University

Evaluation of bridges strengthened or newly constructed with innovative materials

by

Yoon-Si Lee

A thesis submitted to the graduate faculty
in partial fulfillment of the requirements for the degree of
MASTER OF SCIENCE

Major: Civil Engineering (Structural Engineering)

Program of Study Committee:
Terry J. Wipf, Co-major Professor
F. Wayne Klaiber, Co-major Professor
Brent M. Phares
Lester W. Schmerr

Iowa State University

Ames, Iowa

2003

Graduate College

Iowa State University

This is to certify that the master's thesis of

Yoon-Si Lee

has met the thesis requirements of Iowa State University

Signatures have been redacted for privacy

For the Major Program

TABLE OF CONTENTS

LIST OF FIGURES

LIST OF TABLES

ACKNOWLEDGEMENTS

Above all, I would like to thank my parents for their consistent support and never-ending love. I also would like to thank my wife, Ji-Hye Kim, for the tremendous encouragement and countless sacrifices she has made to support my study.

I wish to express my sincere appreciations to Dr. Terry J. Wipf, Dr. F. Wayne Klaiber, and Dr. Brent M. Phares for all of their guidance, advise, generous time, and support throughout this study. I also would like to thank Dr. Lester W. Schmerr for serving on my committee. Special thanks are accorded to Douglas L. Wood, Manager of the Structural Engineering Laboratory, who provided significant assistance with the system installation and the laboratory and field testing. I would like to extend my gratitude to fellow students of the Bridge Engineering Center at the Center for Transportation Research and Education, and staff and faculty of the Civil, Construction and Environmental Engineering Department of the Iowa State University for their help and assistance.

The research projects presented in this thesis were initiated by the Iowa DOT and sponsored by the FHWA. Special thanks are extended to the numerous Iowa DOT Office of Bridges and Structures and Iowa DOT maintenance personnel for their help in various phases of this study.

GENERAL INTRODUCTION

BACKGROUND

Based on data from the Federal Highway Administration (FHWA), approximately 30 percent of the nation's 600,000 bridges are in need of repair or replacement due to structural deficiencies or functional obsolescence. As these bridges continue to deteriorate, the problems have become further compounded by increases in legal load limits, limited budgets and substantial cost associated with proper maintenance, rehabilitation or replacement of these deficient bridges. Bridge engineers and owners have spent considerable time and effort researching viable, cost effective solutions to improve the condition, durability, and capacity of bridges and, thus, reduce overall life-cycle costs. In an effort to address this issue, the FHWA's Innovative Bridge Research and Construction (IBRC) Program, established in 1998, launched a new initiative that provides direction and funding to help local agencies and State Department of Transportations (DOTs) incorporate the use of innovative materials in their bridge projects. The goal of the program is to improve mobility by lowering congestion associated with bridge maintenance and rehabilitation projects, and to increase productivity in the nation's highway by reducing the overall life-cycle costs of a bridge, including the costs of new construction, while enhancing the safety.

Among the many projects funded through the IBRC Program, this thesis summarizes three projects that utilize innovative materials to strengthen existing deficient bridges and in the construction of a new bridge. The projects presented in this thesis focus on the demonstration of the use of new, cost-effective, innovative materials and the associated performance evaluation.

OVERVIEW

This thesis contains three parts. In the first two parts (Part I and Part II), the use of carbon fiber reinforced polymer (CFRP) materials to strengthen existing, structurally deficient steel girder bridge is summarized. Among various strengthening materials, CFRP composite materials were selected due to their outstanding mechanical characteristics and non-corrosive nature. Two bridges were strengthened using these materials in an effort to improve the live load carrying capacity of the bridges. In one case (Part I), a bridge was strengthened using CFRP bars that were post-tensioned in the positive moment region. In the other case (Part II), a bridge was strengthened by installing CFRP plates to the bottom flange of girders in the positive moment region.

In Part III, a portion of a project that investigates the use of corrosion resistant reinforcing steel in the deck slab of two, newly constructed, prestressed concrete girder bridges is presented. The decks of the two bridges were constructed with two different types of steel; one with Micro-composite Multi-structural Formable Steel (MMFX) reinforcing steel, a relatively new form of corrosion resistant steel, and the other with epoxy coated steel. During the construction of the bridges, embeddable sensors were installed on selected reinforcing bars in the deck slab to identify signs of corrosion initiation and severity. Data were recorded periodically to assess and compare the performance of two different types of reinforcing steel.

PART I. EVALUATION OF A POST-TENSION STRENGTHENED STEEL GIRDER BRIDGE USING FRP BARS

1. INTRODUCTION

1.1. BACKGROUND

Many state, county, and local agencies are faced with deteriorating bridge infrastructure composed of a large percentage of relatively short to medium span bridges. In many cases, these older structures are rolled or welded longitudinal steel stringers acting compositely with a reinforced concrete deck. Most of these bridges, although still in service, need some level of strengthening due to increases in legal live loads or loss of capacity due to deterioration. Although these bridges are overstressed in most instances, they do not warrant replacement; thus, structurally efficient yet cost-effective strengthening methods need to be developed. In the past, the use of bolted steel cover plates or angles was a common retrofit option for strengthening such bridges. However, the time and labor involved to attach such a strengthening system can sometimes be prohibitive.

In the last decade, the use of fiber-reinforced polymers (FRP) has emerged as a promising technology in structural engineering. This report documents a method of strengthening a structurally deficient bridge through the application of CFRP post-tensioning bars. Among the various strengthening materials, the use of CFRPs is very appealing in that the CFRPs are highly resistant to corrosion, have a low weight, and have a high tensile strength.

The bridge selected for strengthening was a three-span continuous rolled shape bridge in Guthrie County, Iowa on State Highway IA 141 approximately 1.6 miles west of Bayard, Iowa. The goal of this project was to design and install the CFRP post-tensioning bars on the steel girders and to monitor and document the performance and long-term impact of the strengthening system.

1.2. LITERATURE REVIEW

1.2.1. Post-tensioning

The general purpose of using external post-tensioning (P-T) on an existing bridge is to restore its load carrying capacity by applying internal loads that counteract the dead and live load stresses. External P-T can be very economical, adaptable, and effective in that P-T bars can be easily inspected and, if necessary, be replaced. This makes P-T a viable alternative for strengthening existing structures since installation of the strengthening system is independent of other maintenance operations. The major drawback associated with the use of external P-T is exposure of the hardware to both environment conditions and potential impact.

Since the early 1980's, the Iowa DOT has developed the concept of strengthening simple-span and continuous-span bridges by P-T through several research projects. Klaiber et al [1] and Dunker et al [2, 3, 4] completed several projects related to the use of external P-T with high strength steel bars for the purpose of upgrading the live load carrying ability of steel beam, composite concrete deck bridges. This collection of work includes both experimental and analytical results to demonstrate the effectiveness of external P-T. The initial project, entitled " Feasibility Study of Strengthening Existing Single Span Steel Beam Concrete Deck Bridges" [1], published in June 1981 studied the general concepts of strengthening single-span bridges by P-T. To illustrate these concepts, a 1/2-scale simple-span, steel-girder, concrete slab bridge was tested in the laboratory with numerous P-T schemes. The most promising concepts were later tested and demonstrated in the project "Strengthening of Existing Single-Span Steel-Beam and Concrete Deck Bridges" [3]. The general objective of this work was to design and install post-tension strengthening systems on two existing simple span bridges in Iowa. As a follow-up, a document, "Design Manual for Strengthening Single-Span Composite Bridges by P-T" [4] was developed for use by design engineers. Based on the successful implementation on single-span composite bridges, further work was completed to examine the feasibility of strengthening continuous-span bridges using P-T [5]. A design recommendation for the strengthening of continuous-span bridges was then developed by Klaiber et al [6]. The methodology employed was to utilize the P-T technique in the positive moment regions and superimposed trusses in the negative moment regions. A methodology for determining required amount of P-T force and retrofit scheme (location of P-T system) to reduce or eliminate overstresses in bridges of various configurations was presented in the final report. The results of these research projects verified that the P-T system could effectively be used on continuous-span bridges. Although the P-T system did not significantly reduce live load deflections, it did slightly increase the load carrying capacity of the bridge, thus allowing the bridges to carry additional live loads.

The proven methodology presented in these reports has been successfully used on single-span as well as continuous bridges by engineers in the Iowa DOT and other agencies to improve or upgrade the condition of those bridges such that they meet the demands of modern transportation standards. This collection of work was the basis for the system described in this report.

1.2.2. Carbon Fiber Reinforced Polymer

CFRP materials have been predominantly used by the aerospace industry where cost is generally a secondary consideration to weight [7]. Although the initial cost is typically higher than other conventional materials, CFRP is high in strength and modulus, low in density, chemically resistant, and has outstanding thermal and electrical conductivity properties.

Carbon fibers were first used in a civil application at the Swiss Federal Testing Laboratories [8]. Although it was viewed as generally uneconomical due to the material cost, it was found to be more effective when the reduced on-site construction time was considered.

Since 1975 when the first pedestrian FRP bridge was built by the Israelis, FRP materials have been used in the construction of pedestrian bridges in many continents [9]. Based on the knowledge and experience obtained from working with pedestrian bridges, many engineers, scientists, and researchers have attempted to extend the applicability of FRP to vehicular bridges. Since the early 1990's, many bridge deck systems have been developed and tested utilizing this innovative material. In addition, structural shapes have been developed and tested for use in replacing deteriorated superstructure elements. However, it has typically been found that the most economical use of FRP occurs when it is used with conventional bridge materials.

1.3. OBJECTIVES

The primary objective of the project was to investigate and evaluate the effectiveness of CFRP bars to strengthen an existing, structurally deficient, steel girder bridge. Secondary objectives of this project were:

- To document the construction and performance of the innovative material used.
- To monitor the behavior of the bridge during the application of the P-T.
- To identify changes in structural behavior due to the addition of the strengthening system and with time through field inspection and periodic load tests.

1.4. SCOPE

The research program consisted of several tasks with the main emphasis being the installation of the strengthening system and associated field testing. Before the P-T system was installed, a diagnostic load test was conducted on the subject bridge to establish a baseline behavior of the unstrengthened bridge. During the process of installing the P-T hardware and stressing the system,

both the bridge and the P-T system were monitored. The installation of the hardware was followed by a follow-up diagnostic load test to assess the immediate effectiveness of the P-T strengthening system. Additional load tests were performed over a two-year period to identify any changes in the strengthening system with time. After the last follow-up test (two years of service) was completed, the P-T force was removed from the bridge (and re-applied) to investigate any losses that may have occurred over the two-year period. Laboratory testing of several typical CFRP bar specimens was also conducted to more thoroughly understand their behavior.

A detailed description of the subject bridge and the strengthening system employed is given in Chapter 2. The various tests conducted in the laboratory and in the field are described in Chapter 3, and the corresponding test results are summarized in Chapter 4. Following the test results, the summary and conclusions are presented in Chapter 5.

2. BRIDGE AND STRENGTHENING SYSTEM DESCRIPTION

This chapter describes the physical characteristics of the strengthened bridge. Also, a description of the strengthening system and its installation is given.

2.1. BRIDGE DESCRIPTION

The bridge (Number 3903.0S 141) selected for strengthening is a 210 ft x 26 ft, three-span continuous, rolled shape steel girder bridge constructed in 1956 (shown in Fig. I-1). It is located in southwest-central Iowa in Guthrie County approximately 1.6 miles west of Bayard, Iowa carrying State Highway IA 141 over Willow creek. The bridge consists of two 64 ft end spans and a 82-ft center span. Bridge beams are spliced at locations 20 ft from the two piers in all spans (i.e., four splices per beam line). The bridge deck is a nominal 7-in. thick cast-in-place, reinforced concrete slab that was overlaid with dense low-slump portland cement concrete (PCC) in 1987. The current average deck thickness is approximately 10 in., including 3 in. of wearing surface with 2 1/2 in. of crown. The bridge deck is supported by two WF 30x116 exterior and two WF 33 1/4x141 interior I-beams spaced at 8 ft-3 in. on center as shown in Fig. I-2. The abutments are stub reinforced concrete and the piers consist of open-two-concrete columns with cantilevers. Abutments and piers are both supported on steel piling. The abutments have sliding steel plate bearings while the piers have rocker-type bearings.

The roadway width is 26 ft allowing two traffic lanes with one lane in each direction and a narrow shoulder on each side. The bridge has moderate curbs that are integral with the deck and concrete guardrails connected to the curbs.

Both abutments show a few hairline cracks. Severe corrosion was found at the abutment bearings and moderate to severe spalls were found near the back wall and the bottom of the concrete deck (see Fig. I-1d). There are signs of moderate to severe corrosion on the exterior beams, and areas with moderate to severe corrosion on the bottom flanges of the abutment diaphragms. Also, a considerable amount of corrosion is present on the deck channels and the top of the web of the curb channels (see Fig. I-1e). The bridge deck has several hairlines and narrow transverse cracks. Both curbs show moderate hairline cracks and small spalls at several locations.

(a) Side view

(b) End view

Figure 1-1. Overall bridge photographs.

(c) Bottom view

(d) Typical east abutment condition

Figure I-1. Overall bridge photographs - continued.

(e) Typical condition of deck soffit and deck channel

Figure I-1. Overall bridge photographs - continued.

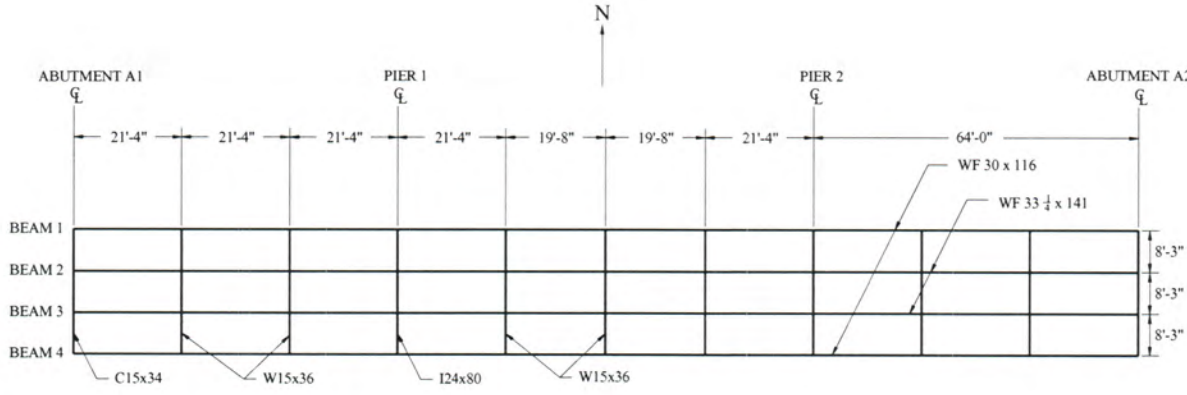

Figure I-2. Bridge framing plan.

2.2. STRENGTHENING SYSTEM

The P-T based strengthening system utilized was developed based on the strengthening recommendations of Klaiber et al [6] and material performance data provided by the manufacturer. CFRP bars were selected due to their outstanding mechanical characteristics and non-corrosive nature. The installation of the P-T system was completed in the positive moment region of the exterior girders in all three spans. The bridge has welded cover plates in the negative moment regions which were determined to be adequate and, therefore, not in need of strengthening. A total of 12 kips was applied to each bar (four bars per location). The descriptions of the design process, the strengthening system components, and the installation procedures are presented in the following sections.

2.2.1. Design Process of Post-Tensioning Strengthening System

The design of the CFRP P-T strengthening system was completed for the HS-20 load [10] utilizing the Allowable Stress Design (ASD) approach. Based on analysis completed by the bridge owner, it was found that the positive moment region of the exterior beams (Beam 1 and Beam 4) in both the end and center spans were overstressed. This section describes the several steps followed in designing the P-T strengthening system. Although some hand calculations were required, a spreadsheet was utilized for a majority of the computations needed to determine the required P-T force at each location. A description of detailed design methodologies and use of the design spreadsheet is presented in Reference 6. The steps to determine the required P-T forces are summarized as follows:

1. Section properties of all girders are computed.
2. All loads and load fractions for each beam are computed for dead load, long-term dead load, and live load plus impact.
3. Internal moments and resulting stresses in each girder induced by the loads computed in Step 2 are determined at various sections along the length of the bridge.
4. The strengthening scheme, bar lengths, and location are selected.
5. Overstresses that need to be reduced are computed.
6. The P-T forces that would generate the desired stress reduction at the critical sections are determined.
7. The final stresses in all girders are checked to ensure that stresses are within the allowable stress limit.

8. The P-T strengthening forces are increased by 8% to account for time-dependent losses and errors due to approximations in the design methodology [6].
9. With the increased P-T force, the stress check procedure (Step 7) is repeated.

2.2.2. CFRP Post-Tensioning Strengthening System Components

The CFRP bar used in this project is 3/8 in. in diameter and has a high tensile strength, a moderate modulus of elasticity, low creep properties, and a high resistance to corrosion. For connection to the other P-T system components, the CFRP bar is embedded into steel tube anchors that have threaded ends. Material properties of the CFRP bars are listed in Table I-1.

Table I-1. Material properties of CFRP bar.

Diameter, (in.)	Tensile Strength, (ksi)	Tensile Modulus, (ksi)	Elongation at ultimate	Fiber Content
3/8	300	20,000	1.5%	65% by Volume

The CFRP bars were connected to the steel beams with 5 in. x 5 in. x 3/4 in. stiffened angles 7 in. in length. Each of these stiffened angle assemblies, which are connected to the web of the steel beams with two 1 in. diameter, and 3 1/2 in. long A325 high-strength bolts, connects four CFRP bars to the web of the beam (two on each side) near the bottom flange. The details of the anchorage assemblies are illustrated in Figs. I-3 and 4.

2.2.3. Installation Procedure of CFRP P-T Bars

As previously stated, the P-T system was installed in the positive moment region of the exterior girders in all three spans of the bridge. Installation of the complete system was completed in just one day by a three-man crew with no special training required. Given accessibility limitations, some of the installation procedures were completed from a man-lift located below the bridge. The following lists and briefly describes the principal installation steps:

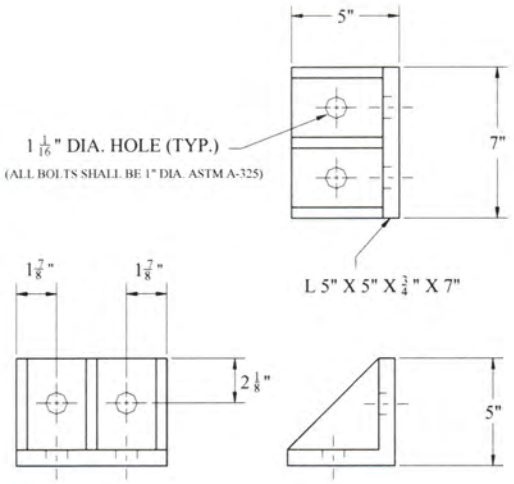

(a) Stiffened steel angle assembly

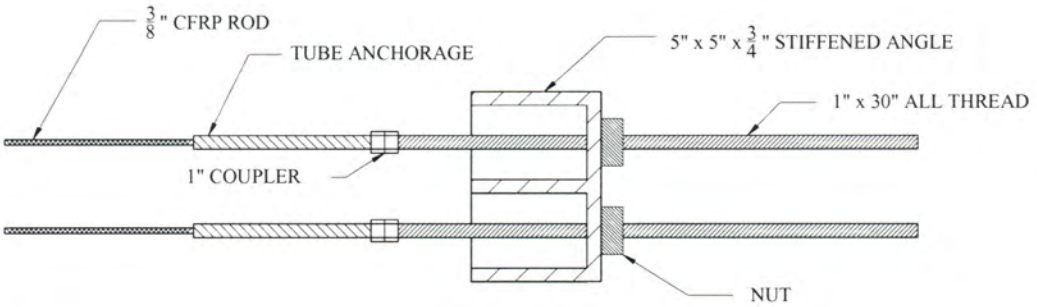

JACKING END

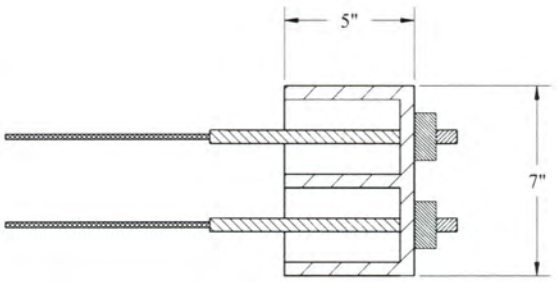

FIXED END

(b) CFRP bar to bracket connection detail

Figure I-3. Anchorage assembly detail for P-T bars.

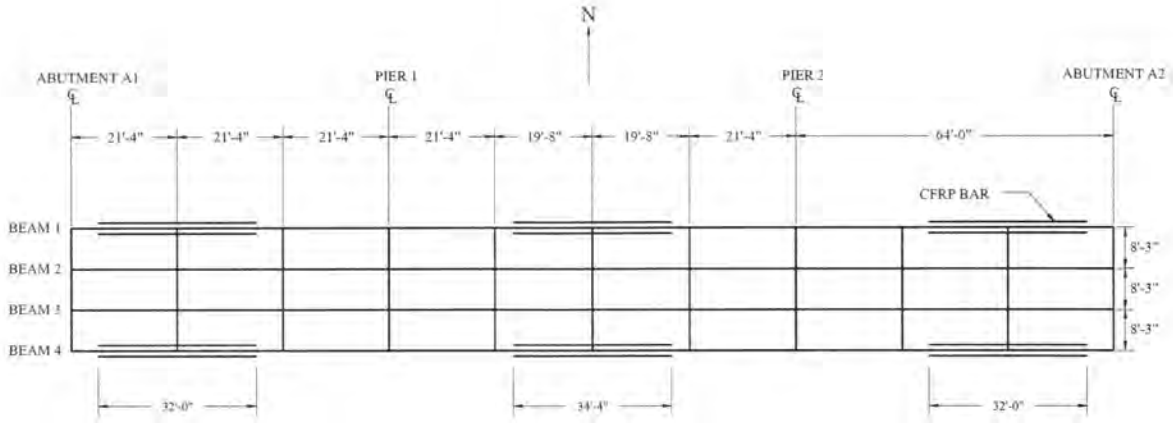

(a) Plan view

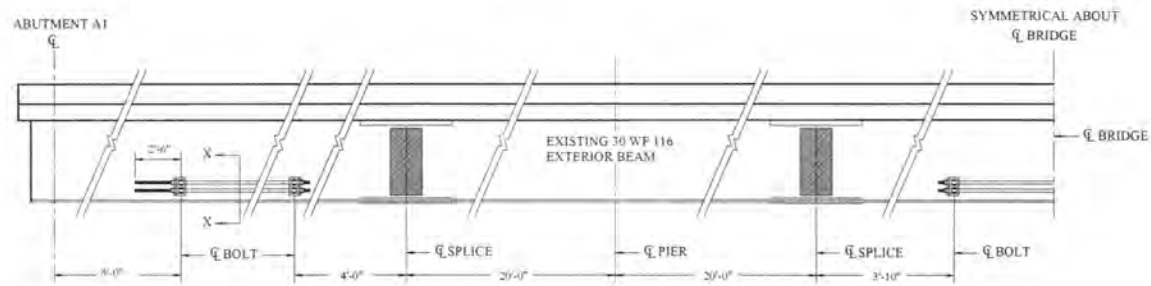

(b) Side view

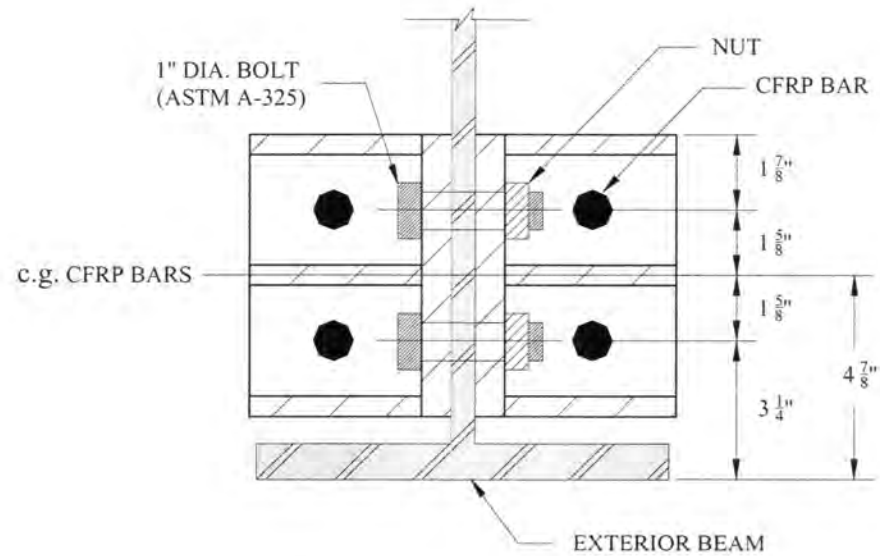

(c) Cross-section view (X-X)

Figure I-4. Location of the P-T system on the bridge.

1. The location of the anchorage assemblies shown in Fig. I-4 was determined based upon the original design and field measurements.
2. 1 1/16 in. diameter holes were drilled through the web of each exterior beam for attaching the stiffened angle anchorage assemblies.
3. The surface of the web that was to be in contact with each stiffened angle anchorage assembly was cleaned without paint removal. All other foreign materials, such as burrs and metal shavings due to drilling of holes were removed to allow for a satisfactory surface contact for a bolted friction connection.
4. The anchorage assemblies were then bolted to the webs of the beams with 1 in. diameter A325 high-strength bolts torqued in accordance with the manufacturer's recommendation (Fig. I-5).
5. As shown in Fig. I-6, interference between the CFRP bars and the diaphragms was corrected by removal of a portion of the diaphragm/stiffener assembly with an acetylene torch.
6. The CFRP P-T bars were placed in position between anchorage assemblies on both sides of the web (Fig. I-7). Extra caution was taken during the erection not to damage any of the bars by scratching or excessive sagging.
7. A nominal force of 12 kips was applied to all bars (four bars per location) with a hollow-core hydraulic jack in a symmetrical manner following the sequence of steps listed below and illustrated in Fig. I-8, where each event defines a specific step in the P-T process:

    a. A nominal force of 6 kips was applied to the bottom and then to the top bar on the south side of the south exterior girder (Beam 4) in the west end span (Events 1-4).
    b. A nominal force of 6 kips was applied to the bottom and then the top bar on the north side of the south exterior girder (Beam 4) in the west end span (Events 5-8).
    c. Steps 1 and 2 were repeated in reverse order to increase the nominal force of 6 kips in each bar to the intended force of 12 kips (Events 9-16), thus completed the P-T at one location.
    d. The jacking equipment was then moved to the north exterior girder (Beam 1) and Steps a through c were repeated (Events 17-32) for the four bars at that location.
    e. Steps a through d were then repeated in the center span (Events 33-64) and in the east end span (Events 65-96) to complete the P-T.

A complete list of "Events" occurring during the application of the P-T force is presented in the Appendix. Photographs of the application of P-T force in the west end span and center span are shown in Fig. I-9, and the overall construction sequence is illustrated in Fig. I-10. Also, photographs of the completed installation can be seen in Fig. I-11.

Generally, the handling and installation process of the CFRP P-T system was relatively simple and not labor intensive requiring less than five man-days to install. It is recommended, however, that a visual inspection be made at each rod grip after the force is applied to the system to make sure that no slippage has occurred between the bars and the grips.

Figure I-5. Installing anchorage assembly.

Figure I-6. Removal of a portion of the diaphragm/stiffener assembly.

(a) Placement of a CFRP bar

(b) Top CFRP bar in place

Figure I-7. Installation of CFRP bars.

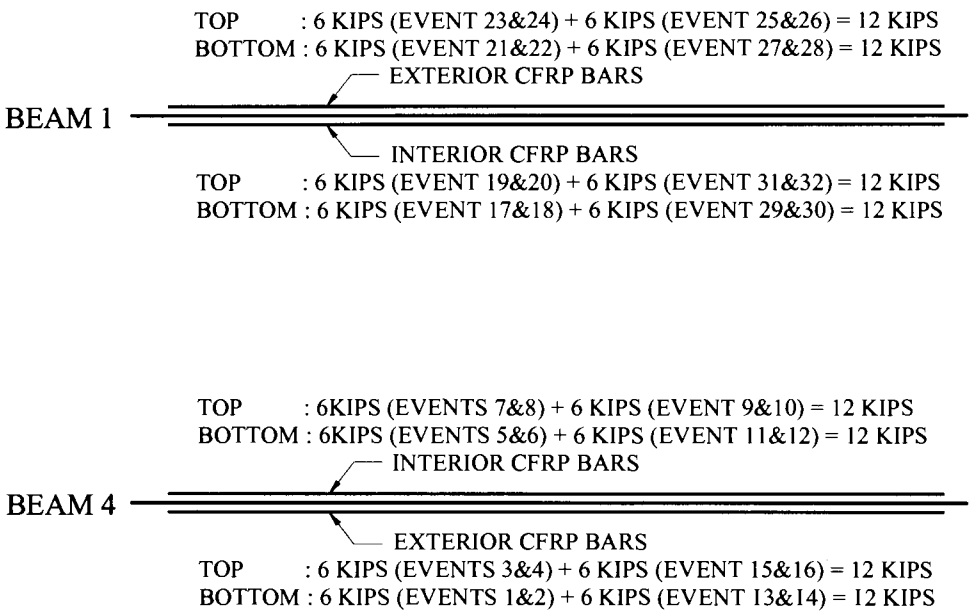

Figure I-8. Typical P-T application sequence.

(a) Application of P-T force in the west end span

(b) Application of P-T force in the center span

Figure I-9. Application of P-T force.

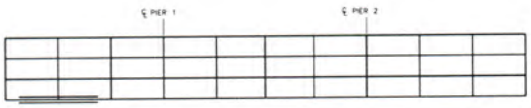

(a) Beam 4 – west end span

(b) Beam 1 – west end span

(c) Beam 4 – center span

(d) Beam 1 – center span

(e) Beam 4 – east end span

(f) Beam 1 – east end span

Figure I-10. Overall P-T sequence.

(a) Exterior CFRP bars in west end span

Figure I-11. Photographs of the completed installation.

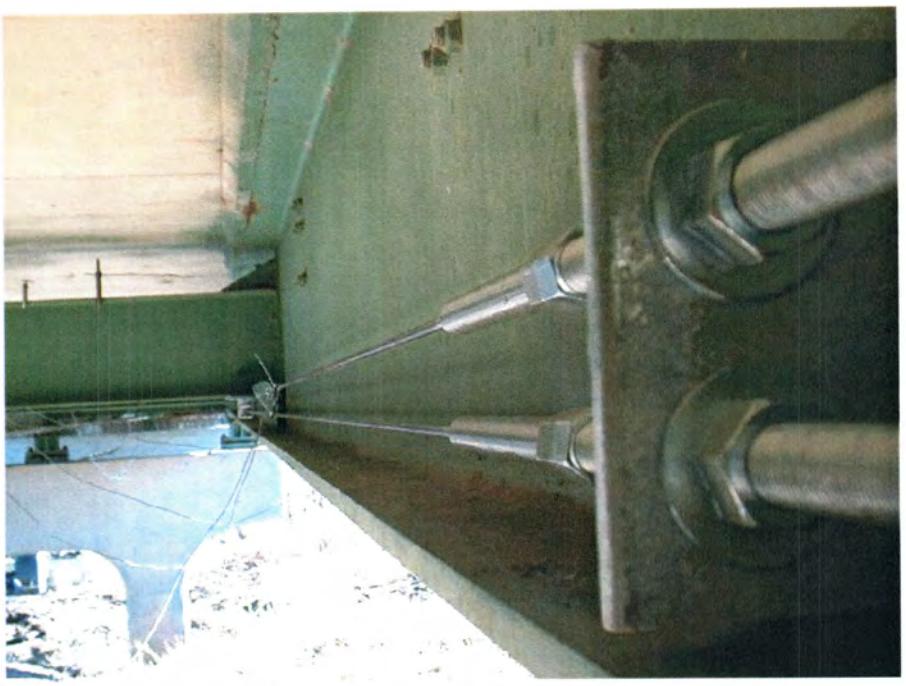

(b) Interior CFRP bars in west end span

(c) CFRP bars in center span

Figure I-11. Photographs of the completed installation - continued.

3. EXPERIMENTAL PROGRAM

This chapter describes the various tests conducted in the laboratory and in the field to evaluate the performance of the CFRP P-T strengthening system. Twenty-four hour, constant load and ultimate tensile strength tests were conducted in the laboratory to evaluate important material characteristics. The bridge described previously was instrumented to measure flexural strains at strategically selected locations; it was tested before installation of the P-T strengthening system, immediately following installation, and after approximately one and two years of service to assess changes in the live load response resulting from the addition of the P-T strengthening system and time. In addition, the behavior of the bridge was monitored during the application of P-T forces. The following sections describe each test performed with the results of the testing and evaluation presented in Chapter 4.

3.1. LABORATORY TESTING

The creep and tensile behavior for conventional materials such as steel are well known; however, these characteristics are not well established for composite materials such as CFRP bars. Laboratory tests were performed to help define the characteristics and to further investigate the feasibility of using this material in P-T strengthening systems. Originally, the laboratory testing program was to include only ultimate strength testing of a sample of CFRP bars. However, within 24 hours of installation of the CFRP bars on the subject bridge, slip was observed to have occurred at the bar to steel tube anchor interface (see Fig. I-12). Although a large slip (approximately 1 in.) occurred at one of the CFRP bars (bottom bar on the west end span Beam 4), most locations had relatively small amount of slip (i.e., in the range of 1/16 in. to 1/8 in.). To this end, the laboratory testing program was modified to include loading sample bars under constant force to study the slippage phenomenon. The following paragraphs describe the specimens tested and the two types of tests performed.

The CFRP bar specimens tested in the laboratory, shown in Fig. I-13, had a total length of 54 in. with the same 3/8 in. diameter and other properties as the CFRP bars used in the field P-T strengthening system. Both ends of the CFRP bar were embedded in 12 in. long steel tube anchorage, as was used in the field.

A total of eight CFRP bars (designated from S1 through S8) were examined. The 24-hour, constant load tests were conducted on three bars (S1, S2, and S3). Ultimate strength tests were conducted on eight bars (S1 through S8), including the three bars that were initially tested under constant load for 24 hours.

The ultimate strength and 24-hour, constant load tests were performed on the eight specimens to examine grip performance, to gain a better understanding of their basic engineering properties, and to study the general suitability as a strengthening material. Both tests required similar setups. All tests were completed using a Satec 400HVL test machine with 400 kips capacity and a 12 in.-stroke in conjunction with an Optim Megadac data acquisition system Model 3415AC. Two Direct Current Displacement Transducers (DCDT) gages were installed on each specimen close to the grips to measure the slip between the bar and tube anchorage (see Fig. I-14). For the 24-hour, constant load test, an electronic extensometer with a 2-in. gage length was mounted at approximately mid-length of the specimens to measure internal strain. Each specimen was installed in the test machine with a connection detail that simulates the connection used in the field P-T strengthening system. Each specimen was installed across the two cross heads of the test machine so that they were aligned with the center of the grips. The top and bottom of the grip ends that had threaded ends were bolted to the top and bottom test machine heads. An example of a fully instrumented specimen and test setup is illustrated in Fig. I-15.

The primary goal of the 24-hour, constant load test was to observe if there were any significant elongation or separation between the bar and the grip connection during the 24 hours after the force was applied. To this end, each specimen was placed under a constant load of 12 kips for 24 hours to simulate the field conditions. The applied load and elongation were recorded continuously for the duration of the test.

The ultimate tensile strength tests were conducted to determine the ultimate capacity of the CFRP bars. Eight specimens were tested under stroke control until failure. Different loading rates were used to study the impact on the performance of the material. The loading rates used were 5% on specimens S6 and S7, 12% on specimens S1, S3, S4, and S5, and 15% on specimens S2 and S8.

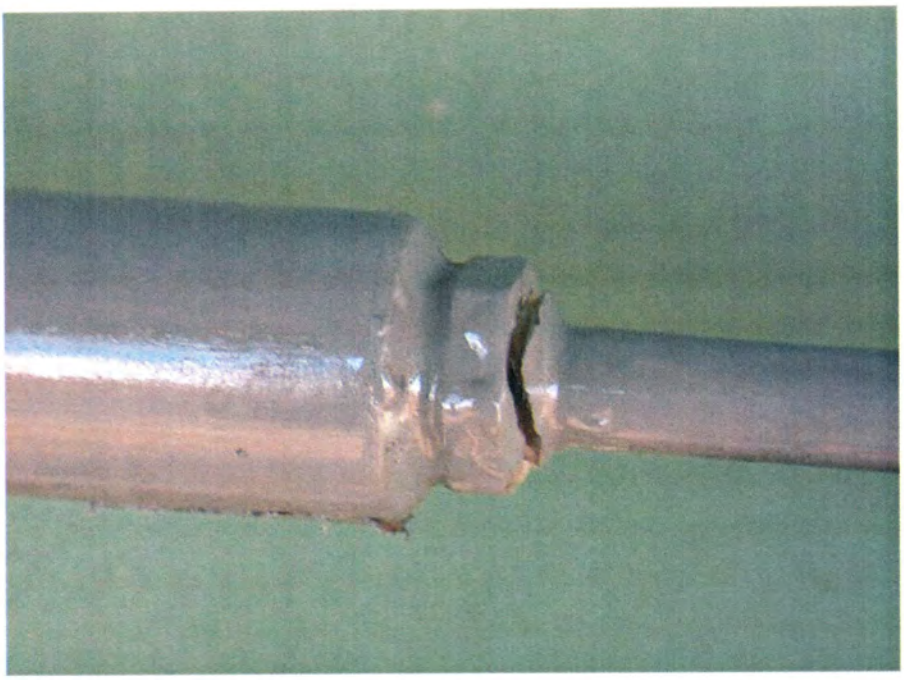

Figure. I-12. Slip between the CFRP bar and the steel tube anchor interface.

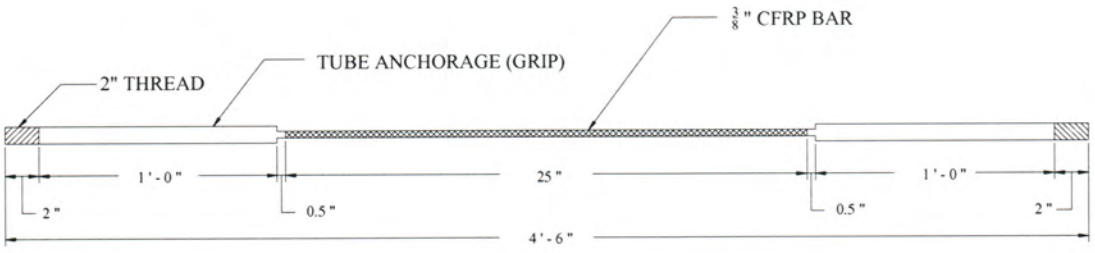

(a) Configuration of CFRP bar specimen

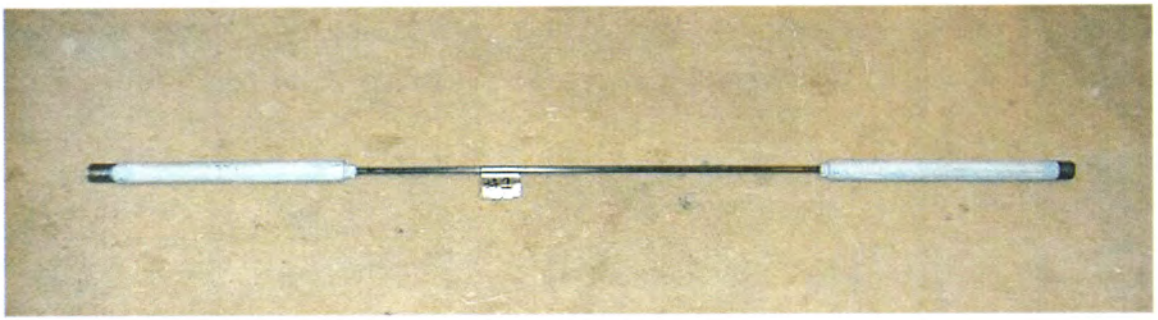

(b) Photograph of CFRP bar

Figure I-13. CFRP laboratory specimen.

(a) Photograph of instrumented specimen

(b) Top grip

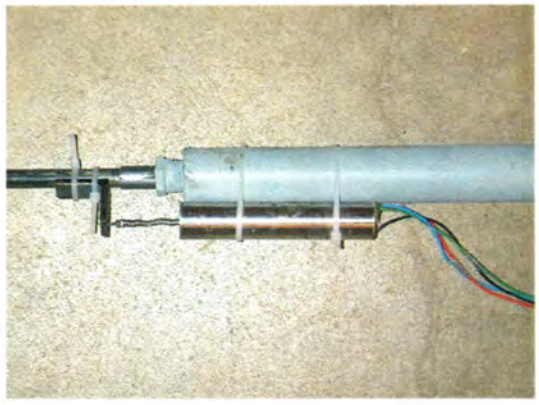

(c) Bottom grip

Figure I-14. Slip measurement instrumentation for the laboratory specimen.

3.2. FIELD LOAD TESTING

The field bridge was tested before and immediately following the installation, and after one and two years of service. The location of the instrumentation was selected so that the live load response of the bridge could be determined, thus providing an overall understanding of global behavior. A total of thirty-six strain gages were installed on the bridge with thirty-two gages on the top and bottom flanges of the beams and four gages on the guardrails as illustrated in Fig. I-16. Due to the structural symmetry of the bridge, only one-half of the bridge was instrumented.

After installation of the instrumentation, a loaded 3-axle dump truck was driven, at crawl speed, across the bridge with strain data collected continuously as the truck crossed the bridge. The initial test was conducted to establish a benchmark response of the bridge, while the follow-up tests were completed to access changes resulting from the addition of the P-T system and time.

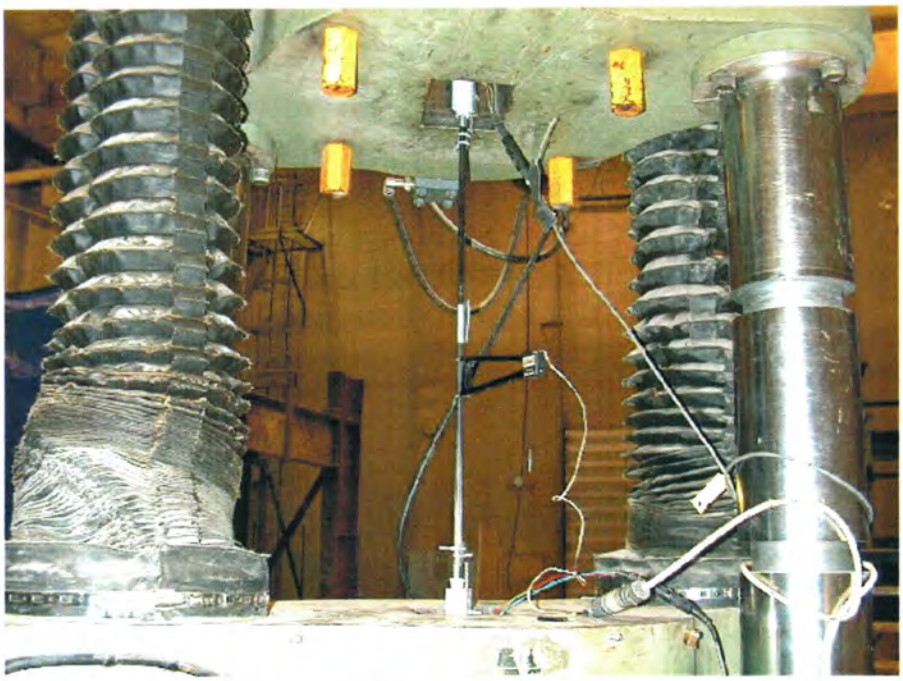

Figure I-15. Test setup for laboratory testing.

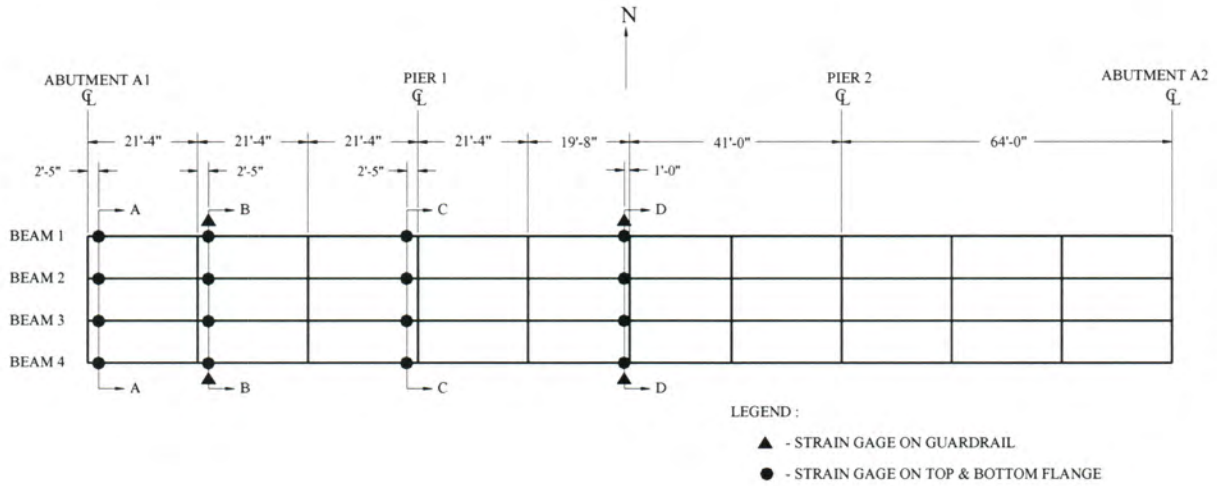

(a) Plan view

Figure I-16. Bridge strain gage location and reference sections.

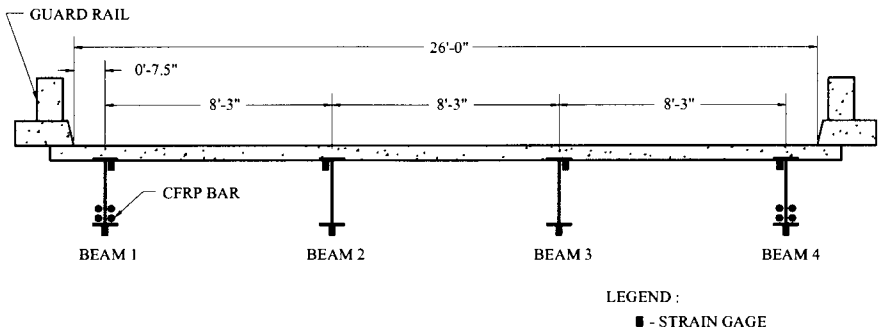

(b) Section A and C

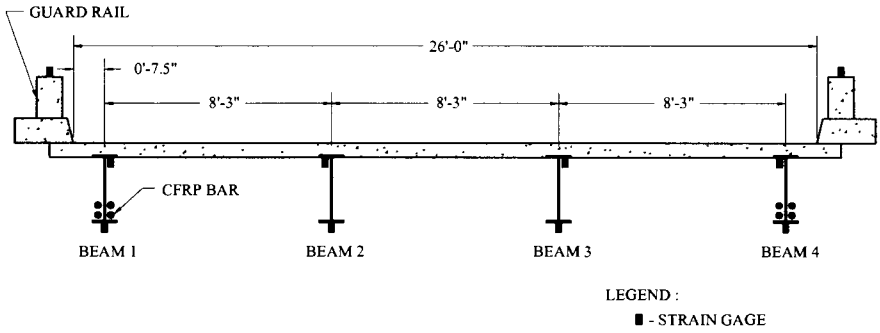

(c) Section B and D

Figure I-16. Bridge strain gage location and reference sections - continued.

3.2.1. Initial Test (October 29, 2001)

A diagnostic initial load test was conducted prior to the installation of the P-T system to establish a baseline static behavior of the unstrengthened bridge. Four different load paths were used to examine the performance of the bridge. For convenience, each load path is referred to as Y1, Y2, Y3, and Y4, respectively, as shown in Fig. I-17. For path Y1, heading east, the driver side wheel was placed 3 ft north of the bridge centerline. For Path Y3, the passenger side wheel was placed on the same path as Y1, but heading west. For path Y2, heading east in north lane, and path Y4, heading west in south lane, the driver side wheels were placed 2 ft from the north and south curbs, respectively. The Iowa DOT provided the loaded truck shown in Fig. I-18. Truck 1, the truck utilized during the initial test, had a total weight of 55.92 kips with 16.40 kips and 39.52 kips on the front and rear axles, respectively.

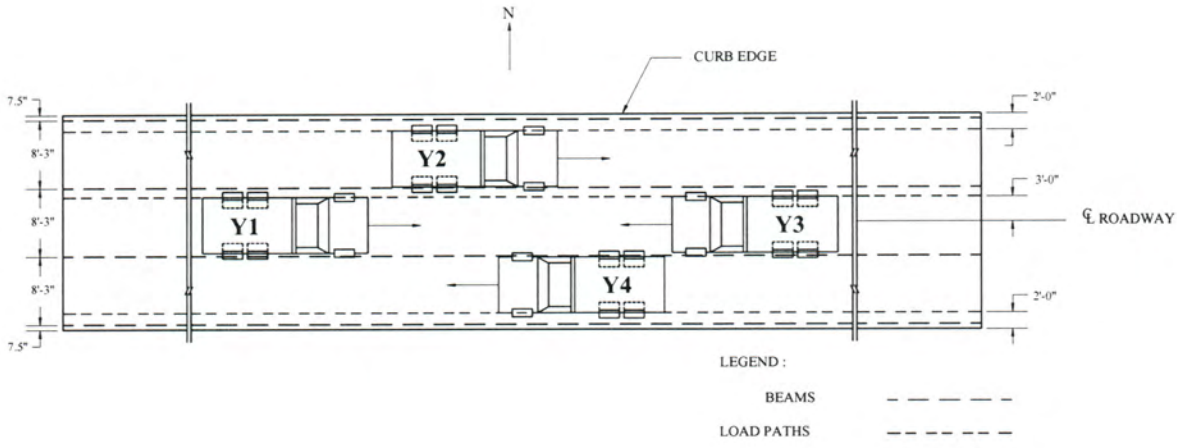

Figure I-17. Truck paths used during load testing.

Figure I-18. Photograph of typical load test truck.

3.2.2. Monitoring During Application of P-T Force

During application of forces to the P-T strengthening system, the bridge and selected CFRP bars were monitored. The goal of this monitoring was to confirm that the design methodology used to predict the distribution of P-T force throughout the bridge was accurate. As illustrated in Fig. I-19, a calibrated system of strain gages was installed on four CFRP bars (Bar 1, Bar 2, Bar 3, and Bar 4) on Beam 4 in the west end span. In addition, the same instrumentation used during the previously described test was again monitored during application of the P-T forces.

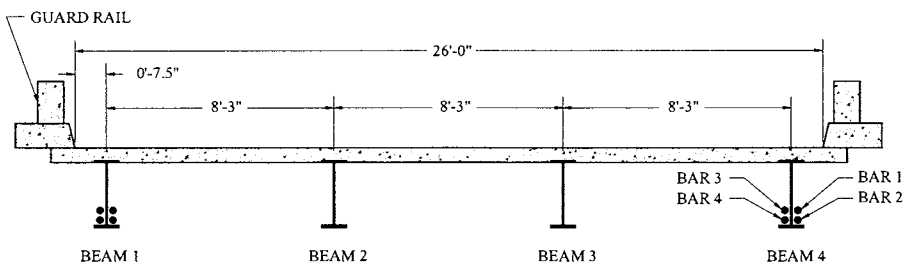

Figure I-19. CFRP bars monitored during application of P-T force.

3.2.3. Immediately After Installation (November 9, 2001)

The second load test was conducted shortly following installation of the P-T system to assess any immediate change in performance resulting from the installation of P-T system. The protocols used for the second load test were the same (e.g., same load paths and sequences, location of the strain gages, etc.) as what was used in the initial test except for the weight of the truck used. The load truck used for the second load test, Truck 2, was again provided by the Iowa DOT and had a total weight of 52.16 kips with 14.74 kips and 37.42 kips on the front and rear axles, respectively.

3.2.4. One Year of Service (October 30, 2002)

On October 30, 2002, another follow-up load test was conducted to investigate any change in the behavior of the bridge over a one year time period. The total weight of the test truck used in this test, Truck 3, was 49.20 kips with 12.52 kips on the front axle and 36.68 kips on the rear axle weight. As before, the same testing protocols were followed.

3.2.5. Two Years of Service (June 11, 2003)

On June 11, 2003, the final test was conducted to assess any change in performance over the two-year life of the P-T system. The bridge was instrumented in the same manner as in previous tests

and the same truck paths were used. The truck utilized for this test, Truck 4, had a total weight of 45.58 kips with 13.20 kips in the front axle and 32.28 kips in the rear axle. Dimensions and weights of the load truck used in each test are illustrated in Fig. I-20 and summarized in Table I-2.

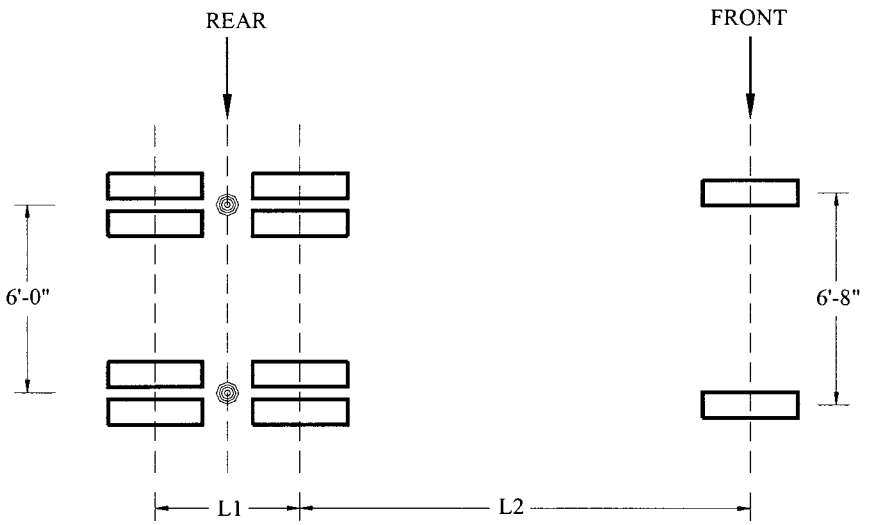

Figure I-20. Dimension and weight of load truck.

Table I-2. Summary of dimensions and weights of load truck.

Truck No.	L1	L2	Weight (lb)		
			Rear	Front	Total
1	4'-7"	14'-3"	39,520	16,400	55,920
2	4'-5"	14'-8"	37,420	14,740	52,160
3	4'-5"	14'-8"	36,680	12,520	49,200
4	4'-6"	15'-0"	32,280	13,200	45,600

After the "two years of service" test was completed, the P-T force was removed from the bridge so that any loss that took place in a two-year period could be determined. Illustrated in Fig. I-21 is the orders used to remove the P-T force from the bridge. Corresponding results are documented in Chapter 4. Note that the P-T force on the top bar on Beam 1 in the west end span was not removed due to the short length of the threaded bar at jacking end (too short to set up the hydraulic jack). Once all the removed forces were determined, the nominal force of 12 kips was re-applied to each P-T bar.

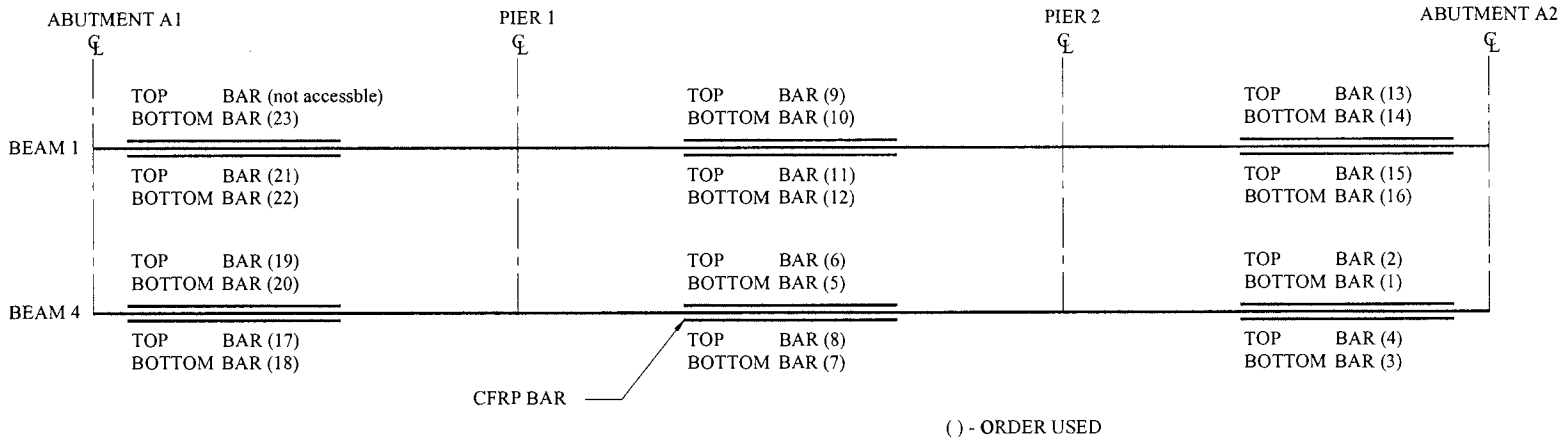

Figure I-21. Order used in removing P-T force from each bar

4. TEST RESULTS

Results from the various tests performed in the laboratory and in the field are presented in this chapter. Where applicable, the experimental results are compared with theoretical analysis results and mechanics based calculations.

4.1. LABORATORY TEST RESULTS

As previously described, the 24-hour, constant load tests were conducted on three bars (S1, S2, and S3) and ultimate tensile strength tests on eight bars (S1 through S8) including the three bars tested under the 24-hour, constant load.

4.1.1. 24-Hour Constant Load Test Results

The constant load of 12 kips was applied to three of the specimens for 24 hours. After the 24 hours of loading, each specimen was removed from the test set up and thoroughly inspected. It was determined from visual inspection that no significant slip occurred during the period of this testing. As can be seen in Table I-3 and Fig. I-22, which summarize the results of this testing, the maximum slip between the grip and the bar was less than 0.0011 in. in all cases. The fact that minimal slip was recorded, unfortunately, means that the source of slip observed in the field could not be determined.

Table I-3. Summary of laboratory 24-hour constant load test results.

Specimen	Maximum slip (in.)	
	Top	Bottom
S1	0.0006	0.0007
S2	0.0005	0.0007
S3	0.0007	0.0011

4.1.2. Ultimate Strength Test Results

Ultimate tensile strength testing was conducted on eight specimens (S1 through S8). The displacement was measured by monitoring the axial deflection of the specimen from the selected reference point on the cross heads that were used to transfer the tensile force to the specimen. Stress-displacement plots were made for each tested specimen as shown in Fig. I-23, and the test results were summarized in Tables I-4 and 5.

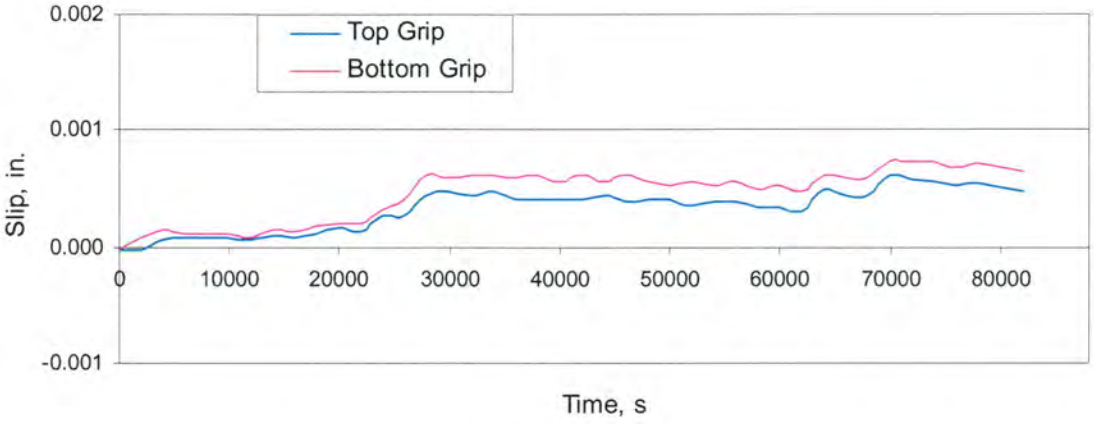

(a) Specimen 1 (S1)

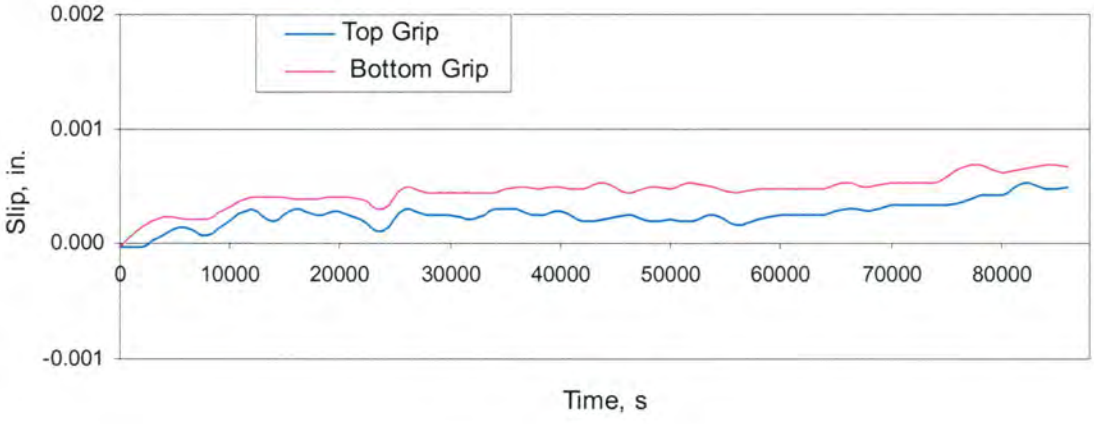

(b) Specimen 2 (S2)

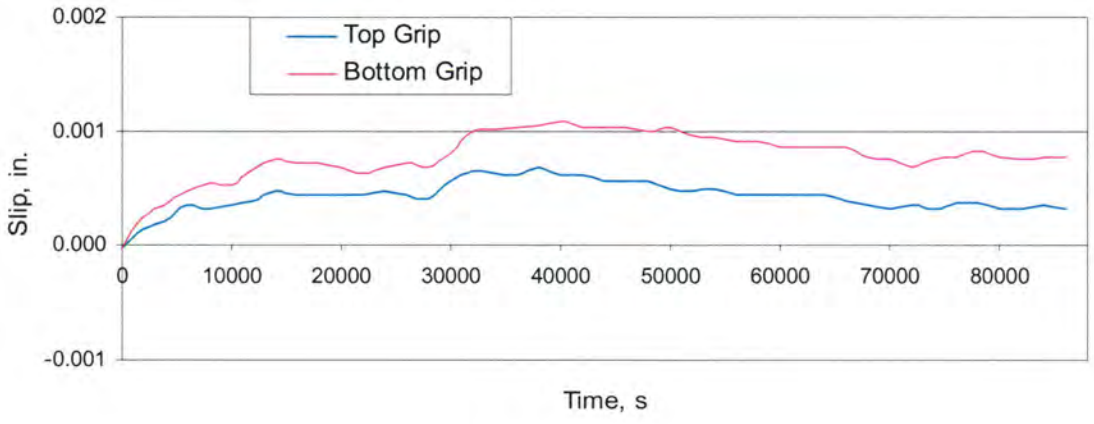

(c) Specimen 3 (S3)

Figure I-22. Laborotory 24-hour constant load test results.

As can be seen in Fig. I-23, it appears that all the CFRP bar specimens experienced several localized internal fiber failures (defined as peaks in Table I-4) before the entire specimen failed. Each internal fiber failure can be identified as a significant stress decrease occurring at each peak in the plot. Based on "post-test" visual inspections of the failed specimens, it was found that failure of the specimens could be generally be grouped into three "modes". Figure I-24 shows typical examples of the three failure modes that were experienced in the ultimate strength test: tensile-rupture failure (Mode 1), grip-slip or pull-out failure (Mode 2), and combination failure (Mode 3). As can be seen in Table I-5, five of eight specimens failed by pull-out (Mode 2); theses specimens with the "pull-out" failure have the first peak at lower stress levels than other specimens.

In summary, the average stress and displacement of the specimen at the first peak were 241.9 ksi and 0.58 in., respectively, with the standard deviation of 68.0 ksi and 0.16 in. (see Table I-4). Also, the maximum average stress and the maximum average displacement of the specimens at failure were 344.5 ksi and 1.43 in., respectively with the standard deviation of 14.9 ksi and 0.66 in. (see Table I-5).

Although only a very small statistical sample was used in this test, the experimental data shows minimal impact from the different loading rates used in the testing as described in section 3.1. The type of failure mode was also found to be unrelated to the ultimate strength of the CFRP bars. However, the specimens used in the 24-hour, constant load test seemed to exhibit higher stress levels at the first peak than the other specimens.

Although some of the specimens experienced internal breaks before they reached the specified ultimate strength (300 ksi) given by manufacturer, it appears from the test results that all specimens reached more than their full capacity.

4.2. FIELD TEST RESULT

The bridge was tested for live load flexural response before and after the installation of the P-T strengthening system as previously described. Data were collected for the four different load paths shown previously in Fig. I-17. Recall also that the weights and dimension of the trucks used were given in Fig. I-20. For ease of interpretation, the data have been normalized based upon the total weight of the truck used in the initial test (i.e., subsequent test data were multiplied by the ratio of the initial test truck weight to the individual test truck weight) so that direct comparisons can be made.

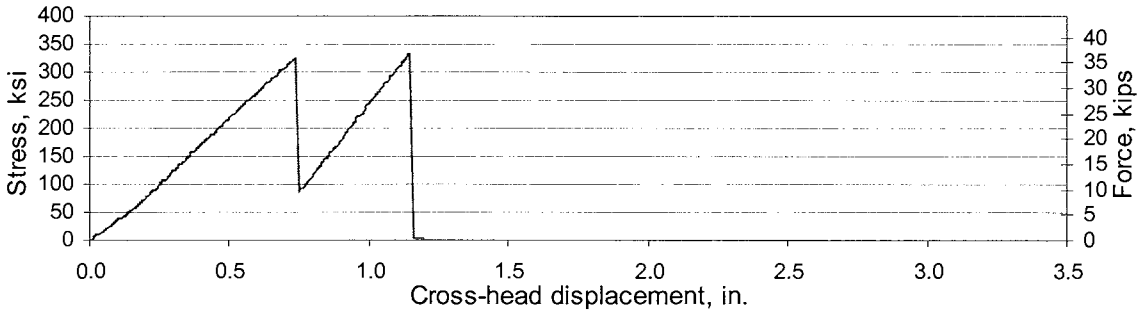

(a) Specimen 1 (S1)

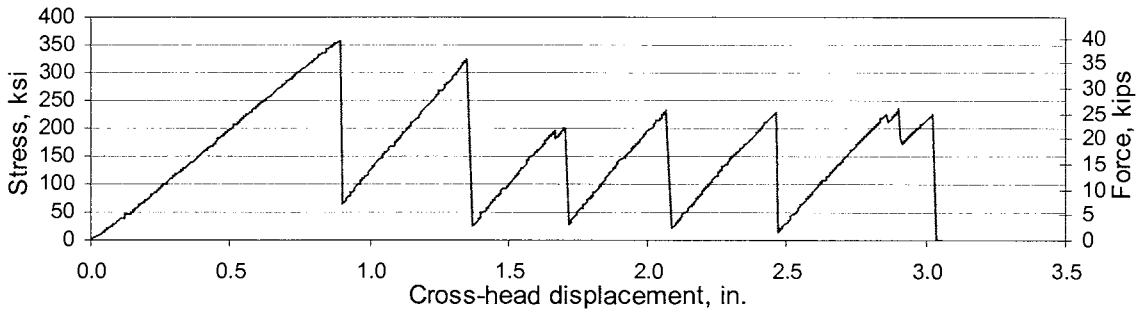

(b) Specimen 2 (S2)

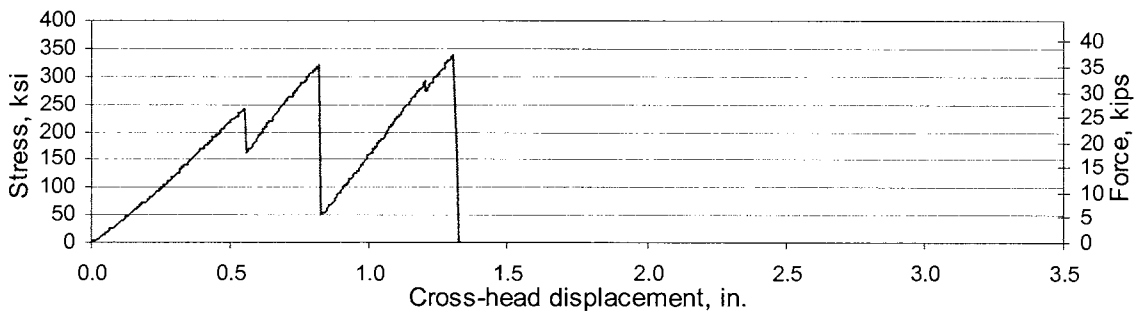

(c) Specimen 3 (S3)

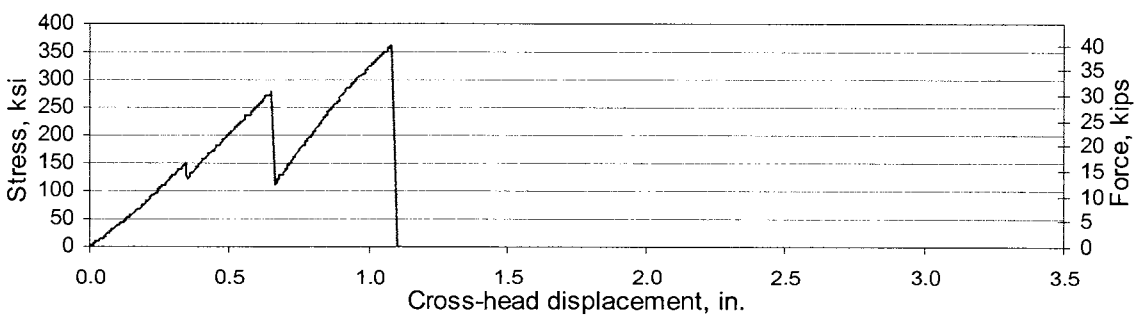

Figure I-23. Ultimate strength test results from laboratory specimens.

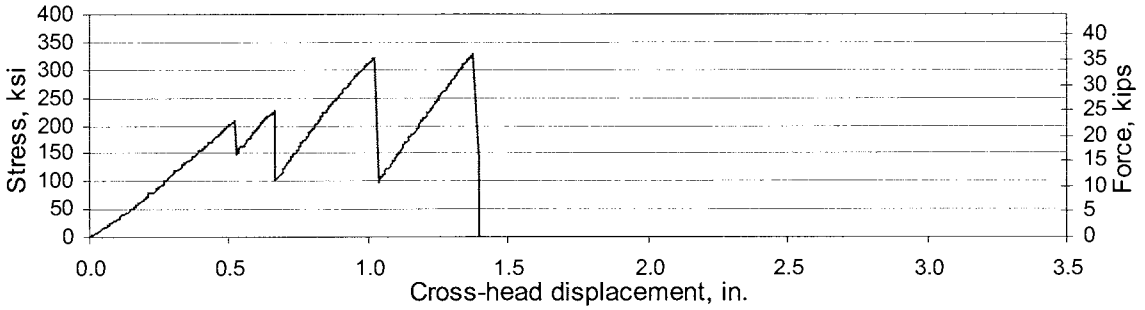

(e) Specimen 5 (S5)

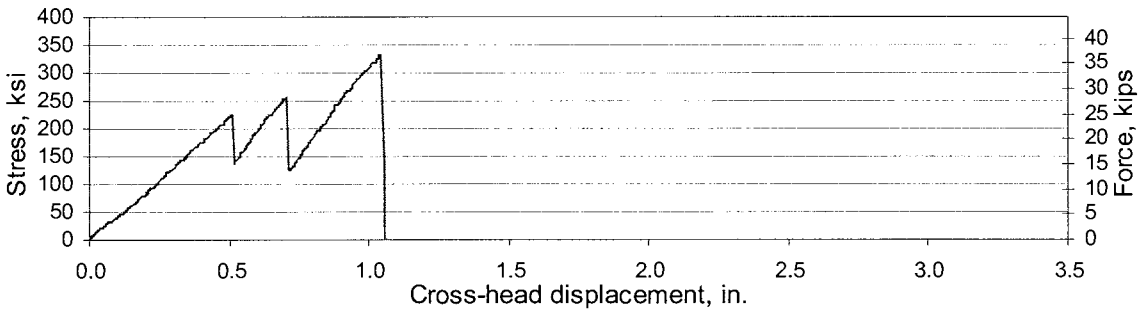

(f) Specimen 6 (S6)

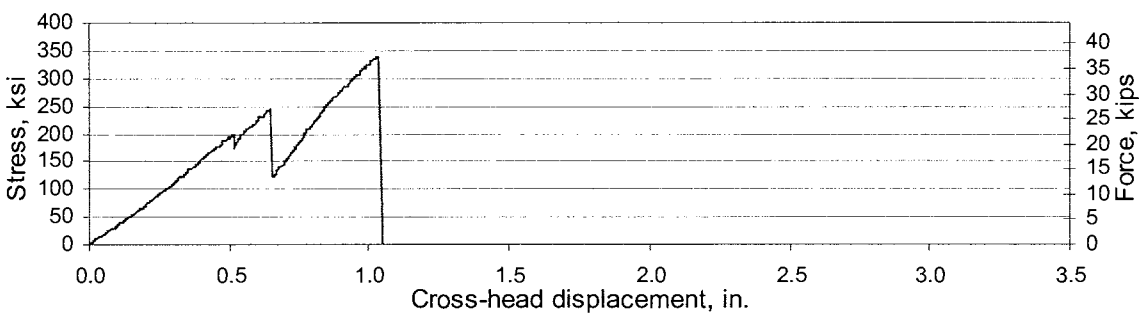

(g) Specimen 7 (S7)

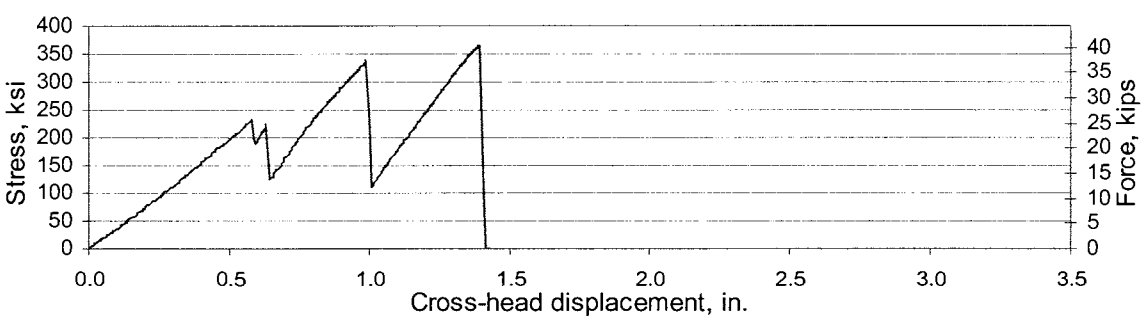

(h) Specimen 8 (S8)

Figure I-23. Ultimate strength test results from laboratory specimens-continued.

Table I-4. Summary of laboratory specimen ultimate strength test result at 1st peak.

Specimen	Applied force at 1st peak (kips)	Stress at 1st peak (ksi)	Displacement at 1st peak (in.)
S1	36.0	326	0.734
S2	39.4	357	0.892
S3	26.6	241	0.549
S4	16.4	149	0.346
S5	22.9	208	0.519
S6	24.7	224	0.510
S7	21.9	199	0.514
S8	25.5	231	0.583

Table I-5. Summary of laboratory specimen ultimate strength test result at failure.

Specimen	Total number of localized fiber failures before specimen failure	Stress at failure (ksi)	Displacement at failure (in.)	Failure mode
S1	2	332	1.143	1
S2	9	357	3.027	1
S3	4	339	1.303	3
S4	3	362	1.084	2
S5	4	328	1.377	2
S6	3	332	1.042	2
S7	3	340	1.033	2
S8	4	366	1.396	2

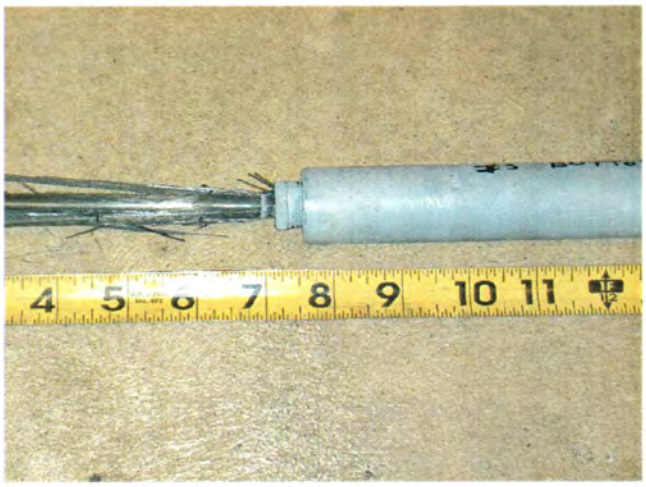

(a) Failure mode 1 (Tensile-rupture)

(b) Failure mode 2 (Pull-out)

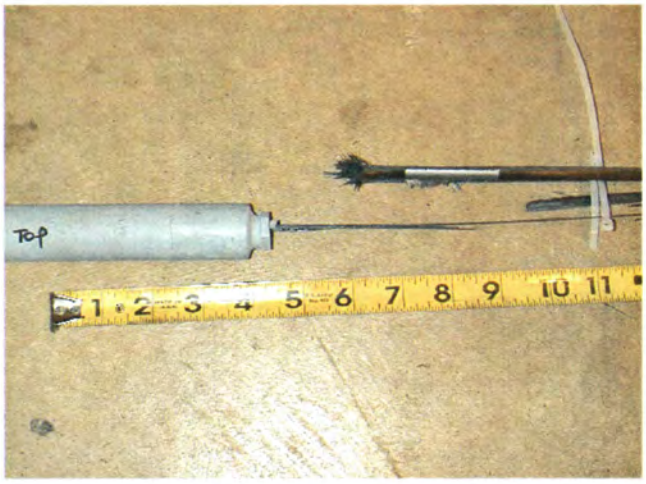

(c) Failure mode 3 (Combination)

Figure I-24. Laboratory specimen failure modes.

In the following discussion, the longitudinal gage position will be referenced to Sections A through D that were shown in Fig. I-16. The following convention was adopted to describe the data in the subsequent figures. The notation starts with a letter "Y" followed by a number such as "Y1" to indicate the truck paths that were illustrated in Fig. I-17. This, in turn, is followed by another letter and a number such as "A1" to indicate a section location (i.e., "A") and a beam number (i.e., "1"). Finally, the notation is completed with a word such as "Top" or "Bottom" to indicate from where on the beam the data are recorded: top flange or bottom flange. For example, "Y2D3 Bottom" represents a data set collected from "Path Y2 - Section D - Beam 3 - Bottom flange". Some other notations used are described as follows:

- "Initial Test" : data set taken during "Initial Test" (Oct. 29, 2001).
- "t = 0 year" : data set taken during "Immediately after installation Test" (Nov. 9, 2001).
- "t = 1 year" : data set taken during "One year of service Test" (Oct. 30, 2002).
- "t = 2 years" : data set taken during 'Two years of service Test" (June 11, 2003).

Note also that in figures showing "Truck Position", this is measured from the front wheel's location with respect to the bridge joints.

4.2.1. Initial Test

As previously mentioned, an initial diagnostic load test was conducted prior to the installation of the P-T strengthening system to establish a baseline static behavior of the unstrengthened bridge. The goal of this testing was to understand the general, global behavior of the bridge and to ensure that any future changes in behavior could be identified.

In general, all collected strains showed an elastic response (i.e., strains from all gages returned to zero after each truck crossed the bridge). The neutral axis location was found to generally be close to the top flange in the positive moment region, thereby verifying the composite behavior of the beam. By observing flexural tensile and compressive strains measured at Section A (near Abutment A1) and their relative magnitudes with respect to midspan strains, as shown in Figs. I-25 and 26, it was observed that some rotational end restraint is present at the abutment. This unintended rotational restraint could be attributed to corrosion of the abutment bearings (see Fig. I-1), accumulation of debris, and the presence of a heavy diaphragm over the abutment bearings. In addition, the strain patterns show a symmetric response that corresponds to the symmetrical nature of

the bridge and the truck paths utilized. For example, strains due to truck paths Y1 and Y3 on Beam 2 and Beam 3 (or Beam 1 and Beam 4), respectively, exhibited a similar, symmetrical behavior as is shown in Fig. I-26b. In general, strains in the positive moment regions exhibited a higher degree of symmetry than in the negative moment region. Some of the differences in transverse symmetry may be attributed to either differences in local stiffness or possible experimental error that might have occurred during the testing (i.e., differences in truck wheel line distribution and/or truck lateral positioning).

4.2.2. Influence of P-T Strengthening System on Live load Response

This section describes the response and behavior of the bridge tested after the installation of the P-T strengthening system by comparing strain measurements from each test. Recall that the gage locations and truck paths used were shown in Figs. I-16 and 17. In the interest of brevity, only bottom flange strains will be presented in this section. However, it should be pointed out that the top flange generally exhibited the same behavior.

Follow-up load tests (immediately after installation, one year of service, and two years of service) were carried out on the post-tensioned bridge to investigate the bridge's behavior before and after the P-T strengthening system installation. Typical strain data from these tests are illustrated in Figs. I-27 through 30. From the follow-up test results, several important observations were made. Each load test produced fairly consistent strain readings with those established during the initial test. This consistency in strain is informative in that it indicates that the P-T system did not significantly alter the behavior of the bridge over the two years of service, as would be expected. Although it is not possible to precisely account for all the sources of strain, it is evident from the consistency of the strain data that the installation of the P-T system had negligible impact on changing the stiffness of the bridge. The data also indicates that the live load distribution characteristics are virtually the same before and after the installation of the P-T system. In general, good agreements in strain data were observed; however, there were some relatively small discrepancies observed at several locations. These strain discrepancies may be attributed to following factors:

- Change in end restraint due to corrosion at the abutment bearings over time in combination with the application of the P-T force.
- Inadvertent variations in truck positions and geometry.

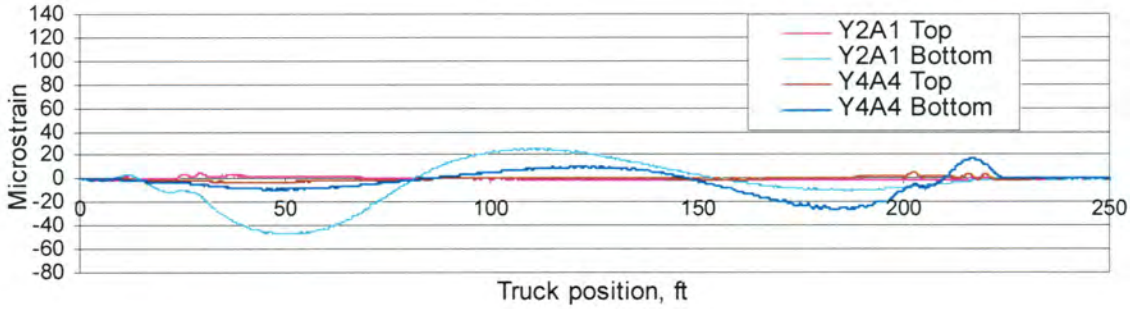

(a) Section A

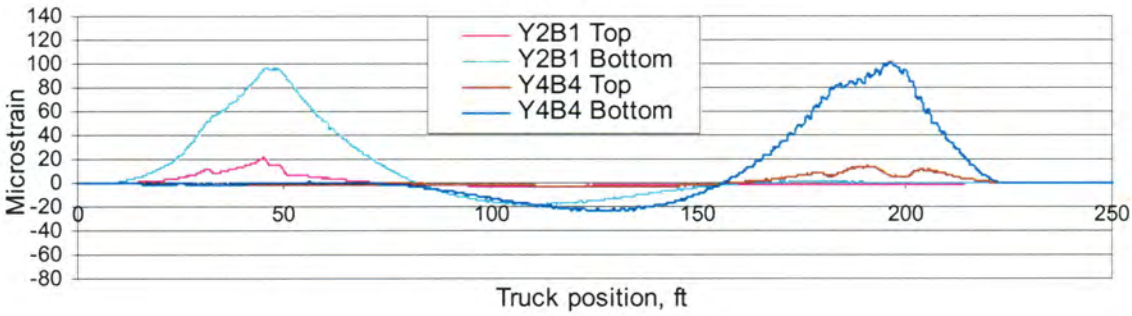

(b) Section B

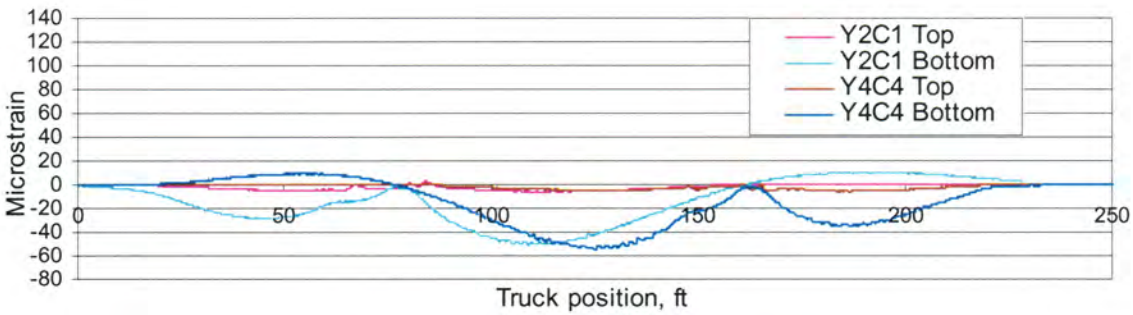

(c) Section C

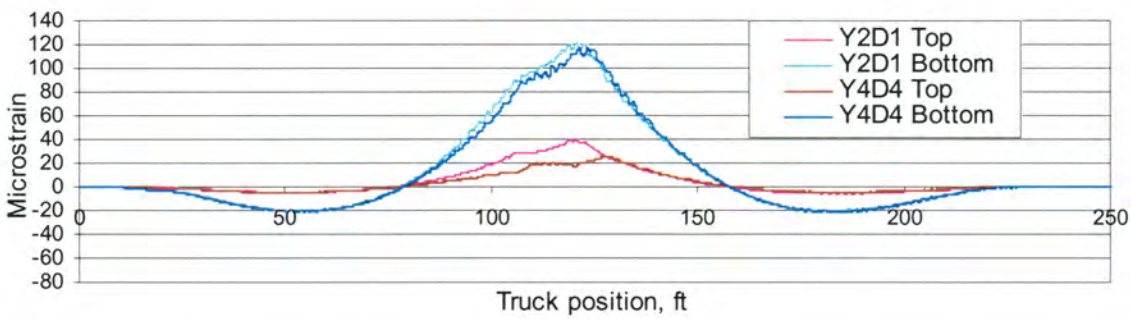

(d) Section D

Figure I-25. Before strengthening: strains in Beam 1 (Path Y2) and Beam 4 (Path Y4).

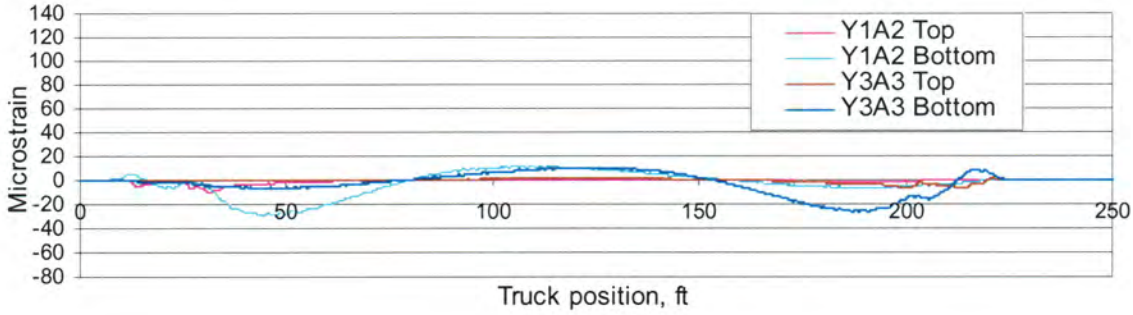

(a) Section A

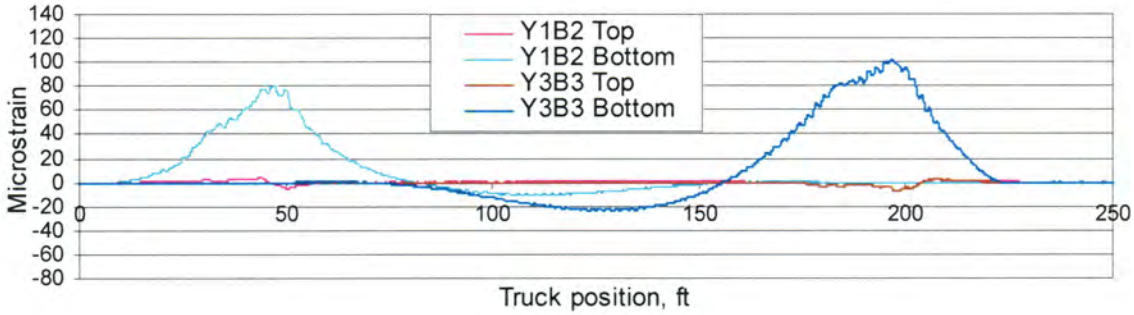

(b) Section B

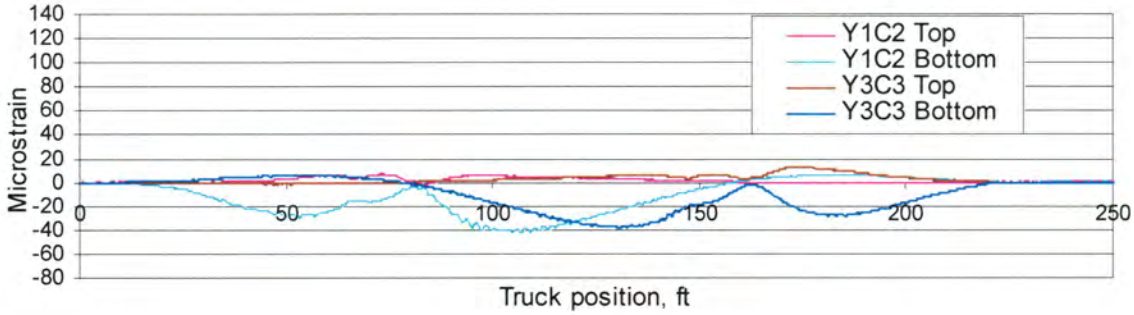

(c) Section C

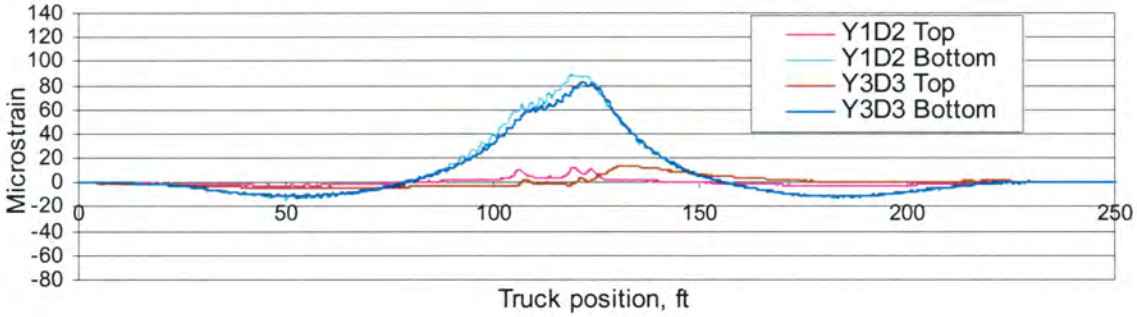

(d) Section D

Figure I-26. Before strengthening: strains in Beam 2 (Path Y1) and Beam 3 (Path Y3).

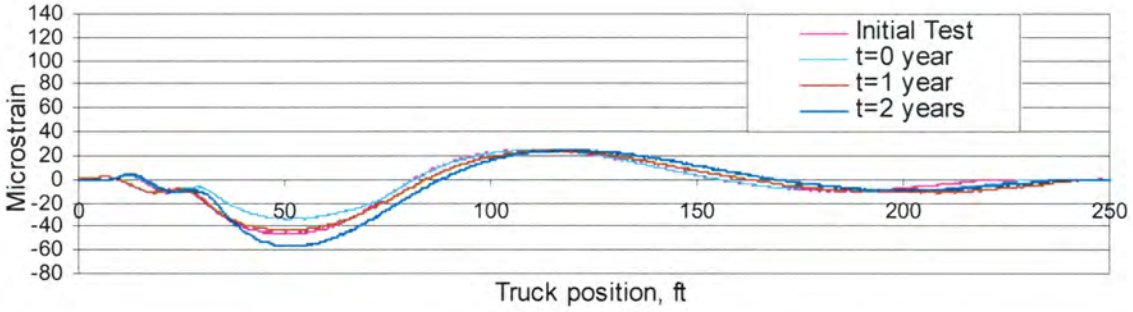

(a) Section A

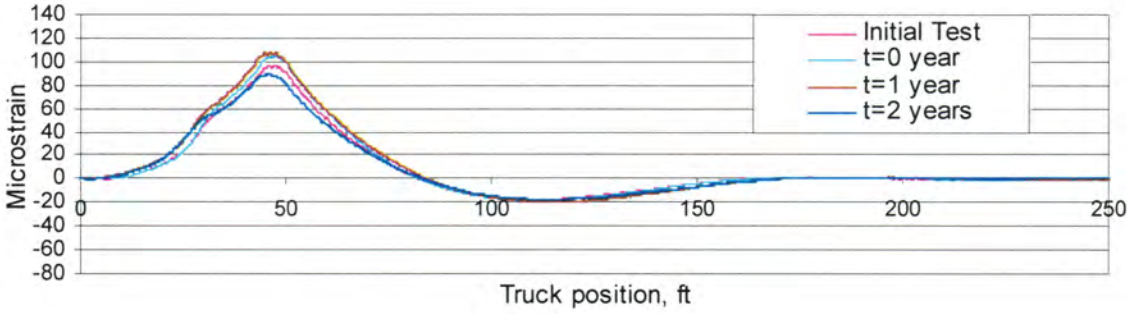

(b) Section B

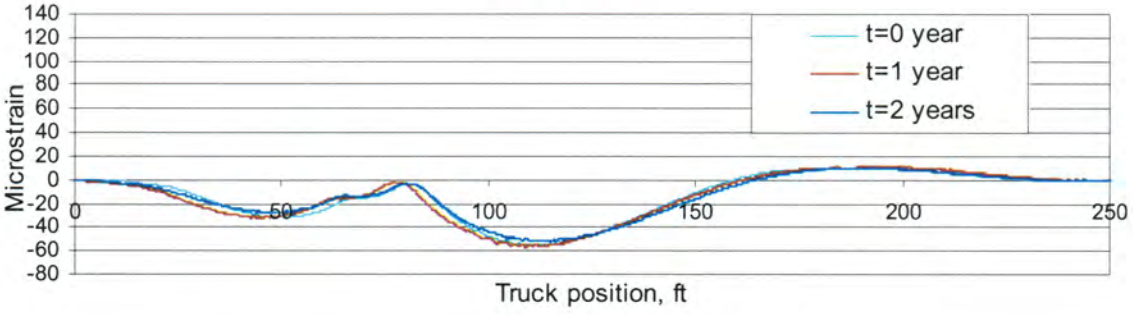

(c) Section C

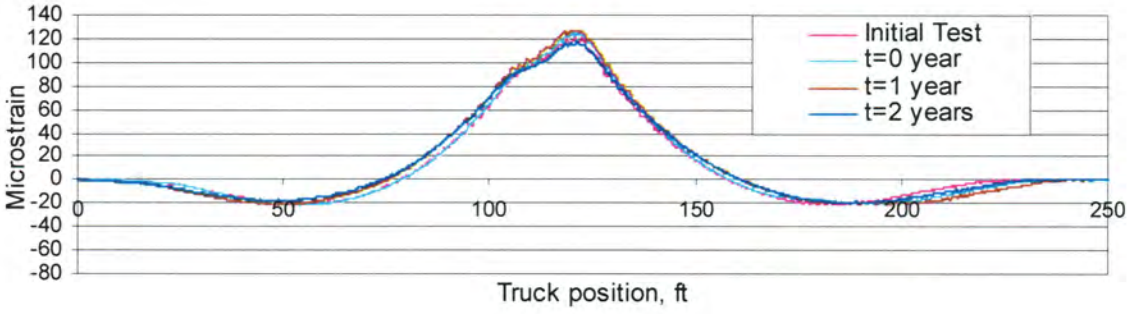

(d) Section D

Figure I-27. Before and after strengthening: strains in Beam 1 (Path Y2).

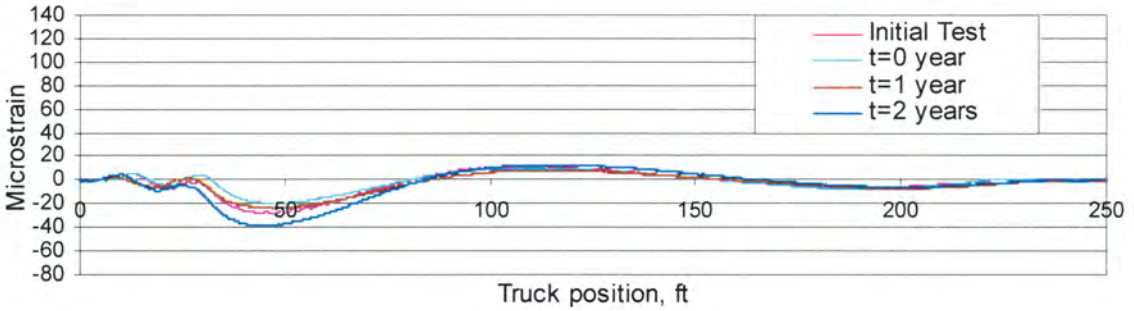

(a) Section A

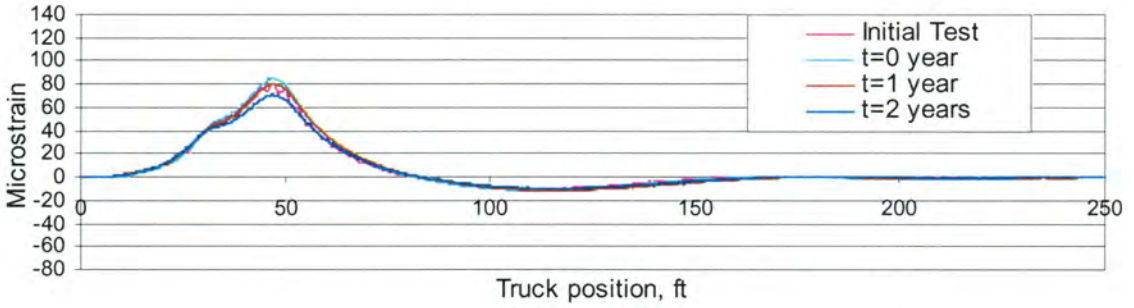

(b) Section B

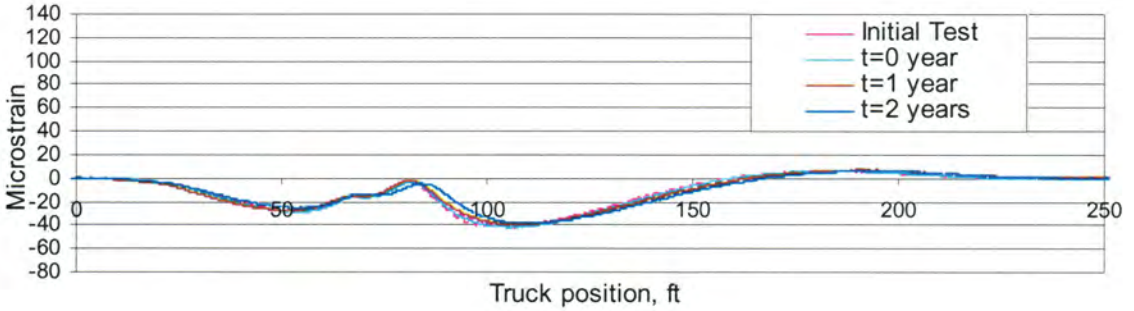

(c) Section C

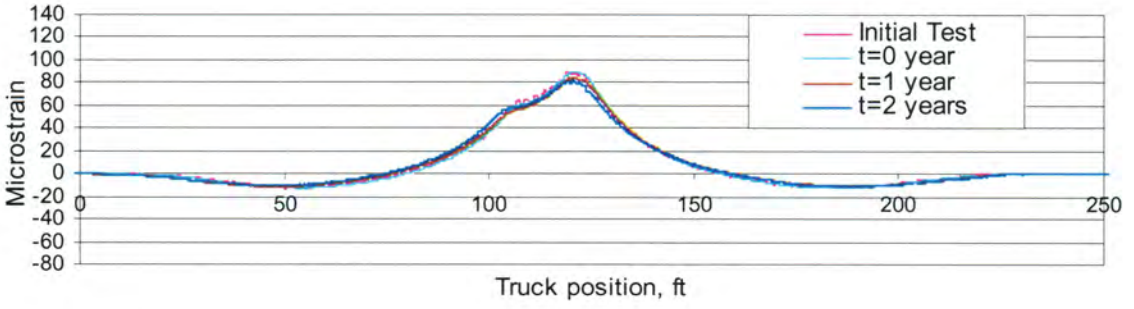

(d) Section D

Figure I-28. Before and after strengthening: strains in Beam 2 (Path Y1).

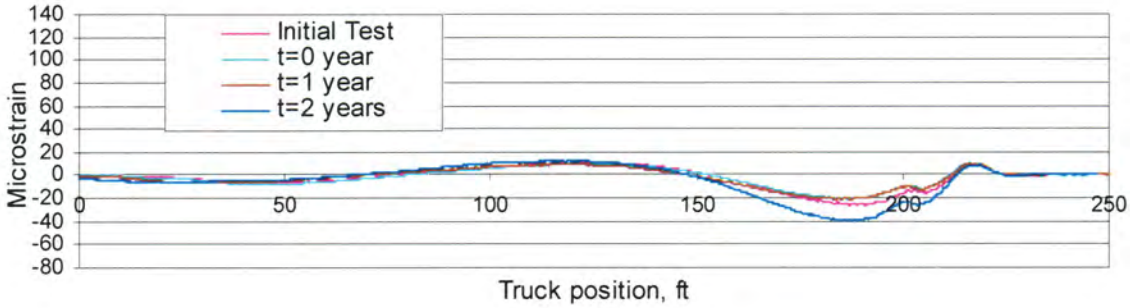

(a) Section A

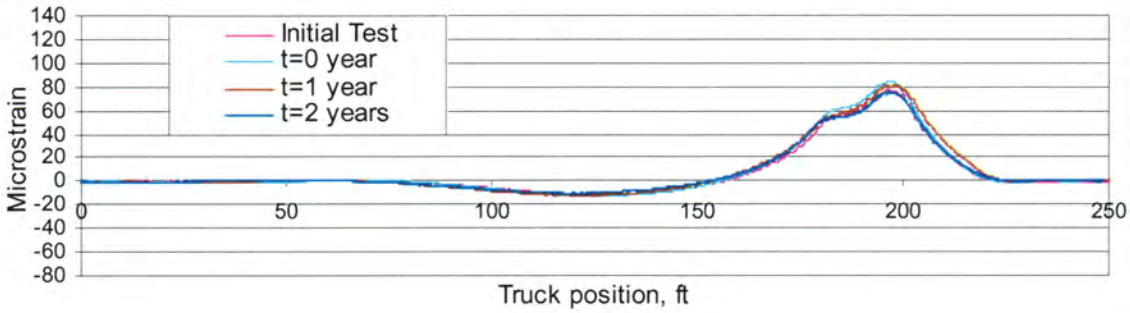

(b) Section B

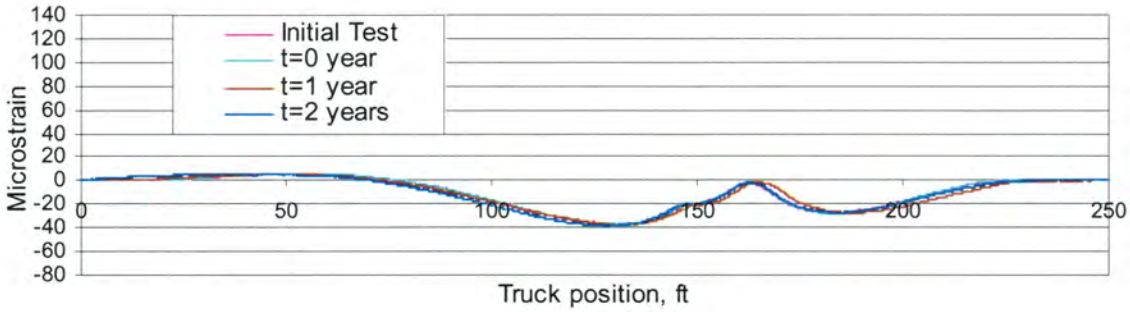

(c) Section C

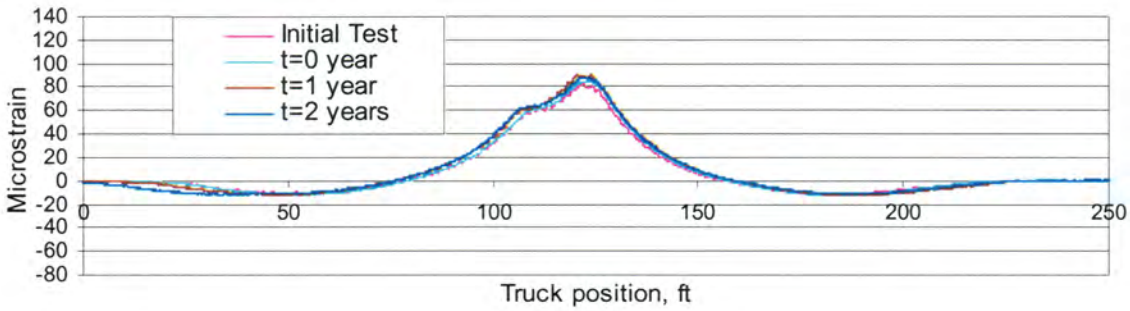

(d) Section D

Figure I-29. Before and after strengthening: strains in Beam 3 (Path Y3).

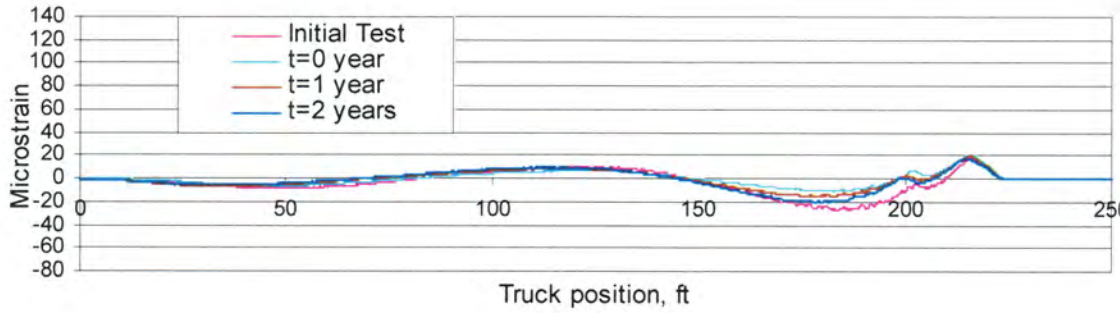

(a) Section A

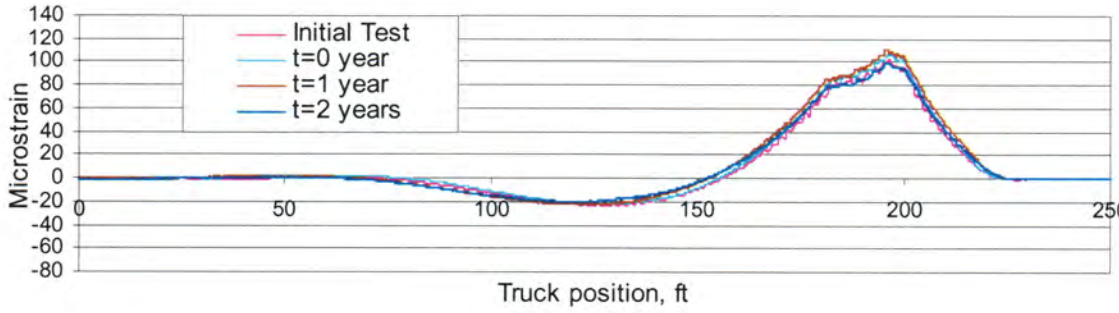

(b) Section B

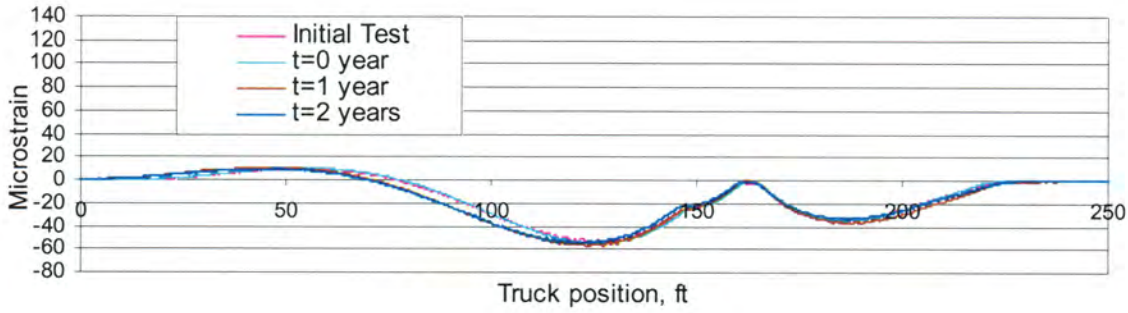

(c) Section C

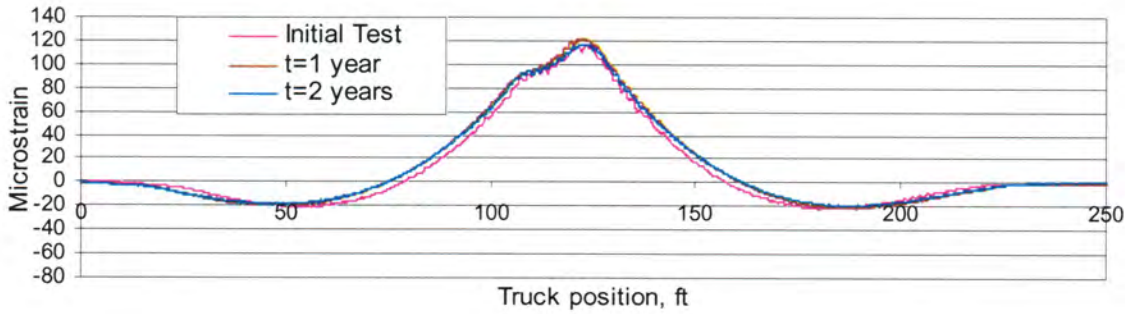

(d) Section D

Figure I-30. Before and after strengthening: strains in Beam 4 (Path Y4).

4.2.3. During Post-tensioning

As mentioned in Chapter 3, during the application of the P-T force, the bridge and the P-T strengthening system were monitored. The behavior of the bridge during the application of the P-T force will be presented in the following sections.

4.2.3.1. STRAIN INCRESE DURING POST-TENSIONING

Proper P-T in the positive moment region generates strain opposite in sign to those produced by dead and live loads. During the application of the P-T strengthening system, strain was measured to investigate the response of the bridge due to the applied P-T force. As expected, when the force was applied to a specific location, that specific beam would experience the greatest change in strain. For example, when the north exterior beam (Beam 1) in the west end span was post-tensioned (Events 17 through 32 in Fig. I-31), the strain due to the P-T force increased significantly compared to other locations where increases in strain were minimal. Likewise, significant increase in strain can be observed during P-T on Beam 1 in the center span (Events 49 through 64 in Fig. I-32). However, it should be noted that a non-trivial level of strain was measured at other locations as well.

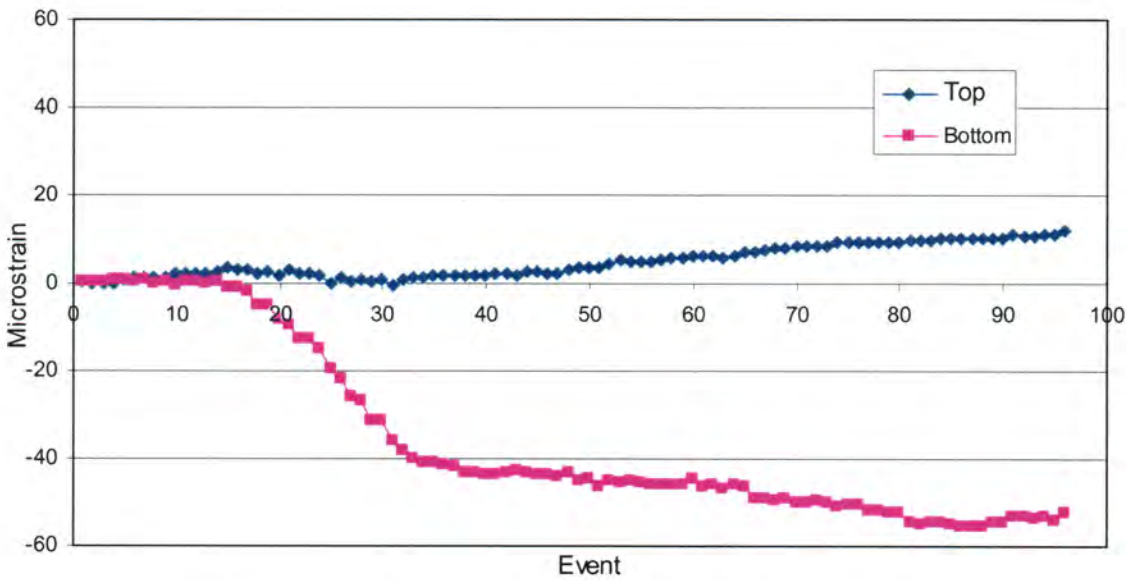

Figure I-31. Strains measured in west end span, Beam 1 during P-T.

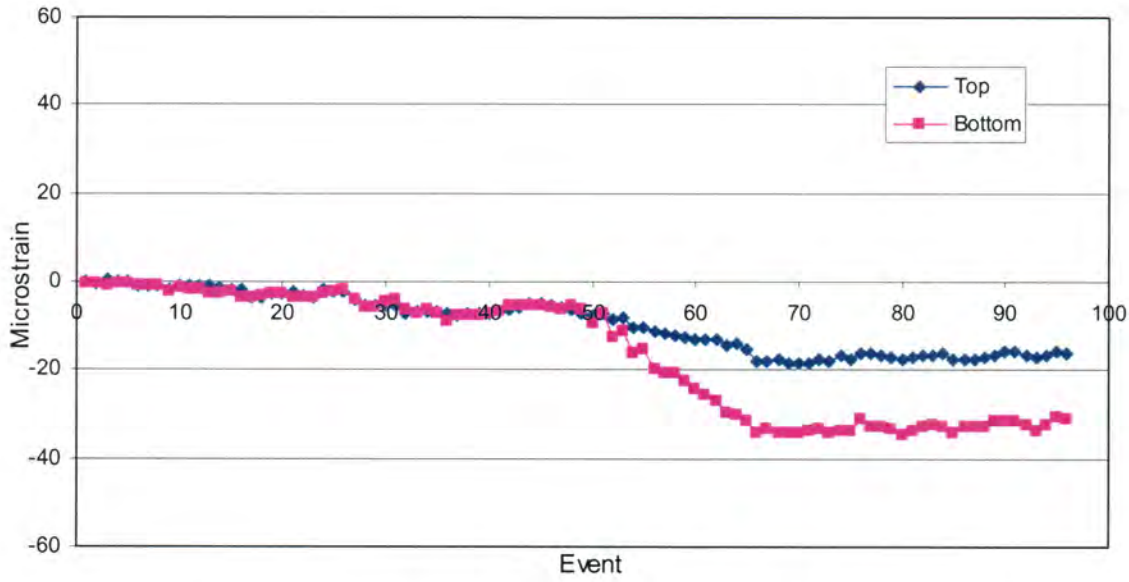

Figure I-32. Strains measured in center span, Beam 1 during P-T.

4.2.3.2. LATERAL DISTRIBUTION

As was mentioned in the previous section, notable amounts of P-T induced strain were recorded at locations away from the applied P-T force. This section investigates the lateral distribution of the P-T force on the bridge. Shown in Fig. I-33 is an overall distribution pattern of the bridge at each section with Beam 1 in each span being post-tensioned. From these figures, it is clear that the effects of the P-T system are distributed throughout the bridge. It is likely that the amount of P-T force distributed is highly dependent upon the deck and diaphragm stiffnesses.

The lateral load distribution can be expressed as a percentage of the P-T force remaining on each beam. Since the exterior beams and the interior beams have different material and section properties, the distribution factor of the individual beams during P-T Beam 1 in the west end span and the center span (referred to as "WSB1" and "CSB1", respectively, in Table I-6) were determined based on the expression presented below. Note that the modulus of elasticity (E) on the exterior and interior beam was assumed to be constant.

$$\%\ DF_i = \frac{\varepsilon_i S_i E_i}{\sum\left(E_i \varepsilon_i S_i\right)} * 100 = \frac{\varepsilon_i S_i}{\sum\left(\varepsilon_i S_i\right)} * 100 \qquad \text{(I-4.1)}$$

where

ε_i = bottom flange strain due to post-tensioning in i th beam.

S_i = section modulus of i th beam.

E_i = modulus of elasticity.

With the above equation, the lateral distribution was determined to be, on average, 58% on Beam 1, 27% on Beam 2, and 15% on Beam 3. It was also found that the application of P-T force on one exterior beam (e.g., Beam 1) has a negligible impact (nearly 0%) on the other side of the exterior beam (e.g., Beam 4). These lateral distributions of bottom strain on each beam are summarized in Table I-6.

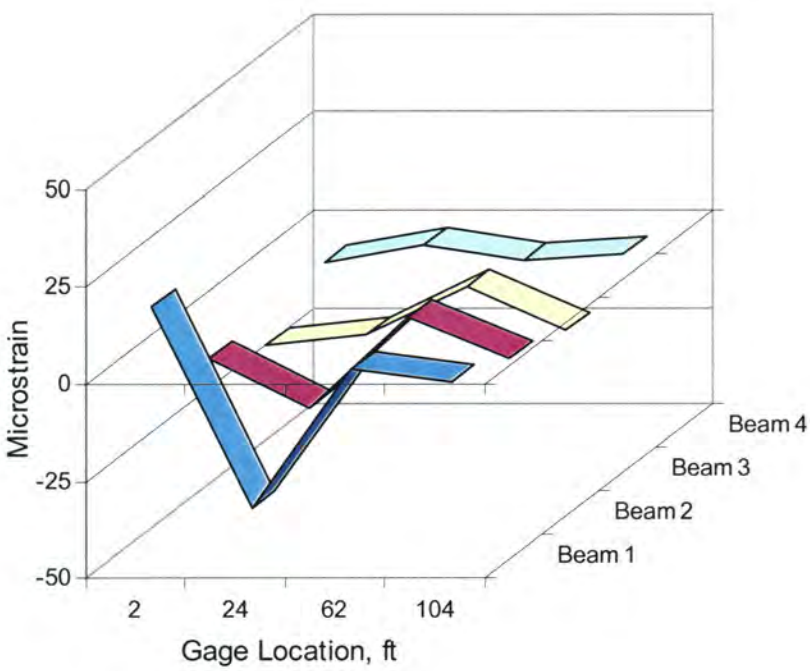

(a) P-T force applied to west end span Beam 1 (Events 17-32)

Figure I-33. Distribution of P-T strains.

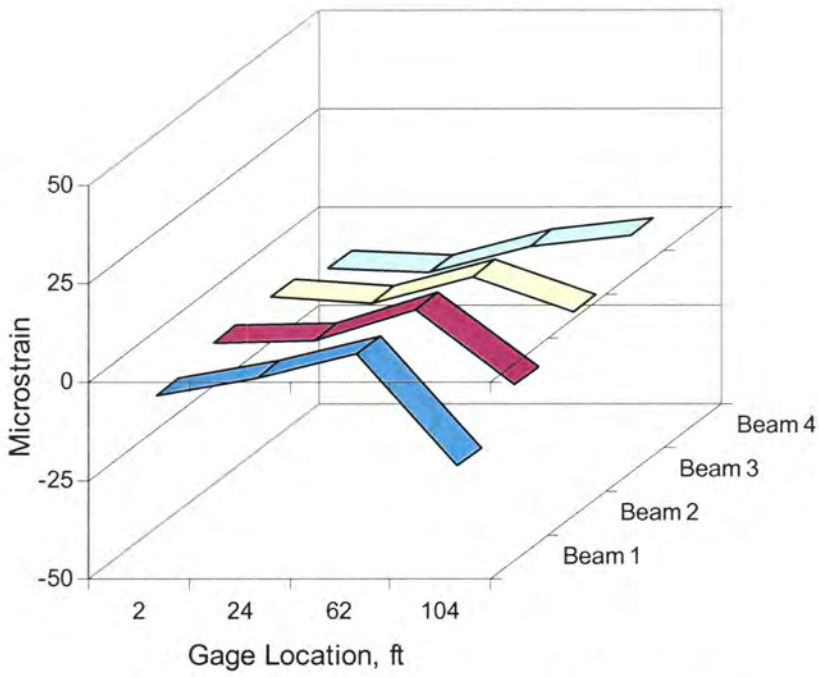

(b) P-T force applied to center span Beam 1 (Events 49-64)

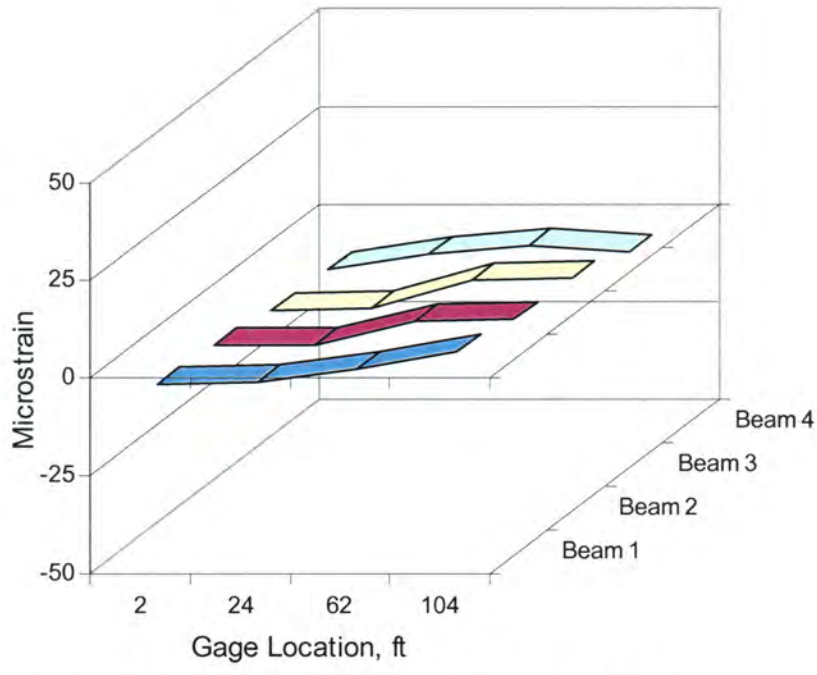

(c) P-T force applied to east end span Beam 1 (Events 81-96)

Figure I-33. Distribution of P-T strains - continued.

Table I-6. Lateral distribution of bottom strain during P-T on Beam 1.

	% of bottom strains			
	Beam 1	Beam 2	Beam 3	Beam 4
During P-T of WSB1	57	26	16	1
During P-T of CSB1	59	28	14	-1
Average	58	27	15	0

From the data presented in Table I-6 and assuming a fairly symmetric response, it was determined that 58% of the P-T force would act on each exterior girder and that 42% would act on each interior girder.

4.2.3.3. VERIFICATION OF P-T FORCE

In order to verify the level of force applied by the P-T strengthening system in the field, a calibration was performed, in the laboratory, on four of the CFRP bars that were to be installed on Beam 4 in the west end span. The strain data measured during the application of P-T force to each of these bars (Events 1 through 16) is shown in Fig. I-34 where each event defines a specific step of the P-T process, as previously described.

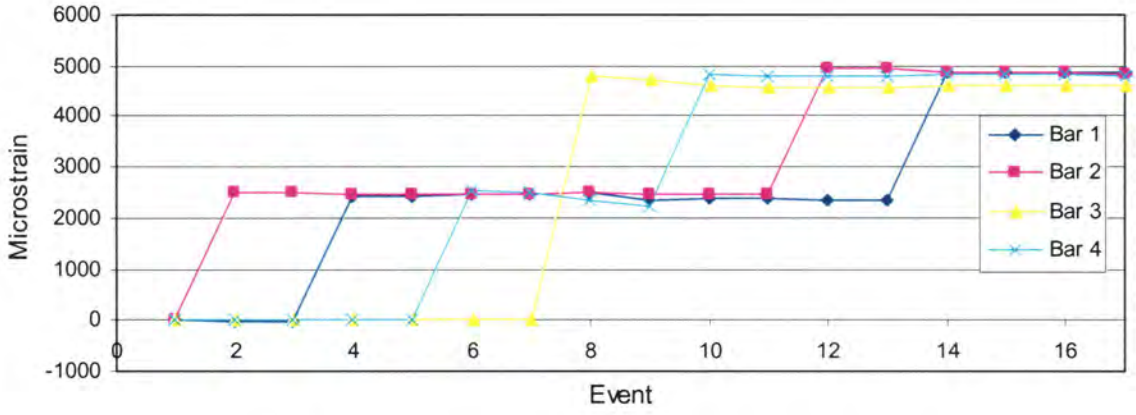

Figure I-34. Bar strains resulting from P-T west end span, Beam 4.

From these data and the laboratory calibration, the actual forces in each bar during P-T application could be determined. As summarized in Table I-7, all bars are slightly under-tensioned.

Bars 1 and 2 were under-tensioned by 10.8%, and Bars 3 and 4 were under-tensioned by 15.8% and 11.6%, respectively. Also, note that the force in each bar changed as force was applied to other bars. The final force in each bar after all four bars at this location had been tensioned was 10.7 kips (Bars 1 and 2), 10.1 kips (Bar 3), and 10.6 kips (Bar 4). By adding the force applied to each bar, it was determined that the total of 42.2 kips were actually applied on Beam 4 in the west end span.

Table I-7. Summary of P-T forces in bars on west end span Beam 4.

	Bar 1		Bar 2		Bar 3		Bar 4	
Event	(4)	(14)	(2)	(12)	(7)	(9)	(6)	(10)
Strain, με	2,445	4,855	2,460	4,850	0	4,590	2,510	4,815
Intended force, kips	6	12	6	12	6	12	6	12
Applied force, kips	5.4	10.7	5.4	10.7	0	10.1	5.5	10.6
% of under-tensioned		10.8		10.8		15.8		11.6

In the previous section, a general study of how P-T forces are laterally distributed was discussed. In an effort to account for longitudinal distribution, an analysis utilizing STAAD Pro. was conducted. Based on this analysis, it was found that approximately 10% of the P-T force applied on the exterior girder in the end span (P-T force being applied only to one location) is longitudinally distributed. Likewise, 27.5% of the P-T force on the exterior beam in the center span is longitudinally distributed to other spans (13.8% to each adjacent span). Having accounted for these longitudinal distributions, the "remaining P-T force" at each section could be determined; a product of 42.2 kips and percentage of the longitudinal distribution of the P-T force (38.0 kips at Section B and 30.6 kips at Section D). Following this, an attempt was made through mechanics principles to account for all of the P-T force. To accomplish this, a relatively simple mathematical model (see Fig. I-35) was developed to represent the beams during P-T application. From this model and the measured strain, discrete forces acting at each location were estimated. The sum of these discrete forces was then compared to the computed "remaining P-T force".

The mathematical model used is illustrated in Fig. I-35 where the application of an eccentric P-T force can be resolved into 42.2 kips of a concentric axial force and 100 ft-kips of applied moment (42.2 kips at an eccentricity, e, of 28.4 in.).

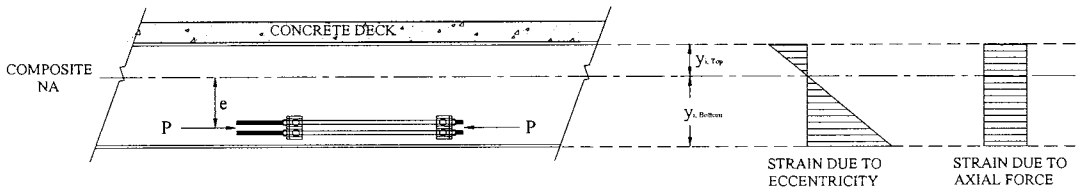

(a) Applied post-tensioning force and corresponding strain diagrams

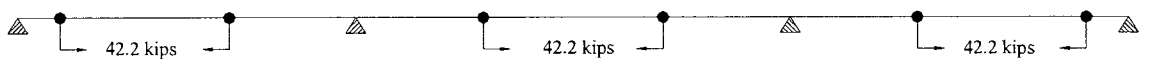

(b) Idealized beam with eccentric forces

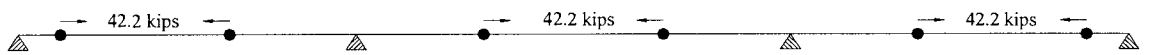

(c) Idealized beam with axial forces

(d) Idealized beam with moment forces

Figure I-35. Idealized beams with applied forces.

A total strain (ε_{Total}) can be expressed as a sum of strains due to an axial force and moment that is a product of the axial force and the eccentricity.

$$\varepsilon_{Total} = \pm \frac{Pey}{EI} \pm \frac{P}{AE} \qquad \text{(I-4.2)}$$

where

P = applied post-tensioning force.

e = eccentricity (distance between axial force and composite NA).

y = distance from composite NA to bottom flange gage.

E = modulus of elasticity of beam.

I = moment of inertia.

A = cross sectional area of composite beam.

This equation can be re-written and solved for the discrete force acting on each individual beam.

$$P_i = \frac{\varepsilon_i}{\frac{ey_i}{EI_i} \pm \frac{1}{EA_i}} \qquad \text{(I-4.3)}$$

where

P_i = P-T force acting on i^{th} beam.

ε_i = strain obtained from i^{th} beam.

y_i = distance from composite NA to bottom flange on i^{th} beam.

I_i = moment of inertia of i^{th} beam.

A_i = cross sectional area of i^{th} beam.

Now, the sum of the discrete force on each beam can be determined.

$$P_{Total} = \sum P_i \qquad \text{(I-4.4)}$$

Using the relationships presented above and the measured strain data, the discrete force acting on each beam was determined. Results at Section B and Section D are shown in Fig. I-36 and summarized in Table I-8.

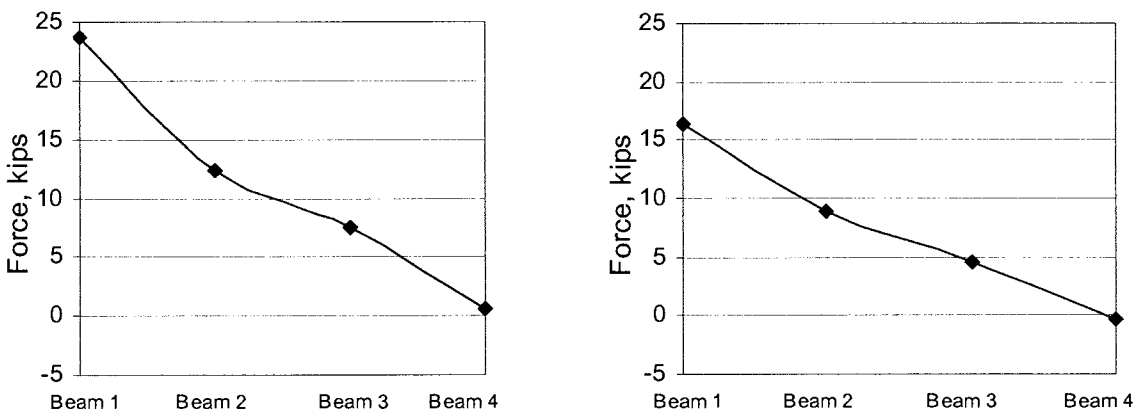

(a) P-T in west end span Beam 1 (WSB1)

(b) P-T in center span Beam 1 (CSB1)

Figure I-36. Discrete forces acting on each beam.

Table I-8. Summary of discrete forces acting on each beam.

	Discrete force acting on each beam (kips)					Sum of discrete force (kips)	Remaining P-T force (kips)	% Difference
	Beam 1 +	Beam 2 +	Beam 3 +	Beam 4	=			
Section B during P-T WSB1	23.6	12.4	7.5	0.6	=	42.8	38	11.2
Section D during P-T CSB1	16.5	8.9	4.6	-0.3	=	28.7	30.6	-6.6

With a higher percentage difference in the west end span, it was generally found that the sum of the discrete forces computed based on experimental strains were higher in the west end span and lower in the center span than the "remaining P-T force".

4.2.4. Effect of Post-tensioning

As stated previously, the goal of the P-T strengthening system is to create an effective way of introducing stresses in the bridge that counteract the stresses produced by dead and live loads. The impact of the P-T strengthening system on individual beams as well as the entire bridge will be discussed in following sections.

4.2.4.1. ANALYTICAL MODELING

A mathematical model was developed to better understand the impact of the P-T strengthening system by investigating the overall behavior of the bridge due to P-T force application. To accomplish this, a grillage model was developed to study the global behavior. Where possible, results from this model are compared with the field test results.

4.2.4.1.1. Grillage Modeling

A model was developed utilizing a commercially available structural analysis package. Due to the difficulty in quantifying end restraint, all supports were modeled as rotationally free. As was

used in the model shown in Fig. I-35, a concentric axial force and an applied couple was used in this analysis to simulate the eccentric P-T force acting on the bridge.

The flexural moment of inertia (I) and torsional constant (J), which are two important properties that are required to construct a grillage model, were calculated as follows [11]:

For all longitudinal members:

$$I_L = (I_{girder} + e_g^2 A_{girder})*n + I_{deck} \quad \text{(I-4.5)}$$

$$J_L = \sum J_{girder} + J_{deck} \quad \text{(I-4.6)}$$

For transverse members:

$$I_T = \frac{bt^3}{12} \quad \text{(I-4.7)}$$

$$J_T = \frac{bt^3}{6} \quad \text{(I-4.8)}$$

where

I = moment of inertia.

A = cross-sectional area.

e_g = eccentricity of the centroid of the girder from mid-height of the deck.

n = modular ratio.

J = torsoinal constant.

b = unit width of concrete deck.

t = concrete deck thickness.

To facilitate the analysis, several assumptions were made:

- The steel and concrete deck are perfectly connected by means of shear connector; thus, the beams behave compositely, acting as a homogeneous section. Computations are based on full interaction without slip between concrete deck and steel beam.
- Section properties of the analytical model are constant along the beam.
- Difference in elastic properties between the concrete deck and steel beam can be properly adjusted through the use of an elastic modular ratio based on AASHTO Standard Specification [10].

- Stiffness contribution of CFRP bars to the composite beam is negligible and thus not included.
- Partial end restraints at the abutment were neglected.

4.2.4.1.2. Illustration of Post-tensioning Effect

The construction sequence for the application of P-T forces was documented in Section 2.2.2. In order to better understand how the bridge behaves during the application of the P-T strengthening system, the same application sequence was applied in the grillage model. The resulting internal moment diagrams are shown in Fig. I-37.

From this analysis, it appears that the P-T strengthening system impacts both the positive and negative moment regions by producing moments opposite in sign to those induced by dead and live loads. Note that for the exterior beams, the larger moment was generated at the anchorage locations rather than at midspan region (i.e., maximum positive moment region). A different pattern, however, was observed on the interior beams; the effect of the P-T strengthening system is the highest near the maximum positive moment location. The grillage analysis also verified that significant P-T forces could be distributed to adjacent beam. It was also observed that larger moments were generated in the end spans than the center span.

4.2.4.1.3. Comparison of Lateral Distribution During Post-tensioning

The theoretical bottom flange strain distribution at Sections B and D during the P-T process was determined from the grillage analysis. These analytical results were then compared with the experimentally determined lateral load distribution characteristics previously presented.

From the grillage analysis, it was found that, on average, when Beam 1 was post-tensioned, 52% of the total strain occurred in Beam 1 while 31%, 17%, and 0% of the total occurred in Beam 2, Beam 3, and Beam 4, respectively. From the field measurements, these same percentages were 58%, 27%, 15%, and 0%. A comparison between the field and analytical prediction is shown in Figs. I-38 and 39. Both the analysis and the field test results showed that applying P-T force on one of the exterior beams has negligible effect on the other exterior beam. In general, both results produced a good agreement; however, it was generally found that the experimental strains were higher than the theoretical strains.

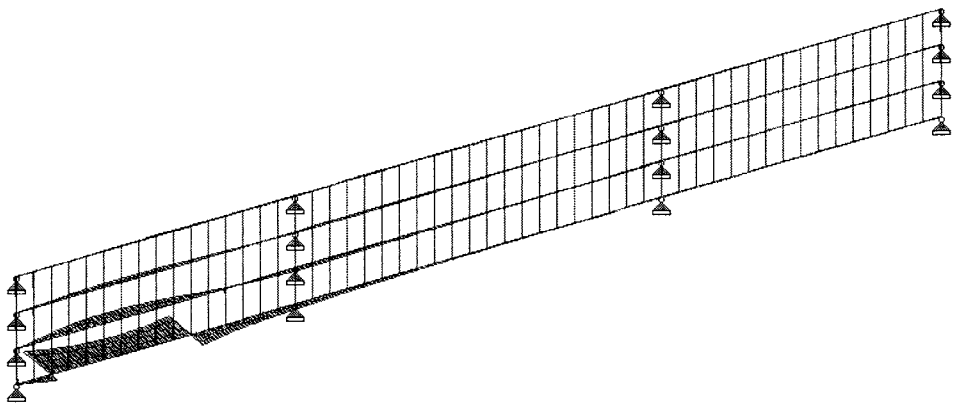

(a) Post-tensioning west end span Beam 4

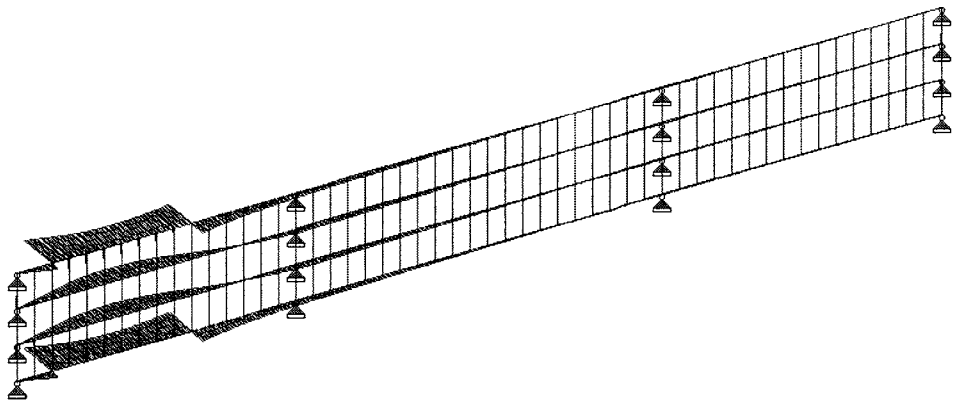

(b) Post-tensioning west end span Beam 1

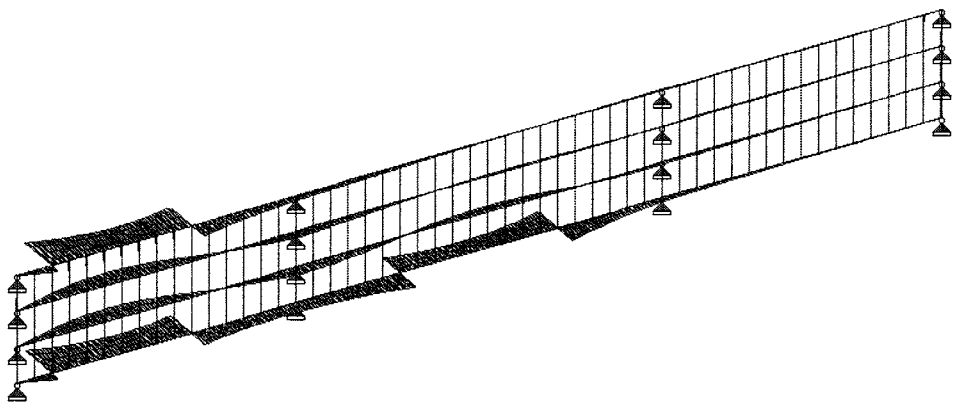

(c) Post-tensioning center span Beam 4

Figure I-37. Theoretical P-T induced internal moments.

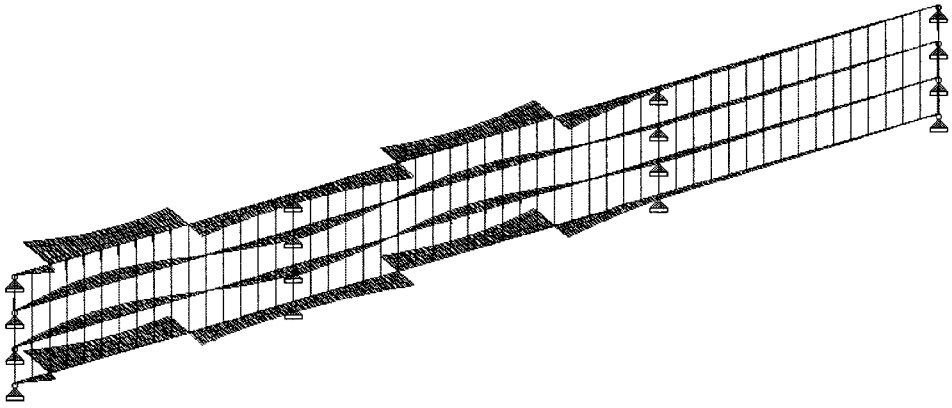

(d) Post-tensioning center span Beam 1

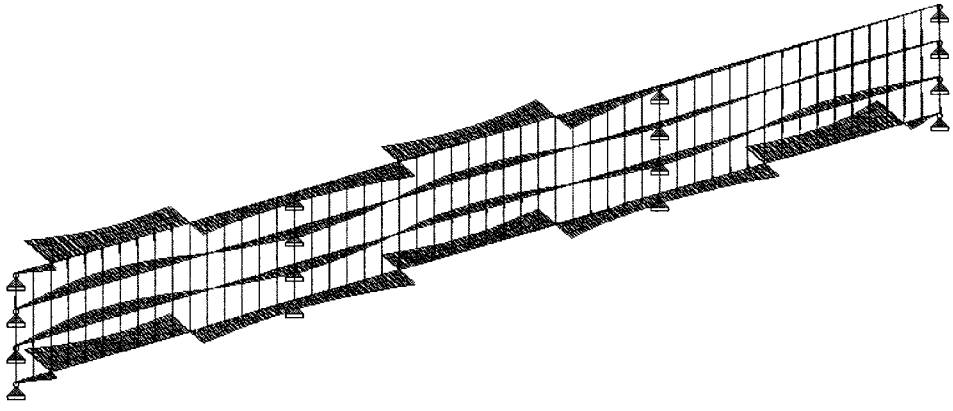

(e) Post-tensioning east end span Beam 4

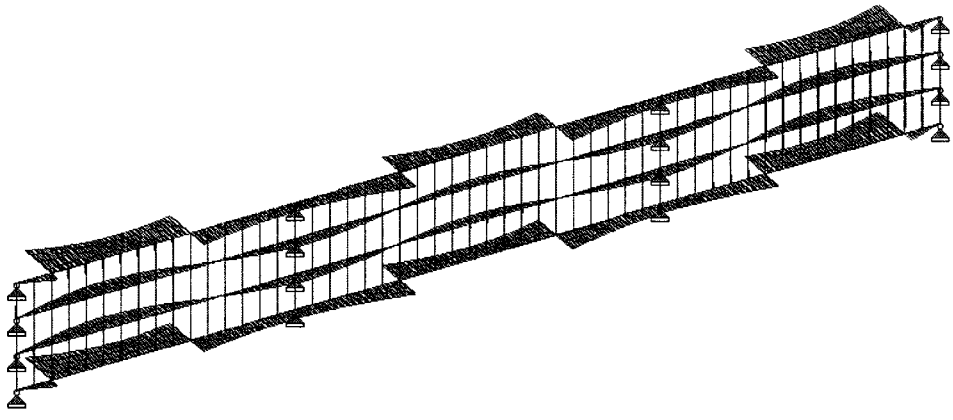

(f) Post-tensioning east end span Beam 1

Figure I-37. Theoretical P-T induced internal moments - continued.

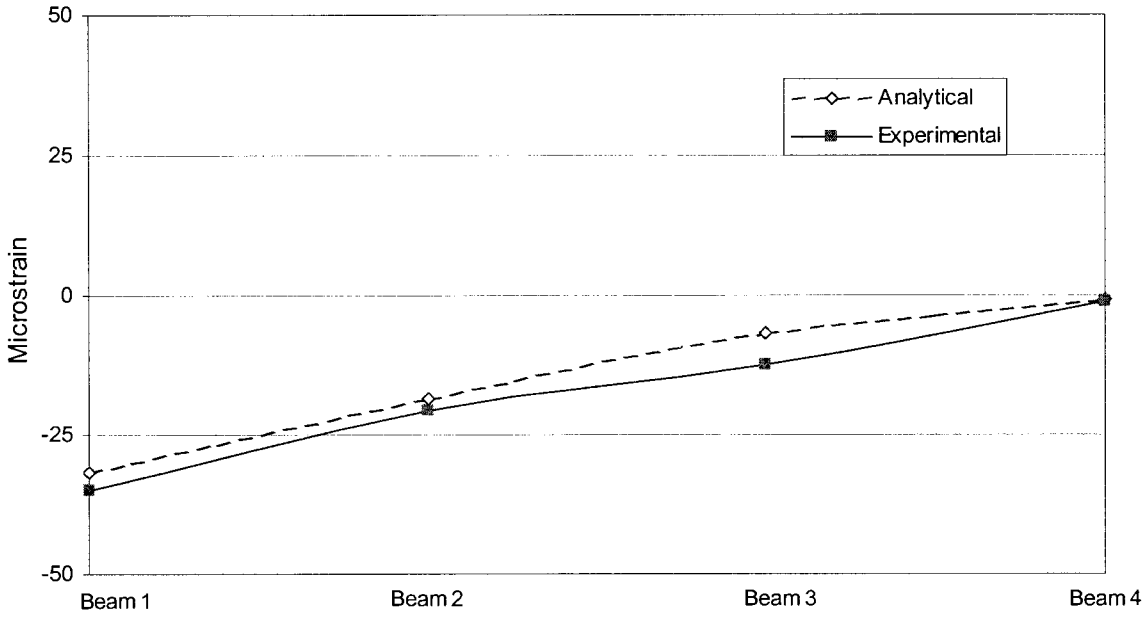

Figure I-38. Strains at Section B during P-T west end span Beam 1.

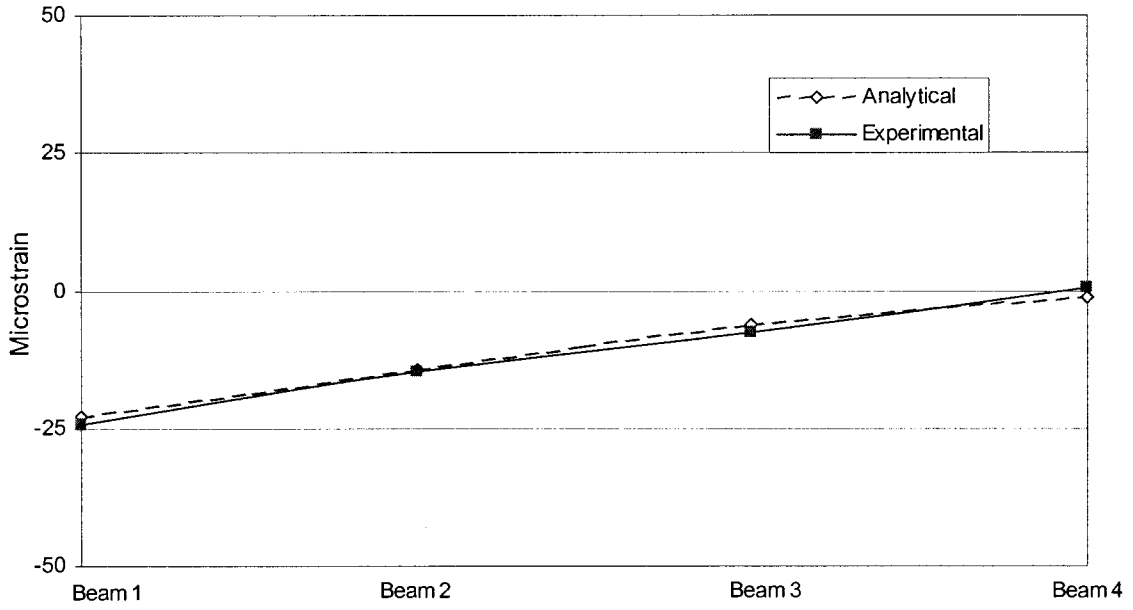

Figure I-39. Strains at Section D during P-T center span Beam 1.

4.2.4.2. INDIVIDUAL BEAM ANALYSIS

To illustrate how the P-T strengthening system improves the live load carrying capacity of the subject bridge, an analysis was performed on both an exterior and interior gider. The moment induced by the P-T force, dead load, and live load at each location of the bridge will be presented first and then combined to illustrate the overall impact of the P-T strengthening system. For this analysis, the live load moment was determined utilizing an HS-20 truck [10] placed so that the maximum positive moment could be generated. Note that the moment diagrams presented in this section are not to scale. Also, from the grillage analysis, the strain induced by the concentric axial force was found to be negligible (i.e., in the range of approximately 0 to 3 microstrain); therefore, a reduction of bottom flange stress due to this axial force component was not included in this analysis.

As was described previously, the lateral distribution factors at the maximum positive moment region were found to be, on average, 58% for the exterior and 42% for the interior beam. Given these distribution factors, the P-T induced moments for the exterior and interior beam at each midspan gage location (Sections B and D) were determined.

Figures. I-40 and 41 show the interior and exterior beam moments induced by the dead load and P-T force, respectively. As can be seen, the P-T force generates moments opposite in sign to those induced by the dead load at both the maximum positive moment region (midspan) and maximum negative moment region (pier). Figures. I-42 presents a moment diagram with these effects combined. From these, it can be seen that the P-T strengthening system has a positive impact on the maximum positive moment region; a portion of dead load moment are reduced by the P-T induced moment at the maximum positive moment regions in both end spans (11.5% for the exterior and the 10.3% for interior beam) and in the center span (6.9% for the exterior and 6.0% for the interior beam).

Three point loads were used to represent the HS-20 truck [10]. These individual point loads were placed so that maximum moments could be generated at the maximum positive moment region in each span. The lateral distribution factors for the exterior and the interior girder determined based upon AASHTO standard specification [10] were applied to the live load induced moment. The experimental lateral distribution factors obtained during the application of the P-T force were used in computing the P-T induced moment. An illustration of the HS-20 truck positioned in each span and corresponding live load moment diagrams are shown in Figs. I-43 and 44.

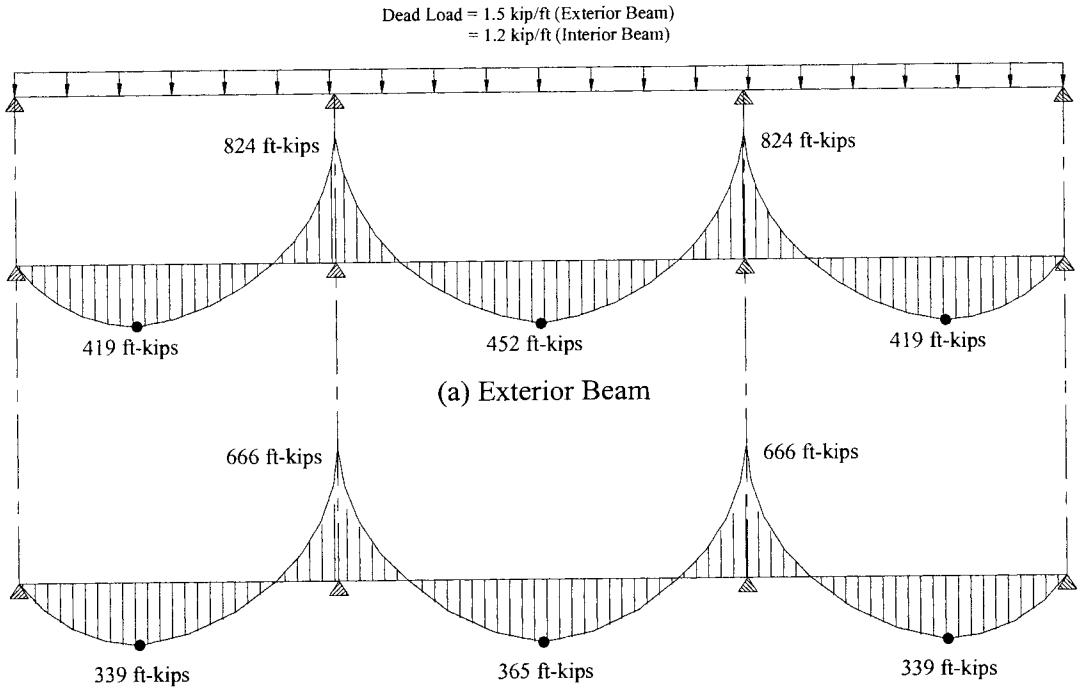

Figure I-40. Dead load induced moments.

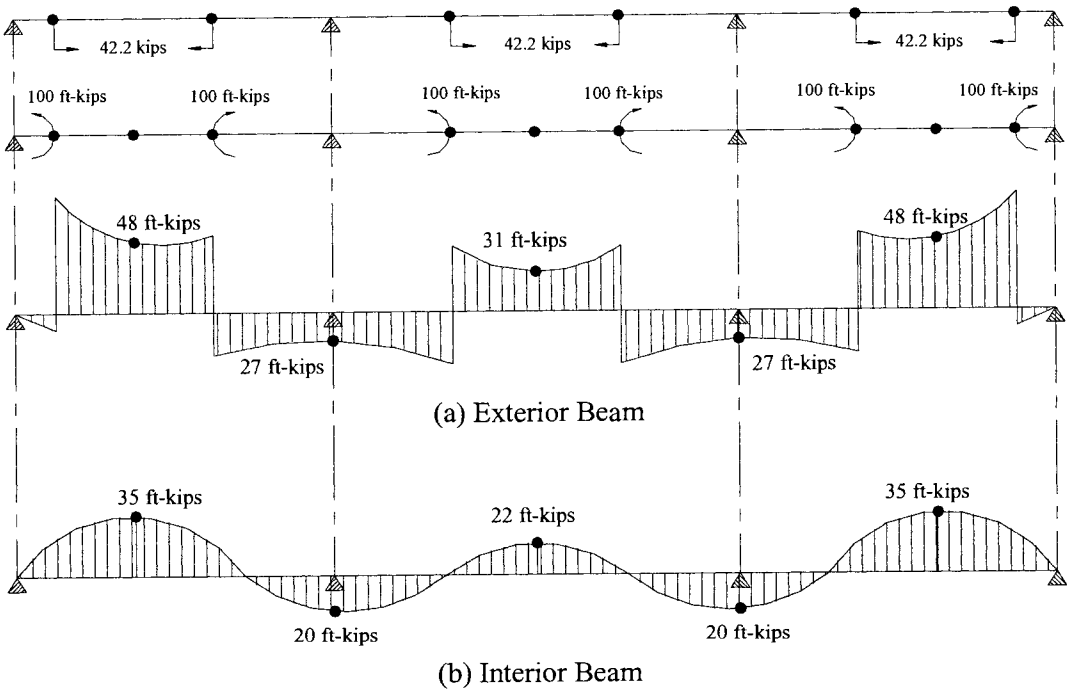

Figure I-41. P-T induced moments.

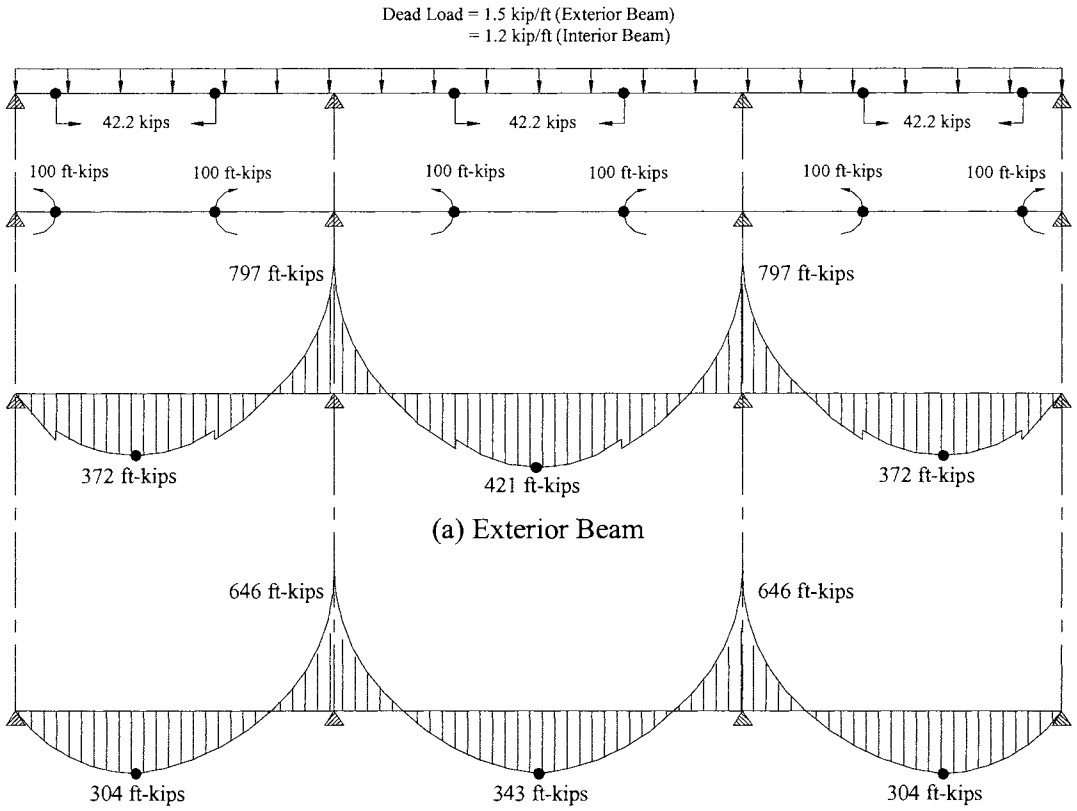

Figure I-42. Dead load plus P-T induced moments.

Given the P-T induced moment ($M_{P\text{-}T}$), dead load moment (M_{DL}) and live load moment (M_{LL}), it is now possible to investigate an overall effect of the P-T strengthening system on the bridge by adding all the moments as if the resulting moment is generated by each individual force acting simultaneously as is illustrated in Figs. I-45 and 46.

As expected, the exterior girder showed a larger reduction in total moment than the interior girder in both the end and the center spans. In general, the end span showed larger moment reductions than the center span. The P-T strengthening system reduced the total moment by 5.3% on the exterior beam and 4.6% on the interior beam in the end span. Similarly, 3.3% and 2.7% of the total moment were reduced on the exterior and the interior beam in the center span, respectively.

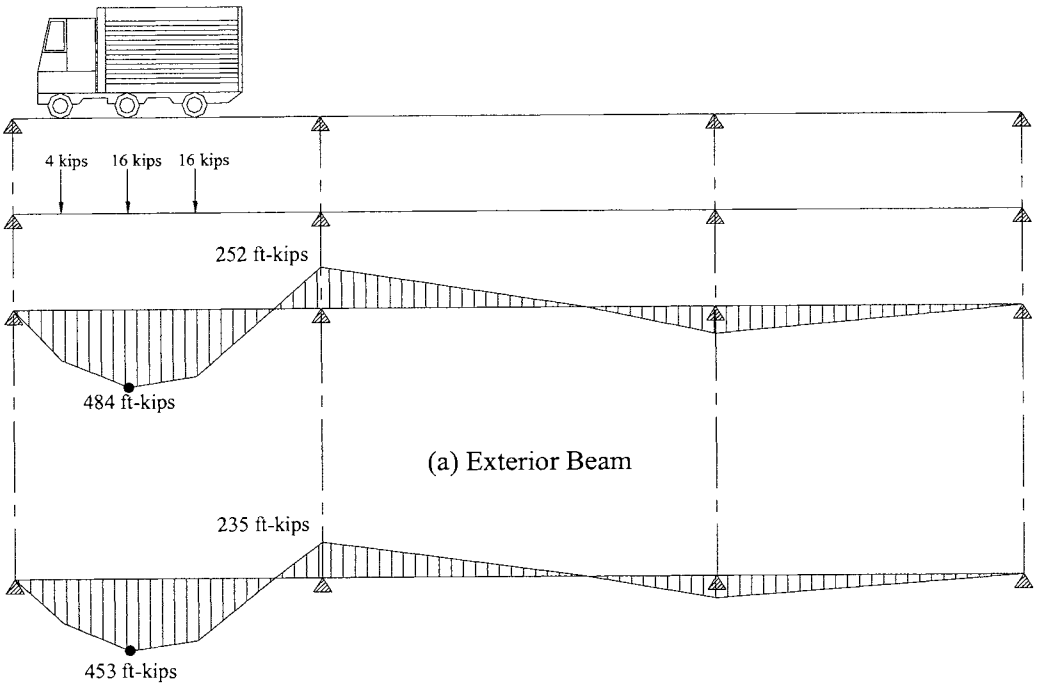

(b) Interior Beam

Figure I-43. Live load moments in the west end span.

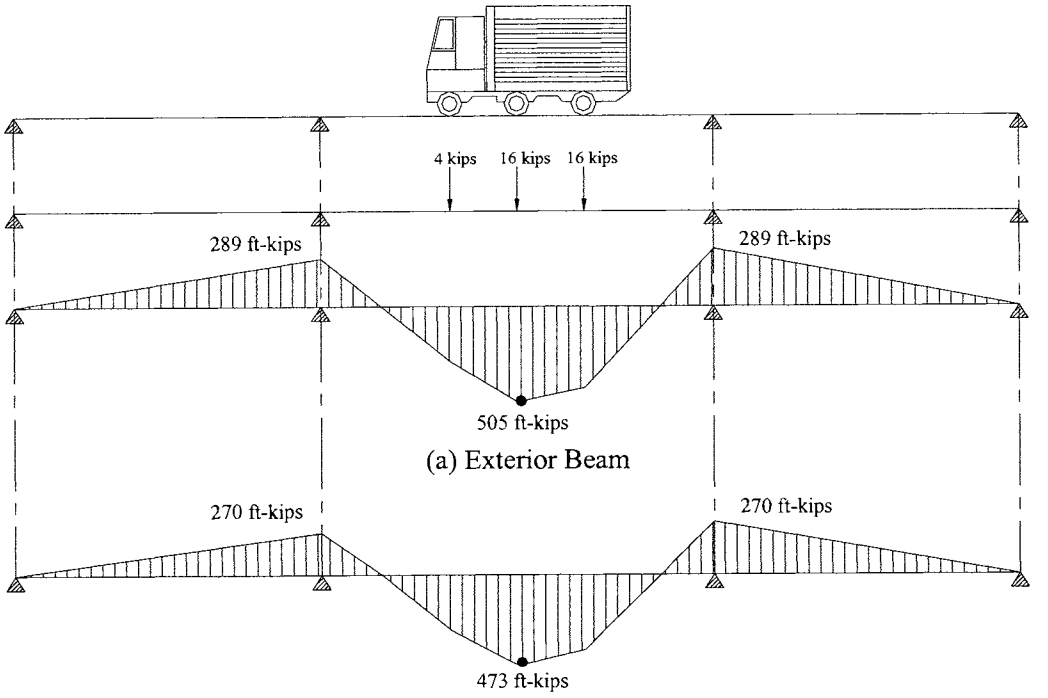

(b) Interior Beam

Figure I-44. Live load moments in the center span.

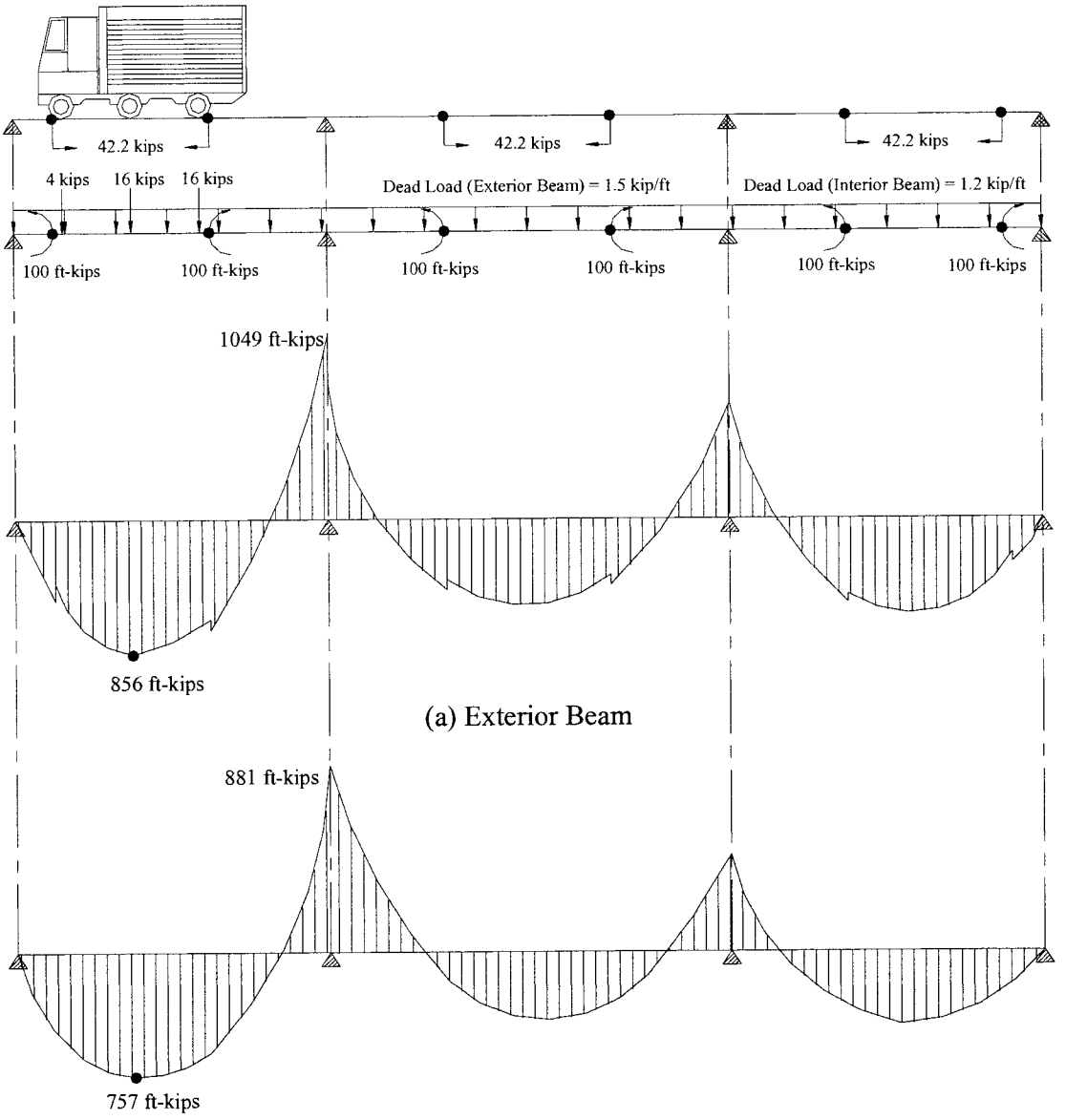

Figure I-45. Effect of P-T on maximum moments in the west end span.

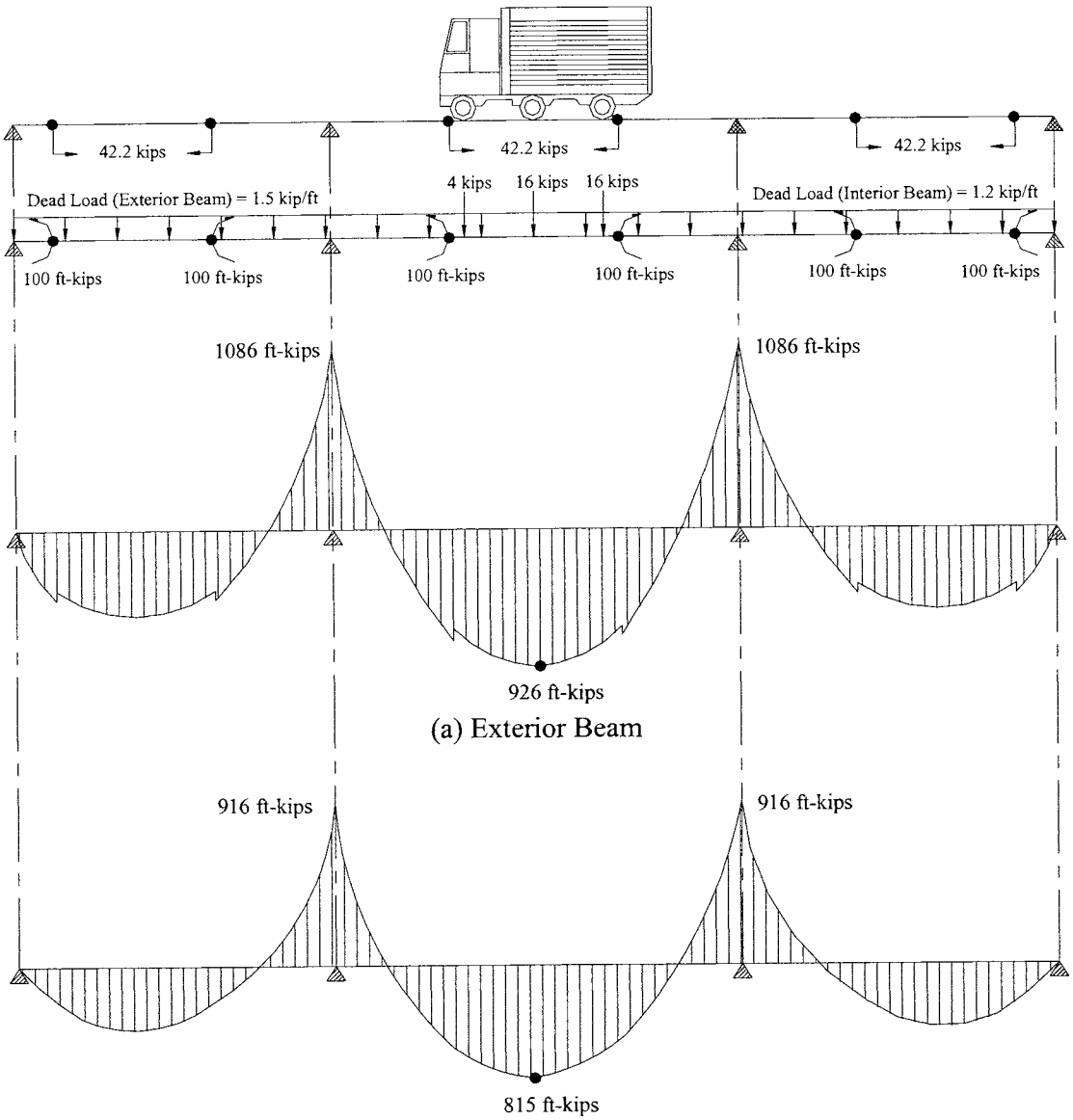

Figure I-46. Effect of P-T on maximum moments in the center span.

Overall, the reduction of these moments indicates the P-T strengthening system was effective in decreasing the total moment by approximately 3 to 5% depending upon the locations, and thereby improving the live load carrying capacity of the bridge at the maximum positive moment region. The reduction in total moment by the P-T strengthening system is summarized in Table I-9.

Table I-9. Reduction in total moment by the P-T strengthening system.

	Section B		Section D	
	Exterior	Interior	Exterior	Interior
$M_{DL} + M_{LL}$ (ft-kips)	904	792	957	838
$M_{P-T} + M_{DL} + M_{LL}$ (ft-kips)	856	757	926	815
Reduction in moment, %	5.3	4.6	3.3	2.7

4.2.5. Change in Post-tensioning Force over Time

As was previously mentioned in Chapter 3, the P-T force was removed from the bridge after two years of service so that any losses could be determined. Recall that the order used to remove the force was shown in Fig. I-21. The P-T force removed from each bar was obtained as shown in Fig. I-47. In comparison with the forces that were originally applied, it was found that the largest loss occurred on Beam 1 in the center span with the magnitude of 3.7 kips (7.8% loss) while the average loss was 2.6 kips (5.4% loss). Although some loss of P-T force occurred in most bars, it should be noted that these time-associated losses were accounted for during the designing phase (see section 2.2.1).

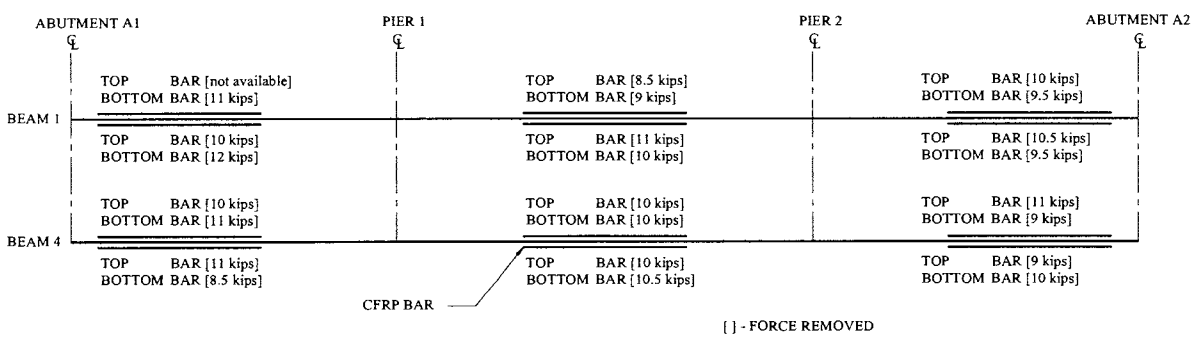

Figure I-47. P-T forces removed from each bar.

5. SUMMARY AND CONCLUSIONS

5.1. SUMMARY

The two primary objectives of this project were to investigate the effectiveness of CFRP composite materials to strengthen existing, structurally deficient steel girder bridge and to identify changes in structural behavior due to addition of strengthening system and time. The bridge selected for strengthening with the CFRP P-T bars was a three-span continuous steel stringer bridge in Guthrie County, Iowa on State Highway IA 141 approximately 1.6 miles west of Bayard, Iowa. The research program consisted of several tasks with the main emphasis being the installation of the strengthening system and associated field testing. Before the P-T system was installed, a diagnostic load test was conducted on the subject bridge to establish a baseline behavior of the unstrengthened bridge. During the process of installing the P-T hardware and stressing the system, both the bridge and the P-T system were monitored. The installation of the hardware was followed by a follow-up diagnostic load test to assess the immediate effectiveness of the P-T strengthening system. Additional load tests were performed over a two-year period to identify any changes in the strengthening system with time. After the last follow-up test (two years of service) was completed, the P-T force was removed from the bridge (and re-applied) to investigate any losses that may have occurred over the two-year period. Laboratory testing of several typical CFRP bar specimens was also conducted to more thoroughly understand their behavior.

5.2. CONCLUSIONS

5.2.1. Laboratory Test

CFRP bars were tested in the laboratory to better understand their characteristics and to assess the feasibility of the CFRP bars as a strengthening material. The following conclusions were generated based upon the test results:

- From visual observation and experimental results from the laboratory 24-hour, constant load test, the slippage between the bar and grip connection was very small (0.0011 in.). Therefore, no conclusions can be drawn from the laboratory test as to the cause of the slip observed in the field.
- During the ultimate strength test, each specimen experienced several localized fiber failures before the specimen failed, and significant strength decrease occurred. However, the tensile strength of all tested specimens exceeded the nominal force (12 kips) applied in the field.

5.2.2. Installation of CFRP Post-tensioning System

- The installation of the P-T system required no special equipment or training other than access equipment, an acetylene torch to remove a portion of several diaphragms, and a hydraulic jack for the application of the P-T force to the CFRP bars. A three-man crew was able to install the system in just over one day.

5.2.3. Field Test

Based upon the monitoring and testing conducted in the field, several conclusions were drawn and summarized as follows:

- The addition of the P-T strengthening system had a negligible impact on changing the stiffness of the bridge. This indicates that the live load distribution characteristics are virtually the same before and after the installation of the P-T strengthening system.
- The P-T system generates strain opposite to those produced by dead and live loads and thereby improves the overall live load carrying capacity of the bridge.
- Based upon an analysis performed utilizing the HS-20 truck, it was found that the P-T strengthening system reduced dead and live load induced moments by approximately 3 to 5%, thus allowing the bridge to carry additional live load.
- An average loss of 2.6 kips of P-T force (per location) occurred over two years of service; therefore, long-term monitoring on the P-T strengthening system maybe needed for further assessment.
- The use of the P-T CFRP bars to strengthen the structurally deficient bridge described in this project was proved to be a viable, effective and practical solution. However, the same CFRP P-T bar used in this project may not be applicable where greater overstresses need to be overcome. In that case, a larger bar with appropriate capacity may be needed.

Overall, this project was completed successfully. The use of CFRP P-T bars in this project provided an opportunity for the Iowa DOT to investigate and demonstrate its effectiveness and feasibility as an innovative, cost-effective bridge strengthening technique.

6. REFERENCES

1. Klaiber, F.W., K.F. Dunker, and W.W. Sanders, Jr., "Feasibility Study of Strengthening Existing Single Span Steel Beam Concrete Deck Bridges." Department of Civil Engineering, Iowa State University, Ames, IA, Iowa DOT Project HR-214, 1981.

2. Dunker, K.F., D.J. Dedic, and Sanders W.W. Sanders, Jr., "Strengthening of Existing Single-Span Steel-Beam and Concrete Deck Bridges." Final Report Part I. Engineering Research Institute, Iowa State University, Ames, IA, 1983.

3. Dunker, K.F., F.W. Klaiber, B.L. Beck and W.W. Sanders, Jr., "Strengthening of Existing Single-Span Steel-Beam and Concrete Deck Bridges." Final Report Part II. Engineering Research Institute, Iowa State University, Ames, IA, Iowa DOT Project HR-238, 1985.

4. Dunker, K.F., F.W. Klaiber, and W.W. Sanders, Jr., "Design Manual for Strengthening of Continuous Span Composite Bridges." Final Report Part III. Engineering Research Institute, Iowa State University, Ames, IA, Iowa DOT Project HR-238, 1985.

5. Dunker, K.F., F.W. Klaiber, F.K. Daoud, W.E. Wiley and W.W. Sanders, Jr., "Strengthening of Existing Continuous Composite Bridges." Engineering Research Institute, Iowa State University, Ames, IA, Iowa DOT Project HR-287, 1987.

6. Klaiber, F.W., F.S. Fanous, T.J. Wipf and H. El-Arabaty, "Design Manual for Strengthening of Continuous Span Composite Bridges." Engineering Research Institute, Iowa State University, Ames, IA, Iowa DOT Project HR-333, 1993.

7. Jones R.F., "Guide to Short Fiber Reinforced Plastics." Chernow Editorial Services, New York, NY, 1998.

8. Burgoyne J.C., "Advanced Composites in Civil Engineering in Europe." University of Cambridge, Cambridge, UK, 1999.

9. Tang, B. and W Podolny, "A Successful Beginning for Fiber Reinforced Polymer (FRP) Composite Materials in Bridge Applications." *FHWA Proceedings*, Orlando, FL, December 1998.

10. American Association of State Highway Officials. *Standard Specifications for Highway Bridges*, 16th Edition, Washington, D.C., 1996.

11. Baker, R.M. and J.A Pucket, "Design of Highway Bridges." John Wilely & Sons, New York, NY, pp. 290-291, 1997.

PART II. EVALUATION OF A STEEL GIRDER BRIDGE STRENGTHENED USING FRP PLATES

1. INTRODUCTION

1.1. BACKGROUND

Recent studies have indicated that approximately three trillion dollars are needed for the rehabilitation/retrofitting of the nation's infrastructure. To this end, nearly half of the nation's highway bridges have become structurally deficient or functionally obsolete. Basically, bridges need to carry loads greater than what they were designed for and at the same time have deteriorated at a rate faster than they could be repaired. Although replacement would be the best solution, a large number of these bridges are not critical enough to warrant replacement. In addition, the number of bridges that can be replaced is limited by financial considerations. Therefore, a structurally efficient but cost effective means of strengthening is needed.

High performance materials such as carbon fiber reinforced polymers (CFRP) have the potential of becoming a cost effective strengthening solution. The use of CFRP materials is very appealing in that they are highly resistant to corrosion, have a low weight, and have a high tensile strength. In the last decade, the use of these types of materials has emerged as a promising technology in structural engineering [1]. With this knowledge, a project, funded through the Federal Highway Administration's Innovative Bridge Research and Construction (IBRC) Program, was initiated to investigate the effectiveness of using CFRP composite materials to strengthen an existing steel girder bridge by installing CFRP plates to the overstressed regions. CFRP plates were chosen due to their outstanding mechanical characteristics, non-corrosive properties and ease of installation. This report documents the design, construction, and evaluation of a CFRP strengthening system.

1.2. LITERATURE REVIEW

Although the use of CFRP plates in concrete (reinforced and prestressed) bridge repair is becoming common practice in the U.S., its use on steel bridges is still limited. The following paragraphs summarize research involving the use of CFRP plates or laminates on steel beams.

Previous research by Al-Saidi [2] at Iowa State University has established the effectiveness of CFRP plates for improving the strength of composite steel beam. The study investigated the behavior of steel-concrete composite beams strengthened with CFRP plates attached to their tension side. To predict the behavior and deformation of a strengthened/repaired composite section, an analytical procedure was developed assuming nonlinear constitutive relationships for both the concrete slab and

steel beam, and a linear relationship for the CFRP plates. Given the computationally intensive nature, a computer program using FROTRAN 77 code was developed to perform the analysis. For the experimental part of the study, a total of ten beams were tested under four-point bending. Six of the beams were in an undamaged condition: two beams were control beams and four were strengthened (without damage) with CFRP plates. The remaining four beams were artificially damaged by reducing the bottom flange area and then repaired (one control beam and three repaired). Different widths and two types (different modulus of elasticity- 29,000 ksi and 22,000 ksi) of CFRP plates were used depending on the strengthening scheme. The test results indicated a significant increase in the strength of the strengthened/repaired beams. It was found that the beam strengthened with CFRP plate with a modulus of elasticity of 22,000 ksi had a more ductile behavior than the beam strengthened with CFRP plate with a modulus of elasticity of 29,000 ksi.

A study was conducted by Mertz and Gillespie [3] to evaluate the feasibility of using advanced composite materials in rehabilitating deteriorated members of steel highway bridges. The study focused on the case of a single span girder where the bottom flange is subjected to tensile stresses. The retrofit was installed on a corroded steel member utilizing adhesive bonding. In the initial phase of this project, modeling, fabricating, and testing of two repair schemes were performed. After service-load testing on the repaired members, the authors found that the composite plates increased the section stiffness moderately. Several rehabilitation schemes were then developed and tested on a variety of field geometries. Analysis and test results determined that an increase in flexural stiffness of 20 to 30% was attainable. It was also found that accelerated bonding through induction heating was a viable field installation technique. Additional service-load testing of fabricated scale beams and large-scale testing of both intact and corroded steel beams were completed in the later phase of the project. The results indicated that composite materials improved the strength and fatigue life of steel components.

The report by Tavakkolizadeh et al [4] presents the results on the behavior of steel-concrete composite girders retrofitted with CFRP sheets (a width of 76 mm and thickness of 1.27 mm per sheet) under static loading. Three large-scale composite girders consisting of a W355x13.6 A36 steel beam and a 75 mm thick by 910 mm concrete slab were tested. A differing number of layers (1, 3, and 5 layers) with constant thickness were used on the specimens. The test results showed that the strengthening system significantly increased the ultimate load-carrying capacities of the girders. It was also found that the efficiency for utilizing the CFRP sheet was reduced when more CFRP layers

were used. For the one-layer system, stress in the CFRP laminates was 75% of its ultimate strength while it decreased to 42% of the ultimate strength for the five-layer system.

A study by Miller [5] addressed the issues of force transfer, development length, and long-term durability of the CFRP/steel bond. First, force transfer and development were studied through the use of small-scale specimen testing and analytical solutions. From this test, it was found that 98% or more of the force transfer between the steel and CFRP plates occurred within 4 inches. It was also found that the force transfer length and force were sensitive to changes in bond-line thickness and CFRP material properties. Seven months of monitoring for the long-term durability of the CFRP/steel bond under sustained loads indicated no signs of significant creep or debonding. The developed rehabilitation scheme was performed on an existing steel bridge girder. Initial and follow-up load tests indicated a reduction in tension flange strains of 11%.

1.3. OBJECTIVES

The primary objective of this project was to investigate and evaluate the effectiveness of CFRP plates to strengthen an existing, structurally deficient steel girder bridge. This objective was met by:

- Documenting the design, construction, and performance of the innovative material used.
- Identifying changes in structural behavior due to the addition of the CFRP plates and with time through field inspection and load testing.

1.4. SCOPE

The research program consisted of several tasks with the primary emphasis on the design process, installation of the strengthening system, and field testing. A detailed description of the subject bridge and the strengthening system employed is given in Chapter 2. The field tests are described in Chapter 3, and the corresponding test results are summarized in Chapter 4. General study conclusions and recommendations are presented in Chapter 5 and Chapter 6, respectively.

2. BRIDGE AND STRENGTHENING SYSTEM DESCRIPTION

This chapter describes the physical characteristics of the bridge strengthened as part of this investigation. Also, a description of the strengthening system including its design and installation is given.

2.1. BRIDGE DESCRIPTION

The bridge (Number 7838.5S092) selected for strengthening is a 150 ft x 30 ft three-span continuous I-beam bridge shown in Fig. II-1. The bridge is located in southwest Iowa in Pottawattamie County carrying State Highway IA 92 over Walnut Creek. The bridge has two 45 ft - 6 in. end spans and a 59-ft center span. The original non-composite bridge was built in 1938 and was widened on both sides in 1967 by the addition of exterior girders that were constructed composite with the deck. The original bridge deck is a nominal 6.5-in. thick case-in-place, reinforced concrete slab. The current average deck thickness is approximately 11 in. with 4 - 1/8 in. of crown from the edge of the roadway to the center of the roadway. The bridge deck is supported by two W27x84 exterior beams and four interior beams (two W27x91s and two W27x98s). Beam spacing, diaphragm location, etc., are shown in Fig. II-2. Note that full depth 8-in. thick concrete diaphragms were installed between the W27x91 interior and W27x84 exterior beams when the bridge was widened in 1967. The bridge has no skew. Both abutments are integral concrete supported on treated wood friction piling, and the original piers are open-two-column concrete supported on untreated wood friction wood piling. The piers were also widened on both sides with the addition of a concrete pile at each end in 1967 (see Fig. II-1a).

The roadway width is 30 ft allowing for two traffic lanes and a shoulder on each side. The bridge has moderate curbs integral with the deck and concrete guardrails connected to the curbs.

Both abutments have a few random vertical and horizontal hairline cracks and the far abutment footing has a delaminated area at the top of a construction joint. The top and bottom of the deck exhibit several hairline and narrow transverse cracks, and a few small delaminated areas. Both curbs show moderate hairline cracks. The top of the deck has Portland Cement (PC) patches at several locations, and a few small spalls and delaminated areas along the construction joints.

(a) Side view

(b) End view

Figure II-1. Overall bridge photographs.

(c) Bottom view

(d) Typical abutment

Figure II-1. Overall bridge photographs - continued.

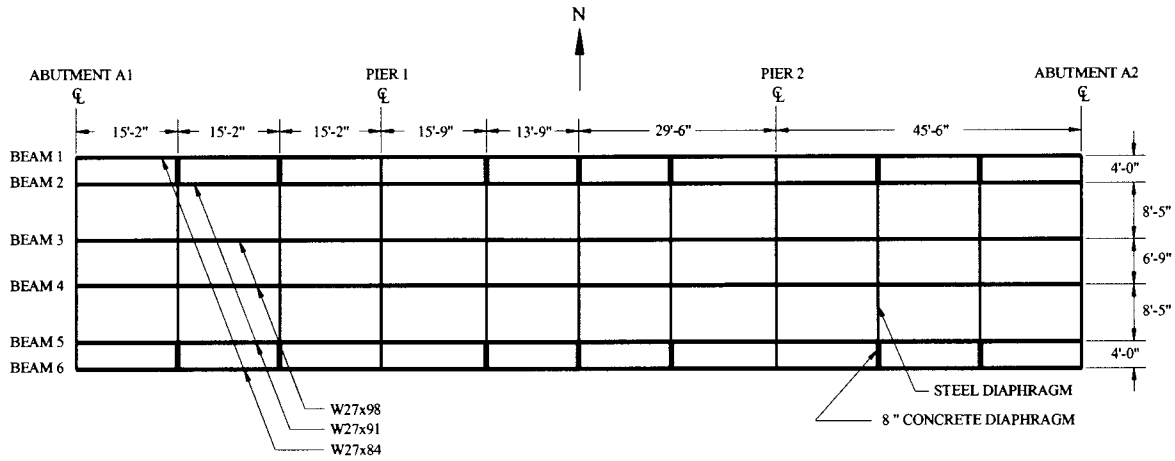

Figure II-2. Bridge framing plan.

2.2. STRENTHENING SYSTEM

The CFRP plate strengthening system consisted of preparing the bonding surface and installation of the CFRP plates. The strengthening system installed consisted of from one to three layers of CFRP plates bonded to the bottom flange in the positive moment region. More specific details are provided in the following sections.

The strengthening system basically consisted of three primary components: CFRP plates, Primer, and Structural epoxy. Each of these components is described in the following paragraphs.

The specific CFRP material selected for this application is a pultruded carbon fiber reinforced polymer consisting of continuous unidirectional carbon fiber in an epoxy matrix. The anisotropic CFRP plates were fabricated utilizing a proprietary pultruding process in which the carbon fibers are pretensioned and aligned during impregnation and curing. The plates have a tensile strength of 300 ksi (ASTM D3039) and modulus of elasticity of 20,000 ksi (ASTM D3039). All plate bonding surfaces were supplied in a "sanded" condition to promote adhesion between the bonding surface of the steel beams and plates. Each plate is 4 in. wide and 0.04 in. thick (see Fig. II-3). The CFRP plates have a tensile linear elastic behavior up to failure; their mechanical properties are summarized in Table II-1.

Figure II-3. CFRP plates being unrolled.

Table II-1. Material properties of CFRP plates.

Ultimate tensile stress, (ksi)	Modulus of elasticity, (ksi)	Ultimate strain	Fiber Content
300	20,000	1.5 %	68 % by volume

A two-part, FRS 1000 Primer was used to provide a base surface between the steel beams and CFRP plates. The primary purpose of the primer application is to prevent corrosion induced by a galvanic reaction between the beam surface and carbon fiber.

A two-part system ECS 104 Structural Epoxy was used for bonding the CFRP plates to the steel beams. The pot life for the epoxy was 3 hours for 3 ounces at 77°F. The properties of the epoxy adhesive are shown in Table II-2.

Table II-2. Properties of ECS 104 Structural Epoxy (units in ksi).

Tensile strength	Adhesion	Flexural strength	Flexural modulus
8.80	>0.29	14.50	310

2.2.1. Design

The design of the CFRP plate strengthening system was completed for the Iowa legal loads utilizing the Load Factor Design (LFD) approach [6]. Based on the analysis completed by the bridge owner, it was found that the positive moment region of Beam 3 and Beam 4 in both the end and center spans was overstressed by 0.55 ksi and 1.57 ksi, respectively. This section describes design process used to predict an increase in moment capacity due to the addition of CFRP plates. In addition, the strengthening scheme that was finally designed for the CFRP plate strengthening system is described.

2.2.1.1. DESIGN MODEL

To design the CFRP plate strengthening system, a design model was developed that satisfied section strain compatibility and force equilibrium. To accomplish this, several assumptions were made:

- The beam is symmetric and initially straight.
- The steel is elastic-perfectly plastic.
- There is a "perfect bond" between CFRP plate and steel beam.
- The CFRP has a linear elastic behavior up to failure.

A summary of the step-by-step design procedure follows:

1. Divide the cross-section into numerous individual elements to idealize the strain distribution with a linear function (see Fig. II-4).
2. Assume the CFRP plate reaches its ultimate strain ($\varepsilon_{CFRP} = 0.015$). Thus, the extreme tension fiber strain (ε_R) can be assumed to be $\varepsilon_R = 0.015$.
3. Assume a neutral axis location, c.
4. Calculate strain in each element and generate a strain profile (see Fig. II-4) based on the strain compatibility relationship.
5. From the strain profile generated in Step 4 and stress-strain relationship for each material shown in Fig. II-5 (constitutive relationship), generate the stress distribution in each section.

For steel,

$$f_{Si} = E_S * \varepsilon_{Si} \quad (\text{if } \varepsilon_{Si} \leq \varepsilon_y)$$

or

$f_{Si} = f_y \qquad (\text{if } \varepsilon_{Si} > \varepsilon_y)$

where f_{Si}, E_S, ε_{Si}, and ε_y are stress in i^{th} steel element, elastic modulus of steel, strain in i^{th} steel element, and yield strain of the steel member, respectively.

For CFRP plates,

$f_{CFRP} = E_{CFRP} * \varepsilon_{CFRP}$

where f_{CFRP} and E_{CFRP} are stress and elastic modulus of CFRP plate, respectively.

6. From the stress distribution, calculate the compressive force, F_C, and the tensile force, F_T, for each element with respect to the centroid of each element.
7. Check the equilibrium of horizontal force, $\sum F_x = 0$:

   if $F_{Compression} \neq F_{Tension}$, assume a new neutral axis location (Step 3) until the solution converges and equilibrium is satisfied.

   if $F_{Compression} = F_{Tension}$, move on to the next step.
8. Calculate the total moment (moment capacity, M_n) by summing the moments of the internal forces about a convenient axis, which can be expressed as below:

$$M_n = \sum(f_{si} * A_{si} * d_{si}) + \sum(f_{CFRP} * A_{CFRP} * d_{CFRP})$$

where A (A_{si} or A_{CFRP}) and d (d_{si} or d_{CFRP}) are cross sectional area of the corresponding element, and distance from the corresponding element to the top surface of the top flange.

The change in moment capacity with increasing numbers of CFRP plate bonded to the bottom of the bottom flange is shown in Table II-3 and Fig. II-6. From this analysis, it was found that the efficiency for using the CFRP plates decreases as amount of CFRP plates used increases. The increase in moment capacity was the greatest (12.3%) with only one layer of CFRP plate utilized while it was 3.2% from the three-layer system to four-layer system.

Stiffness increase due to the addition of CFRP plates to the bottom of the bottom flange was also studied as shown in Fig. II-6. Based on this analysis, it was generally found that an approximately 1.2% stiffness increase per layer was obtained for Beams 3 & 4. The theoretical change in stiffness presented in this section is later compared with field test results, which will be discussed in Chapter 4.

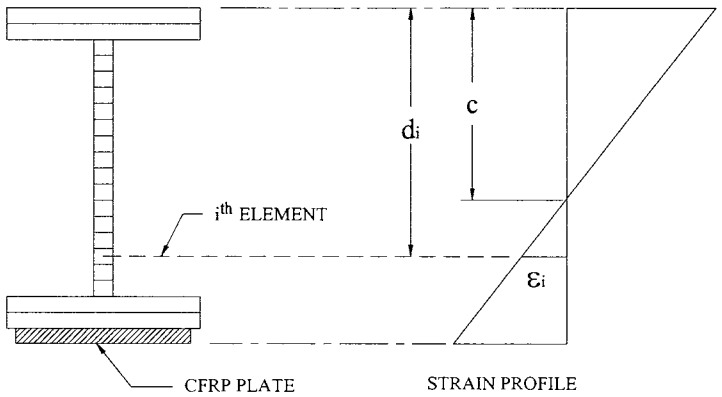

Figure II-4. Subdivision of beam cross-section and strain profile.

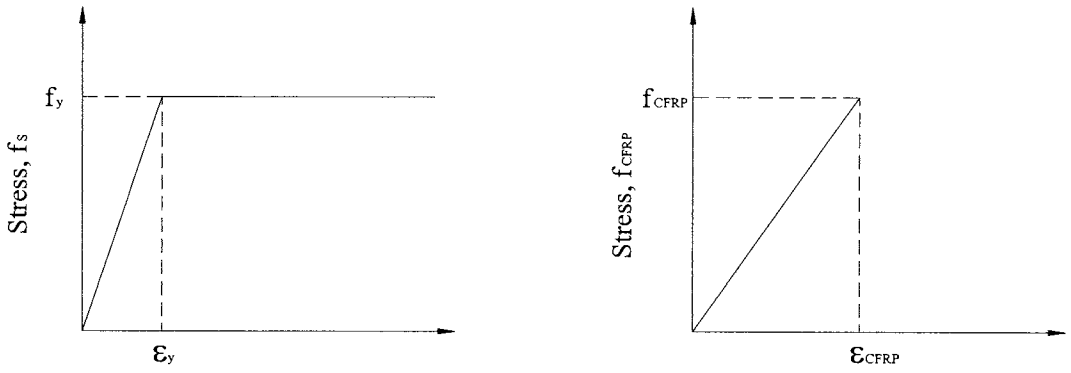

(a) Steel (b) CFRP Plate

Figure II-5. Constitutive relation.

Table II-3. Change in moment capacity in Beams 3 and 4 due to the addition of CFRP plates.

A_{CFRP}, (in^2)	Increase in moment capacity, (%)	Increase in moment capacity per layer, (%)
No CFRP plate	-	-
One layer (0.32)	12.3	12.3
Two layers (0.64)	21.6	9.3
Three layers (0.96)	28.1	6.5
Four layers (1.28)	31.3	3.2

2.2.1.2. STRENGTHENING SCHEME

Following the procedures outlined previously, it was found that the overstressed beams could be adequately strengthened by the addition of CFRP plates bonded to the bottom flange of the beams, and the required amount of CFRP plate needed for strengthening Beams 3 and 4 was determined: one layer in the end spans, and two layers in the center span (each layer with 8 in. x 0.04 in. CFRP plate).

Although only the Beams 3 and 4 were found to be in need of strengthening, several modifications were made to the overall design to:

- Investigate the ease of installation of multiple CFRP layers.
- Evaluate the durability of the installation.
- Compare the behavior of different schemes used in different conditions.

To this end, the following modifications were made with the final layout summarized in Figs. II-7 and 8:

- Beams 1 and 6 were strengthened to investigate CFRP plate durability on exterior girders.
- Beams 1, 3, 4, and 6 in the east end span had three layers installed to evaluate performance and construction of multi layers.
- Beam 6, in all three span, has one-half of the CFRP plate installed on the bottom of the bottom flange and one-half on the top of the bottom flange to investigate durability under direct environmental exposure.

2.2.2. Installation Process

As illustrated in Fig. II-9, temporary scaffolding was constructed underneath the bridge in both end spans to provide an easy access to the beams for the installing of the strengthening system. Access to the center span was provided through the use of a snooper truck. Proper preparation of the bonding surfaces of the plates and beams is critical to achieving a good bond between the beam and plate. The steel beam surfaces to which the CFRP plates were to be bonded were roughened to a coarse sandpaper texture by sandblasting to remove any paint and unsound material. As can be seen in Fig. II-10, the work area was covered with a layer of plastic sheeting during sandblasting to contain the paint debris. The resulting sandblasted beam surface can be seen in Fig. II-11. After the sandblasting, the beam surface was cleaned (see Fig. II-12) with a clean rag wetted with a cleaning

solvent (acetone). The bonding surfaces of the CFRP plates were also cleaned (see Fig. II-13) with acetone to remove all dirt and debris. After the bonding surfaces were dry, the prepared beam surface was treated with a thin layer of FRS Primer (see Fig. II-14) to prevent corrosion induced by a galvanic reaction between the beam surface and carbon fibers. Once the primer had set, a specially designed pneumatic caulking nozzle with a compressed air line attached was used to mix the two-components of the ECS 104 structural epoxy (see Fig. II-15). The structural epoxy was applied to both the pre-cut (see Fig. II-16) CFRP plates (see Fig. II-17a) and the beam surface (see Fig. II-17b) using a 1/8 in. v-notched trowel. The plate was then carefully placed on the beam surface (see Fig. II-18), starting at one end, taking special care to ensure a "straight" application. A smooth, hand roller was then used to apply pressure to the plate to evenly distribute the epoxy and to remove any trapped air (see Fig. II-19). A smooth trowel was then used to remove any excess epoxy (see Fig. II-20) from the edges of the CFRP plates. After all plates were installed, all surfaces were painted. Photographs of the completed installation are presented in Fig. II-21.

The handling and installation of the CFRP plates was relatively labor intensive and required some training. At least a three-man crew was needed to install the system (a day per layer). It is recommended that a periodic visual inspection be made at the bond line on each strengthened beam to investigate any bond failure or slip at the bonding surface; if any signs of delamination or bond failure is detected, appropriate actions be taken since these types of failure would lead to a significant reduction in strength.

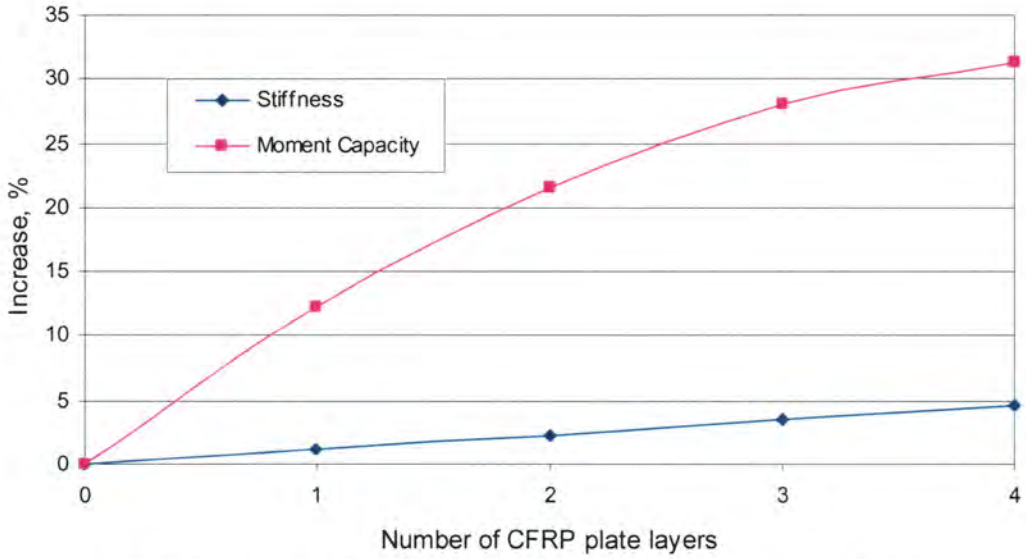

Figure II-6. Change in moment capacity and stiffness on Beams 3 & 4.

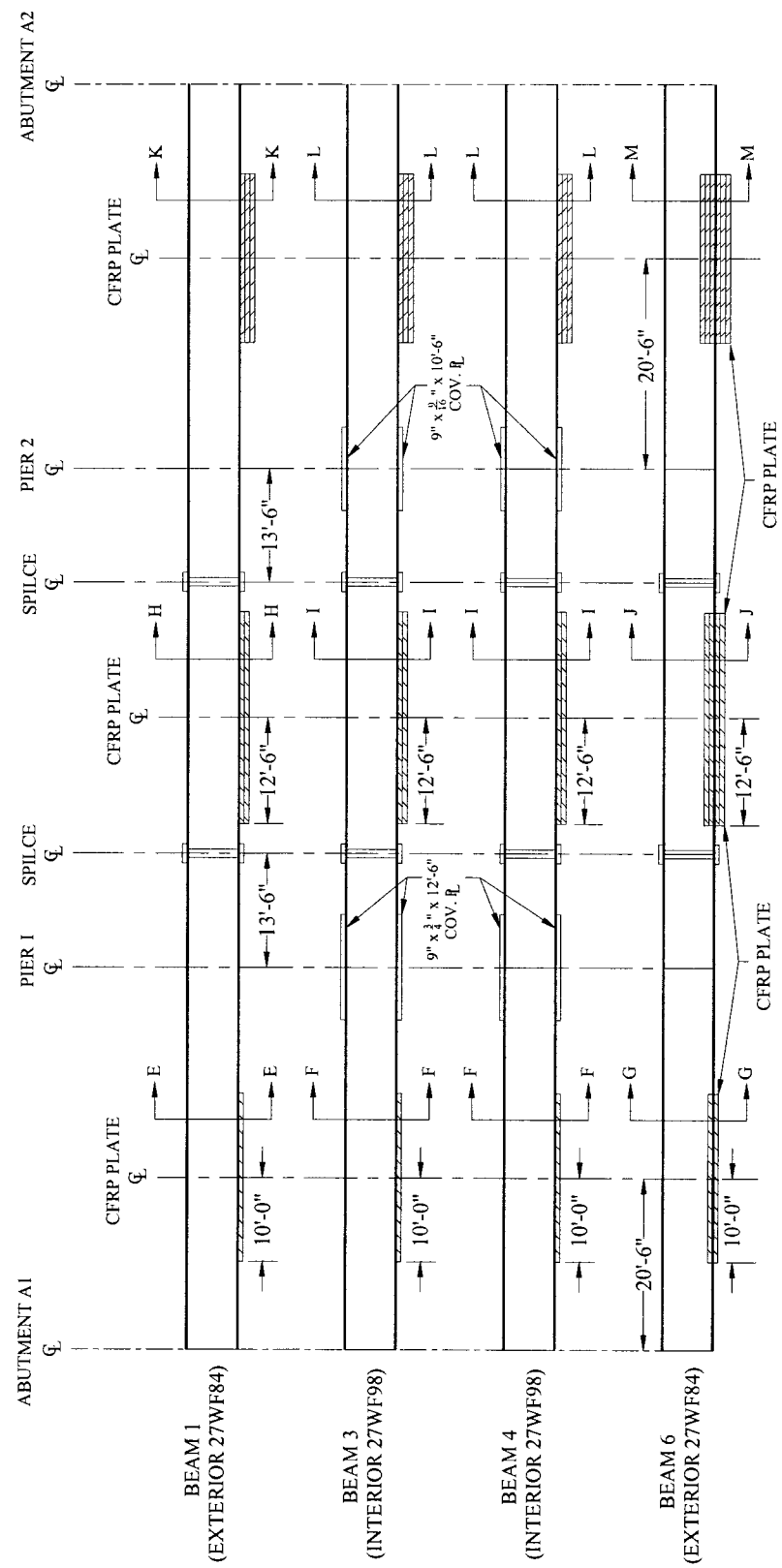

Figure II-7. Final layout of CFRP plates (Side view).

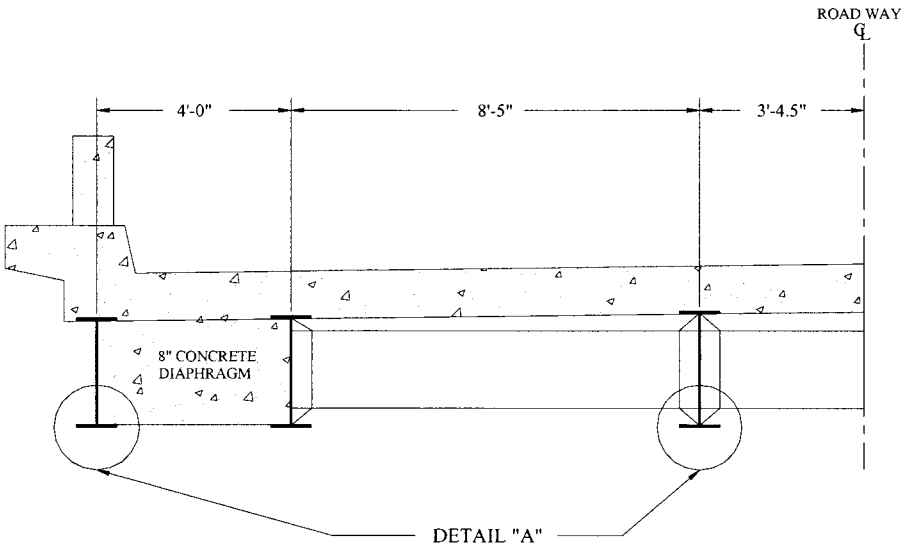

(a) Typical half cross-section

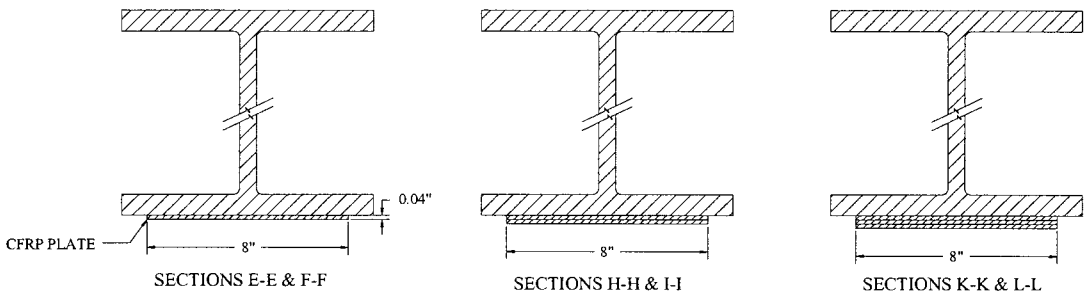

(b) Detail "A" for Beams 1, 3, and 4

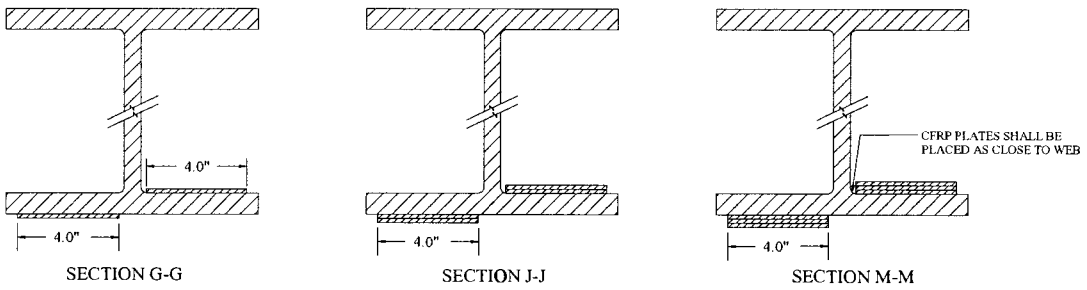

(c) Detail "A" for Beam 6

Figure II-8. Beam cross-sections with CFRP plates.

Figure II-9. Temporary work scaffolding.

Figure II-10. Work area covered with a layer of vinyl during sandblasting.

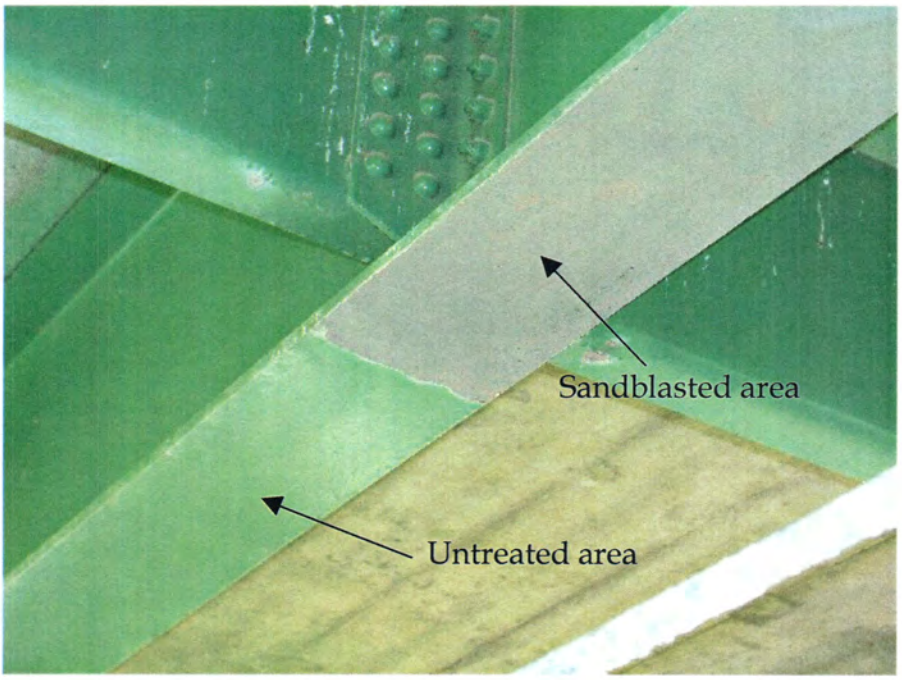

Figure II-11. Sandblasted beam surface.

Figure II-12. Cleaning the beam surface after sandblasting.

Figure II-13. Cleaning the CFRP plate bonding surface.

Figure II-14. Applying FRS 1000 Primer to bottom flange.

Figure II-15. Preparation of ECS 104 structural epoxy (mixing with a compressed air gun).

Figure II-16. Cutting the CFRP plates.

(a) Application of structural epoxy to CFRP plate.

(b) Application of structural epoxy to bottom flange

Figure II-17. Epoxy application.

Figure II-18. Placement of CFRP plate on top of Beam 6 bottom flange.

Figure II-19. Removal of excess air by applying pressure with a roller.

Figure II-20. Removal of excess epoxy.

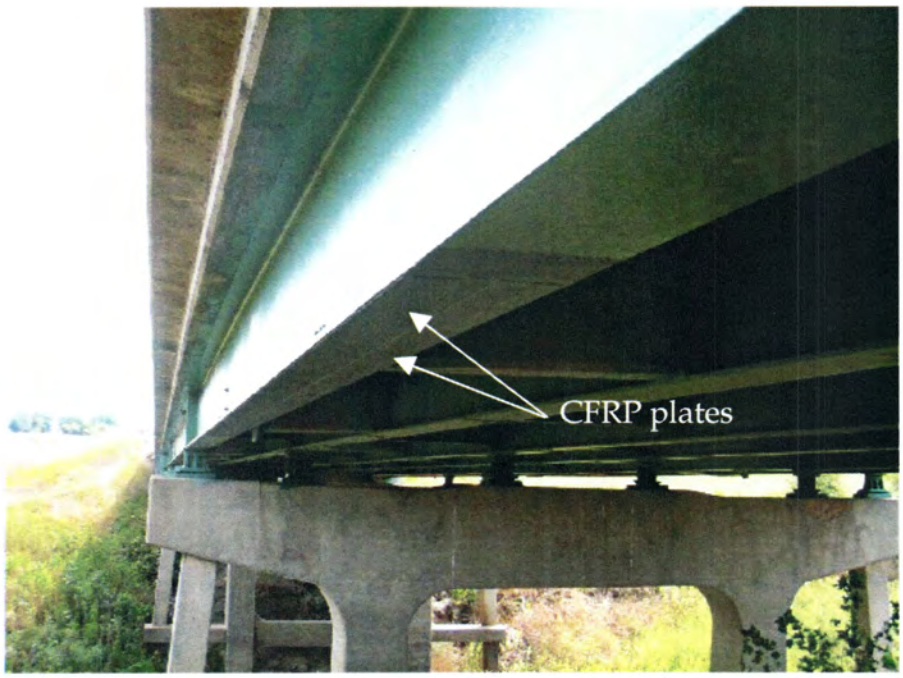

(a) Beam 1 in the west end span

Figure II-21. Photographs of the completed installation.

(b) Beam 3 in the west end span

(c) Beam 4 in the east end span

Figure II-21. Photographs of the completed installation - continued.

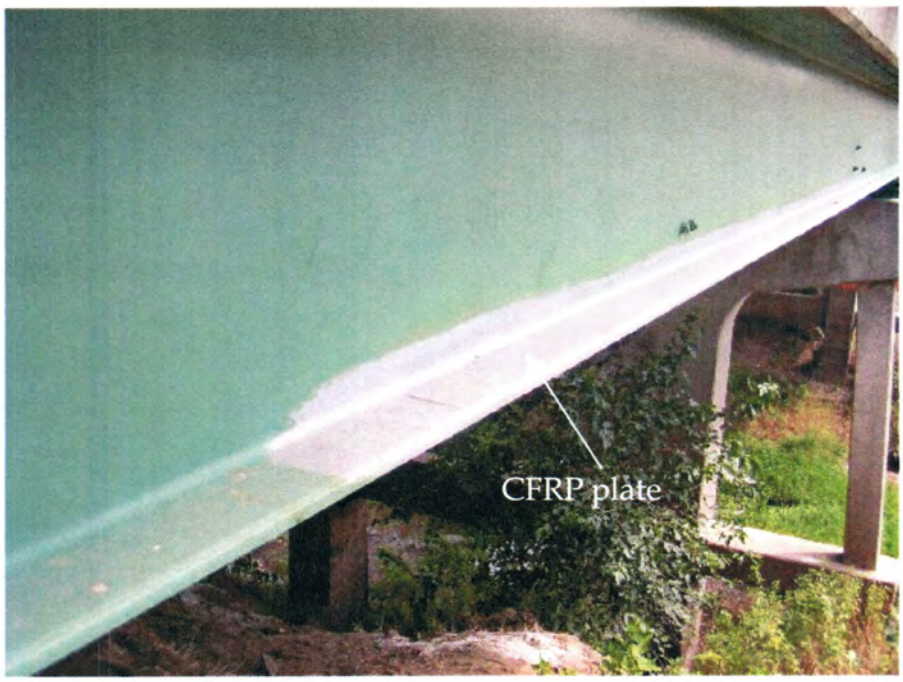

(d) Top of bottom flange of Beam 6 in the west end span

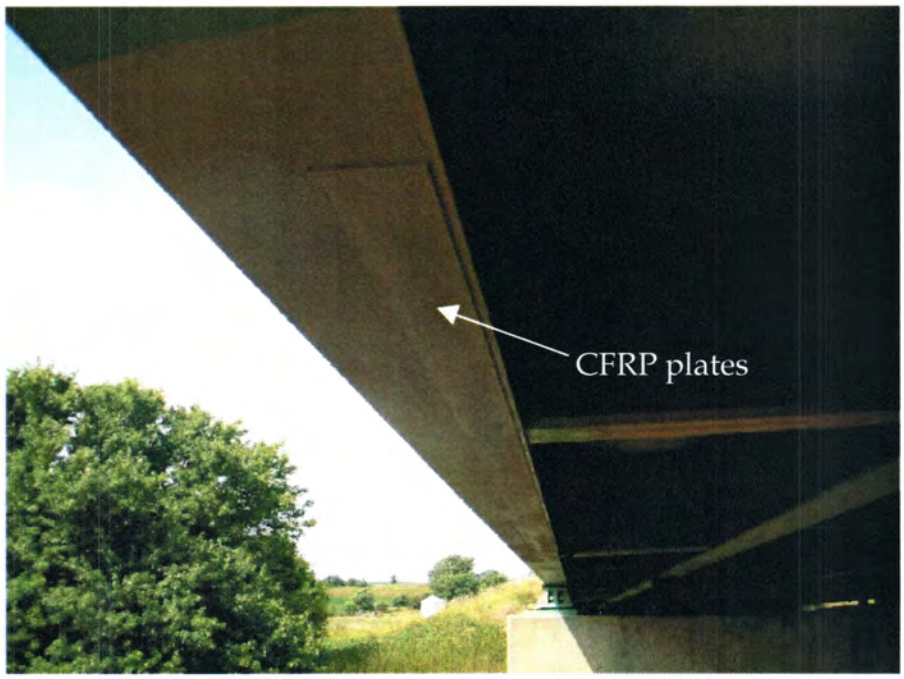

(e) Bottom of bottom flange of Beam 6 in the east end span

Figure II-21. Photographs of the completed installation - continued.

3. EXPERIMENTAL PROGRAM

The subject bridge was instrumented to measure flexural strain at critical locations and tested before installation of the CFRP plates and shortly following the installation to assess changes in performance resulting from the addition of the CFRP plates.

After installation of the instrumentation, standard 3-axle dump trucks, driven at a crawl speed, were used to load the bridge with data collected continuously as the truck crossed the bridge. The initial test was conducted to establish a benchmark response of the bridge, while the follow-up test was completed to access changes resulting from the addition of the strengthening system. For clarity, the load tests that took place before and after the installation will be described separately in the following sections.

3.1. INITIAL TEST (SEPTEMBER 4, 2002)

An initial diagnostic load test was conducted prior to the installation of the CFRP plate strengthening system to establish a baseline static behavior of the unstrengthened bridge. The location of the instrumentation was selected to effectively give an overall understanding of global behavior of the bridge to live load. As can be seen in Fig. II-22, a total of thirty-six strain gages were installed on the bridge with twenty-four gages on the positive bending moment regions and twelve gages on the negative bending moment regions. Due to the structural symmetry of the bridge, only one half of the bridge was instrumented.

Three different truck paths were used to examine the performance of the bridge. These truck paths were chosen so that the maximum strains could be generated in selected girders from the load testing. For convenience, each load path is referred to as Y1, Y2 and Y3 as shown in Fig. II-23. All tests were conducted from west to east. For path Y1 heading east in south lane, the passenger side wheels were placed 4 ft - 1.5 in. north of Beam 6. Path Y2 placed the passenger side wheel 3 ft south of the bridge centerline. For path Y3, heading east in the north lane, the driver side wheel was placed 4 ft - 1.5 in. south of Beam 1. The Iowa DOT provided the load truck shown in Fig. II-24. Truck 1 had a total weight of 52.76 kips with 13.78 kips and 38.98 kips on the front and rear axles, respectively. This truck was 16 ft - 10.5 in. long between the center of the front axle and the center of the rear axles, 6 ft - 8 in. wide between the centers of the front tires, and 6 ft wide between the rear tires.

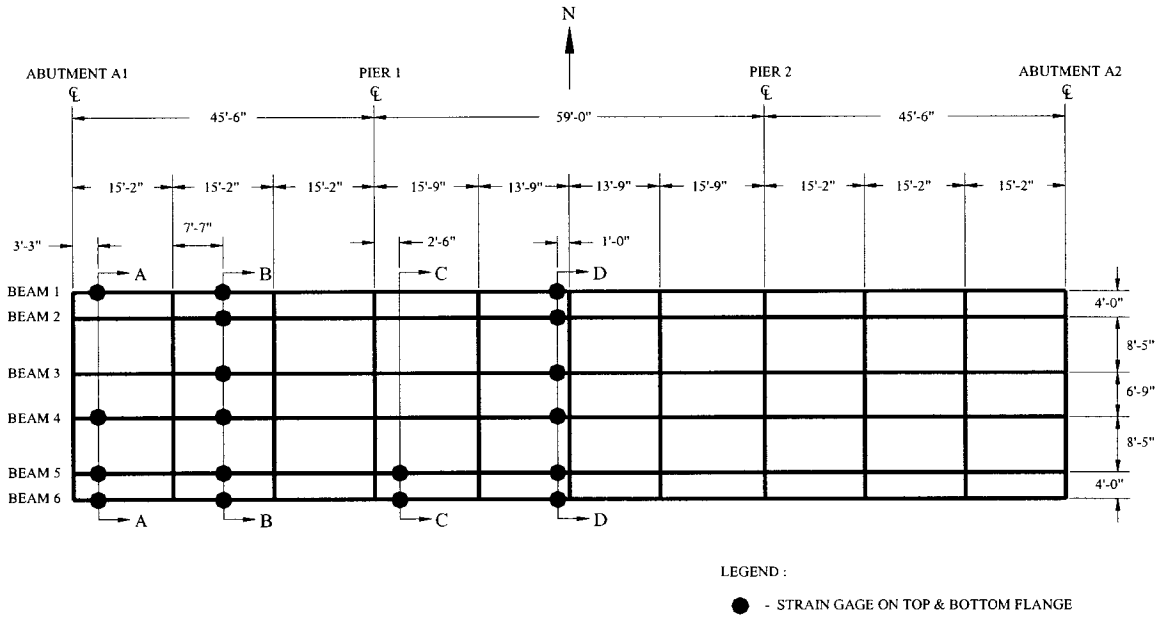

(a) Plan view

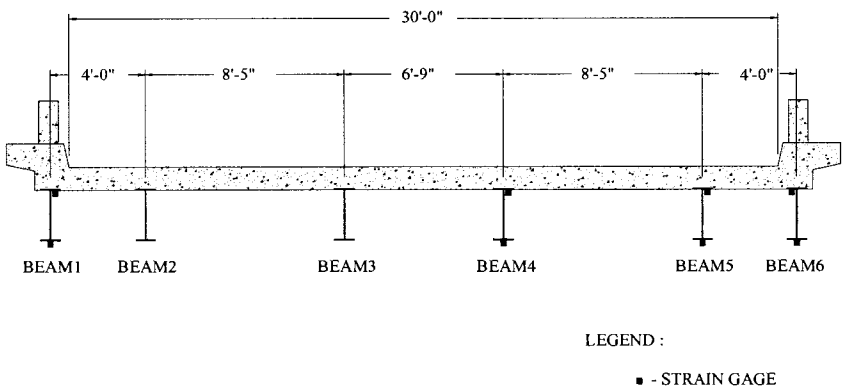

(b) Section A

Figure II-22. Strain gage locations.

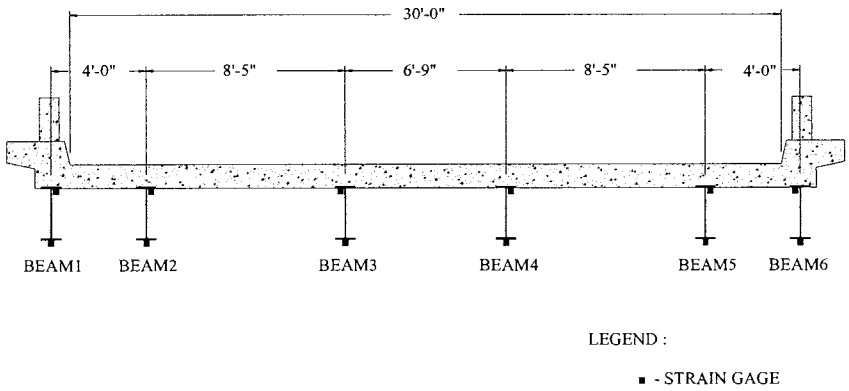

(c) Section B

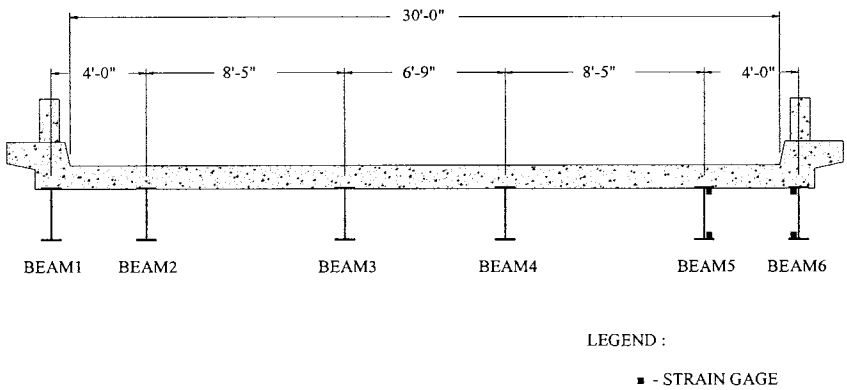

(d) Section C

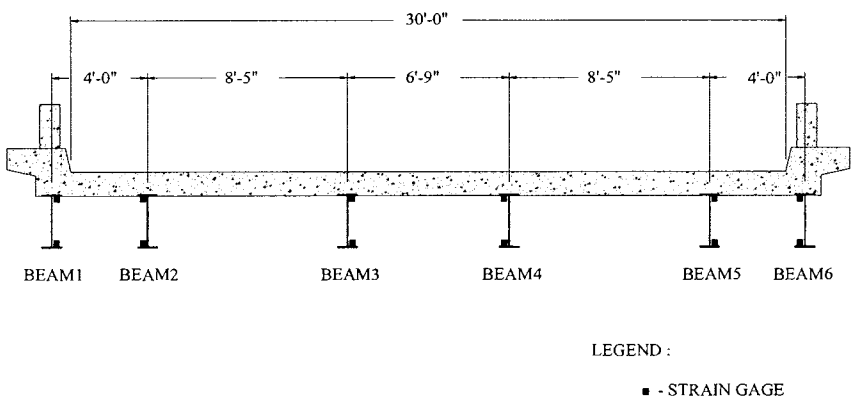

(e) Section D

Figure II-22. Strain gage locations – continued.

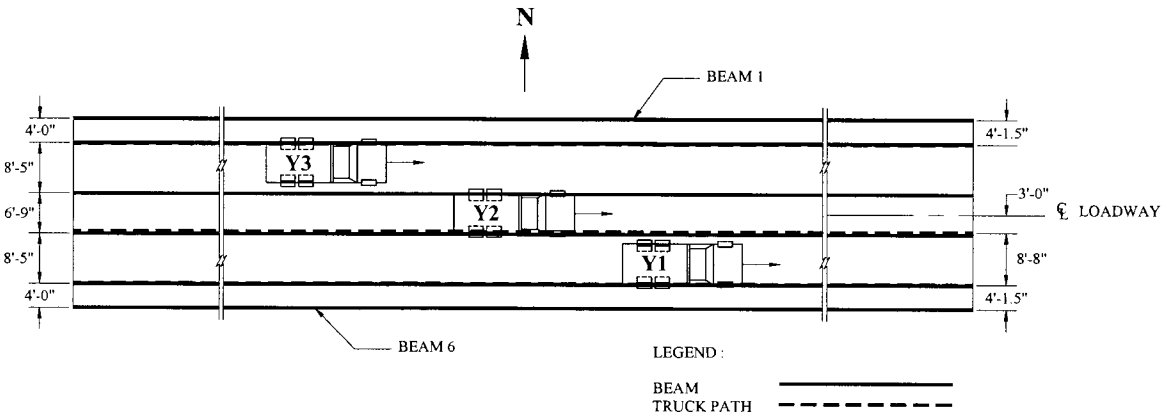

Figure II-23. Truck paths used during load test.

3.2. SHORTLY AFTER INSTALLATION (AUGUST 19, 2003)

The second load test was conducted approximately two months after the installation of the strengthening system to assess any immediate change in performance resulting from the installation of the CFRP plates. The procedures used for the second load test were the same (e.g., same load paths and sequences, etc.) as what was used in the initial test except for the weight of the truck used and the number of strain gages used. In this test, four additional gages were installed on the bottom flange (on the CFRP plates) of the strengthened beams (Beams 1, 3, 4, and 6) in the center span (Section D as shown in Fig. II-25) to investigate the bonding performance of each strengthened beam at that location.

The load truck used for the second load test, Truck 2 was again provided by the Iowa DOT and had a total weight of 53.06 kips with 15.60 kips and 37.46 kips on the front and rear axles, respectively. Dimensions and weights of the testing truck used in each test are illustrated in Fig. II-26 and summarized in Table II-4.

Based on the strains obtained in the follow-up test, the change in stiffness was computed and these results were compared with the preliminary analysis conducted in Chapter 2. Corresponding results will be discussed in section 4.2.3.

Figure II-24. Photograph of typical load test truck.

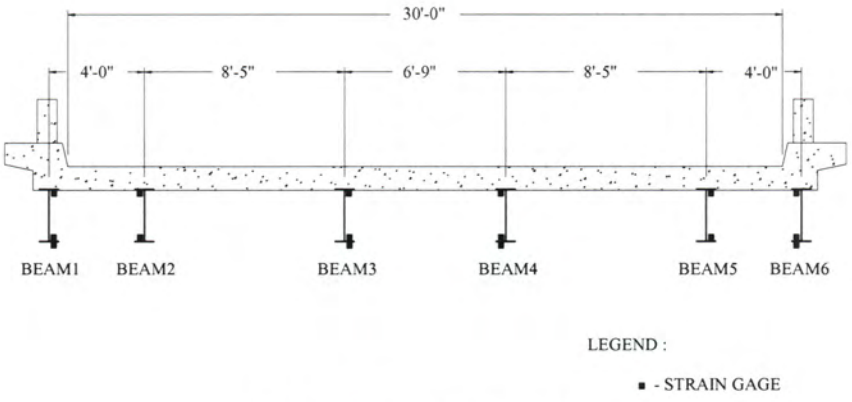

(a) Cross-section (Section D)

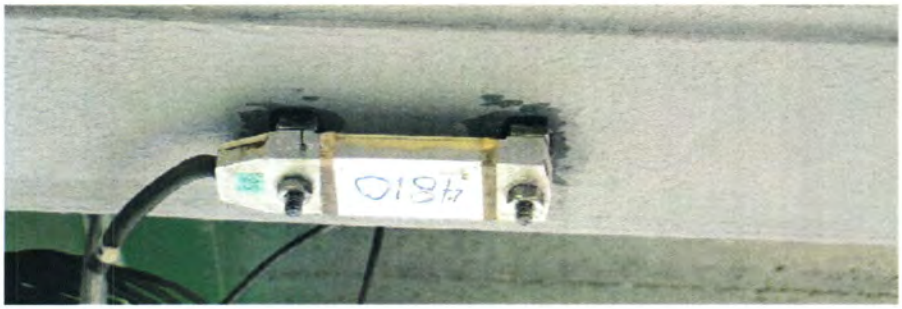

(b) Photograph of typical strain gage installation on CFRP plate

Figure II-25. Strain gage location for "Shortly after installation" test.

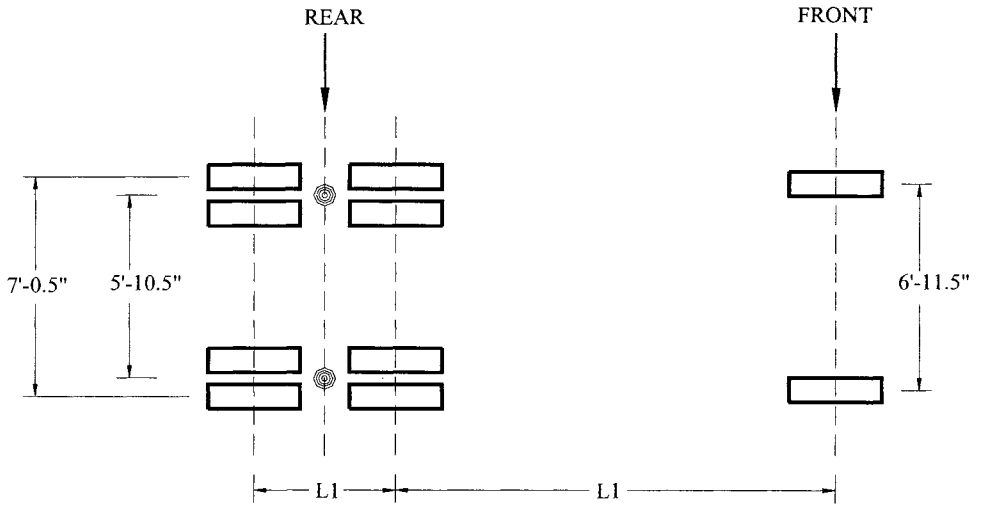

Figure II-26. Dimension and weight of testing truck.

Table II-4. Summary of dimensions and weights of load truck.

Truck No.	L1	L2	Weight (lb)		
			Rear	Front	Total
1	4'-7"	14'-5"	38,980	13,780	52,800
2	4'-7"	14'-5"	37,460	15,600	53,060

4. RESULTS

Results from the field testing and theoretical analysis are presented in this chapter. Where applicable, the field test results will be compared with theoretical analysis results.

For simplification, in the following discussion, the data will be referenced to the sections (A through D) shown in Figs. II-22a and II-25a, and the truck paths shown in Fig. II-23. The same notations used in Part I were again utilized in Part II except that the notation is completed with a letter such as "T" or "B" to indicate the location on the beam. For example, "Y2D3 (TB)" represents a data set collected from "Path Y2 - Section D - Beam 3 - top of bottom flange". Some other notations used are described as follows:

- "Initial Test": data set taken during "Initial Test" (Sep. 4, 2002).
- "t = 0 year" : data set taken during "Shortly after installation Test" (Aug. 19, 2003).
- "(T)" : strain on bottom of top flange.
- "(TB)" : strain on top of bottom flange.
- "(BB)" : strain on bottom of bottom flange.
- "(CFRP)" : strain on CFRP plate (installed on bottom of bottom flange).

All strain data have been normalized for the weight of the Initial Test truck weight (i.e., multiplied by ratio of Initial Test truck weight to individual truck weight).

4.1. INITIAL TEST

As previously mentioned, an initial diagnostic load test was conducted prior to the installation of the strengthening system to establish a baseline static behavior of the unstrengthened bridge. The goal of this testing was to understand the general, global behavior of the bridge and to determine changes in behavior of live load strain.

In general, all strains exhibited an elastic response (i.e., strains from all gages returned to zero after each truck crossed the bridge). Relative magnitudes (with respect to midspan strains) of flexural tensile and compressive strains at Section A (near Abutment A1) were observed (see Figs. II-27a and 28a). This behavior confirms the presence of rotational end restraint at the abutment as one would expect since the bearings at both abutment are encased with concrete (i.e., integral abutment, see Fig.

II-1d). Also, with minor variation, composite action was found to be present at all sections of the exterior beam (i.e., the neutral axis location on the exterior beam was found to be close to the top flange in the positive moment region). As previously described in section 2.1, the bridge was originally a non-composite structure until the bridge was widened in 1967 with the addition of exterior beams that were made composite with the deck. Although, interior beams showed generally non-composite behavior, some composite behavior, however, was observed at several locations.

In addition, strains indicate good lateral symmetric behavior that corresponds to the symmetrical configuration of the bridge and the truck paths utilized. For example, the strains due to the truck paths Y1 on Beam 6 and Y3 on Beam 1, respectively, exhibited a similar lateral symmetrical behavior as shown in Fig. II-27. Similar pattern was observed for the truck path Y2 on Beam 3 and Beam 4 as shown in Fig. II-28. Some of the differences in transverse symmetry may be attributed to either difference in local stiffness, difference in rotational end restraint at the abutment or possible experimental error that might have occurred during the testing (i.e., differences in truck wheel line distribution and/or truck lateral positioning).

4.2. INFLUENCE OF STRENGTHENING SYSTEM ON LIVE LOAD RESPONSE

4.2.1. General Behavior

Follow-up load testing (shortly after installation) was conducted on the strengthened bridge to investigate, by comparing strains, any changes and behavior of the bridge after installation of the strengthening system. Typical strains in the bridge collected during each test are presented in Figs. II-29 through 31.

From the preliminary analysis conducted in Section 2.2.1, it was found that approximately 1.2% stiffness increase per layer was obtained for Beams 3 & 4. By comparing strains in each test, however, it was observed that the follow-up test produced fairly consistent strains with those established during the initial test. This consistency in strain indicates that the strengthening system did not significantly alter the behavior of the bridge. Although it is not possible to precisely account for all the sources of strain, it is evident from the consistency of the strain data that the installation of the CFRP plates had little impact on changing the stiffness of the bridge. It also indicates that the live load distribution characteristics are virtually the same before and after the installation of the strengthening system.

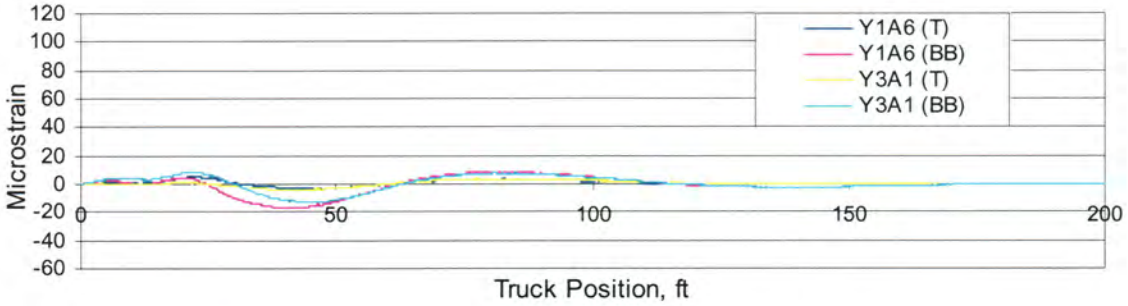

(a) Section A

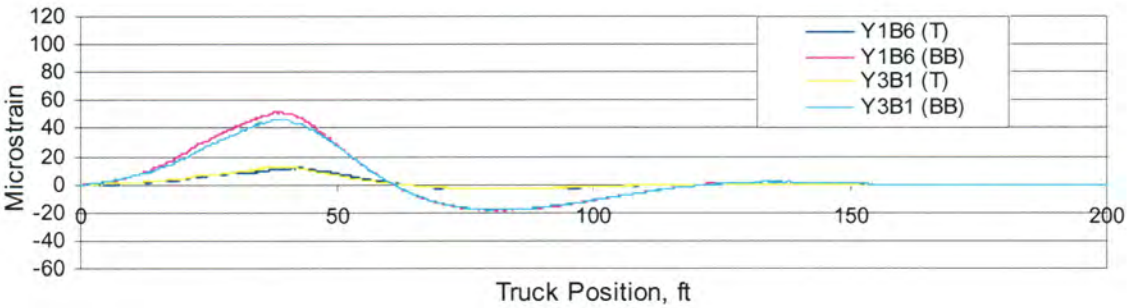

(b) Section B

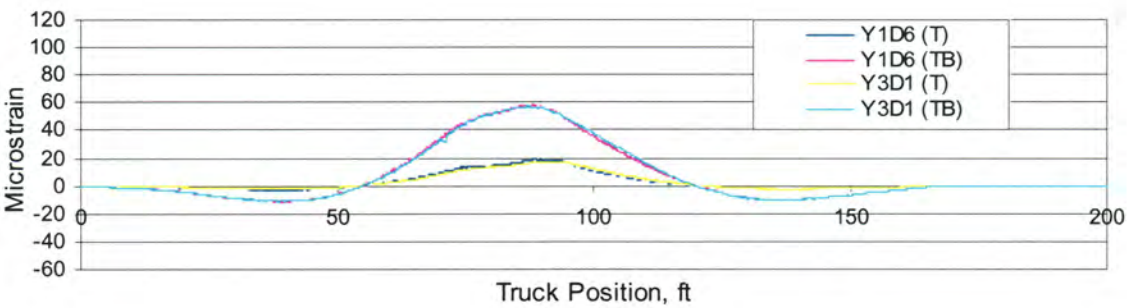

(c) Section D

Figure II-27. Before strengthening: strains in Beam 6 (Path Y1) and Beam 1 (Path Y3).

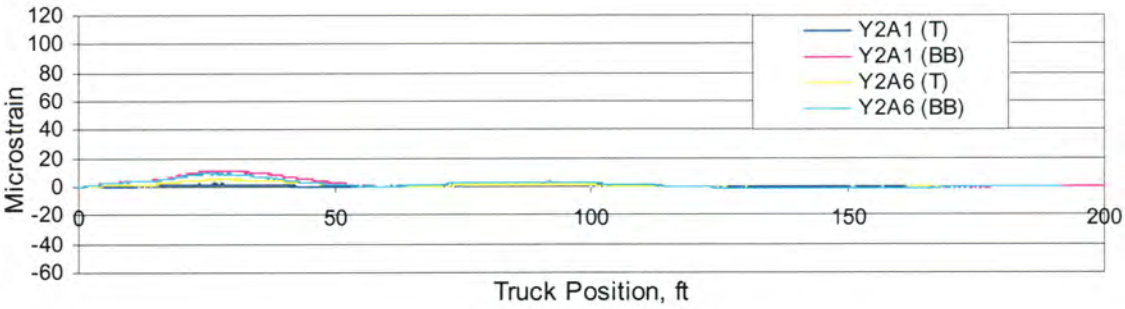

(a) Section A

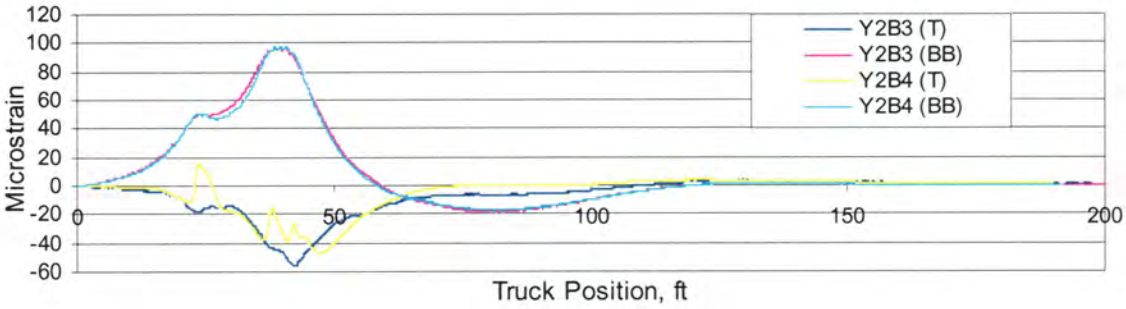

(b) Section B

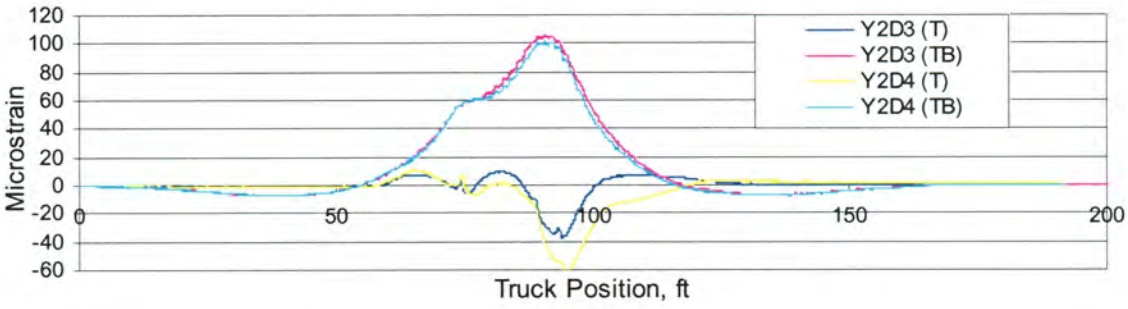

(c) Section D

Figure II-28. Before strengthening: strains in the bridge (Path Y2).

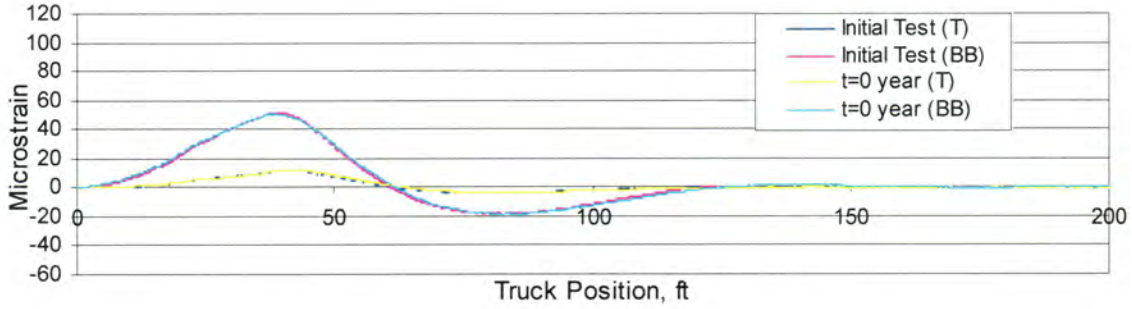

(a) Section B

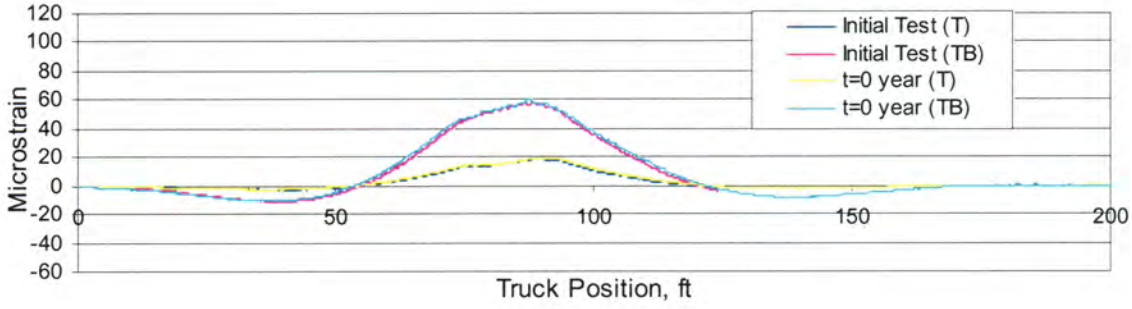

(b) Section D

Figure II-29. Before and after strengthening: strains in Beam 6 (Path Y1).

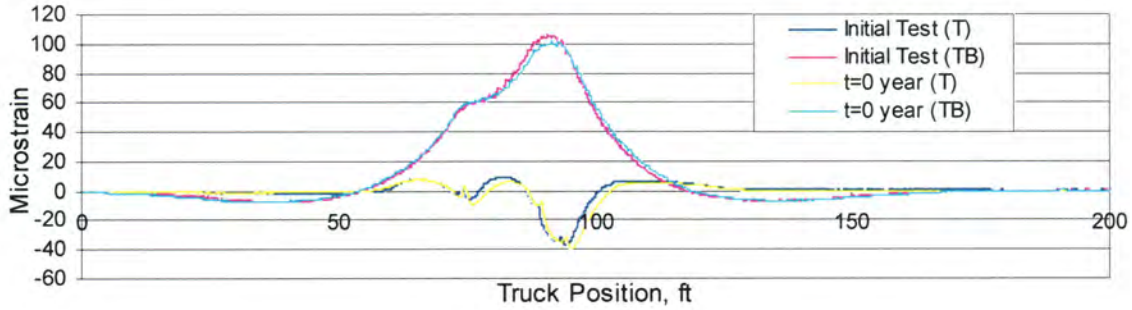

(a) Section D, Beam 3

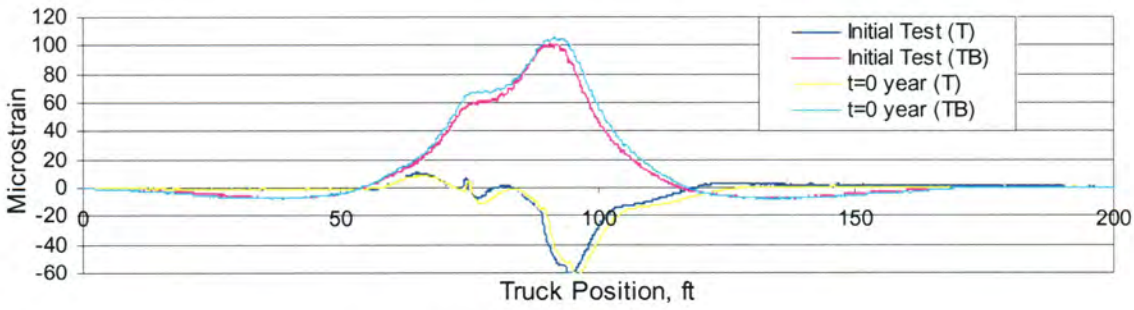

(b) Section D, Beam 4

Figure II-30. Before and after strengthening: strains in Beams 3 and 4 (Path Y2).

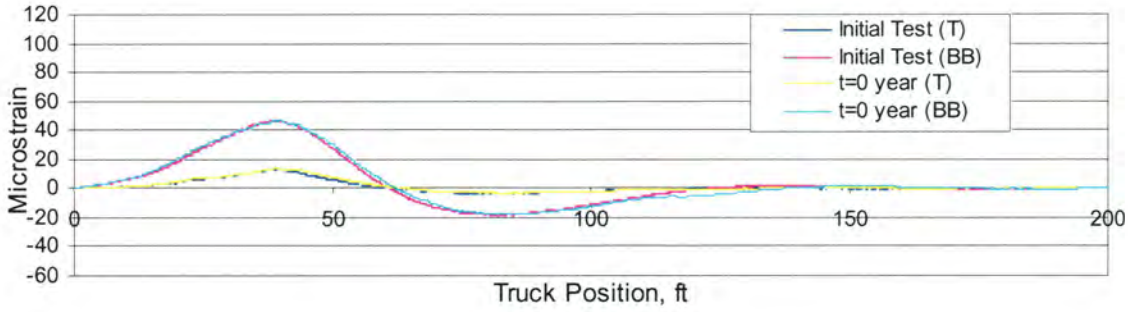

(a) Section B

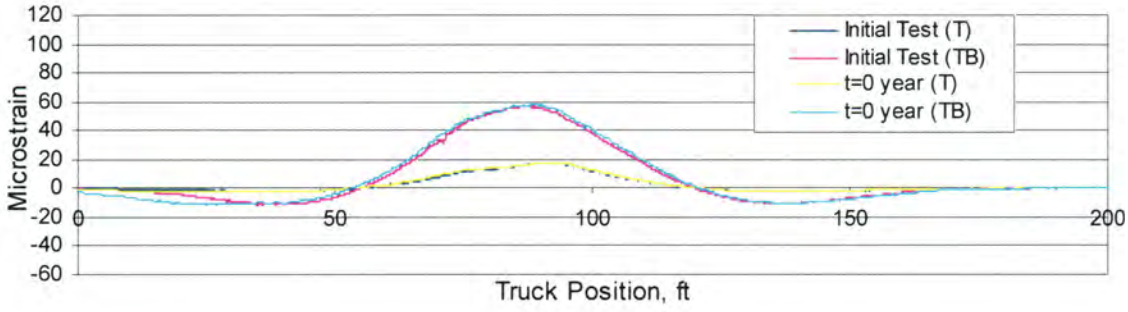

(b) Section D

Figure II-31. Before and after strengthening: strains in Beam 1 (Path Y3).

4.2.2. Bond Performance

When a bonding technique is used for strengthening purpose, it is critical to have adequate bonding performance for the transfer of force to the strengthening material. As was previously mentioned, additional gages were installed on the bottom flange of the strengthened beams (on the CFRP plates) in the center span (Section D) to investigate the bonding performance on each strengthened beam.

A simple analytical tool was developed based on strain compatibility relationship (see Equation II-4.1 and Fig. II-32) to predict the extreme fiber strain on the CFRP plate (ε_{EXT}), and these simple analytical predictions were compared with the strains measured during the post-installation load test (t = 0 year) and illustrated in Figs. II-33 and 34.

$$\varepsilon_{EXT} = \frac{(\varepsilon_T + \varepsilon_{TB}) * h_{CFRP}}{h_{web}} - \varepsilon_T \qquad \text{(II-4.1)}$$

where ε and h are strain at the corresponding location and distance from the bottom of the top flange to the corresponding location shown in Fig. II-32, respectively.

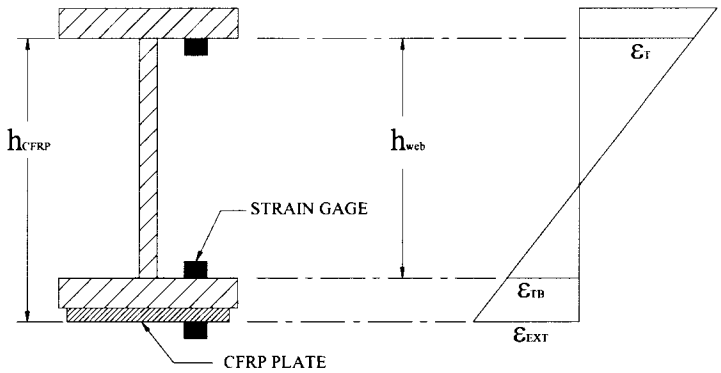

Figure II-32. Beam cross-section with gage location and strain profile.

From the comparison, it was found that the difference between the analytical and experimental strain was 3.8% on average. Considering the sensitivity of the neutral axis location that could change significantly with small change in strain, this percentage error is considered to be relatively small; thus, it appears at this point that there was good bond and no significant debonding between the beam and CFRP plates.

Additional load testing (two more follow-up tests in two years) to collect additional data and occasional visual inspections to document any changes in the integrity of the CFRP plates are planned in this project. Also, bond performance of the CFRP plates will be further assessed based on additional field tesing result in the future.

4.2.3. Change in Stiffness

From the preliminary analysis conducted in Chapter 2, stiffness increase of approximately 1.2% per layer in Beams 3 and 4 (2.34% for two layers of CFRP plates) was predicted. Given these, an attempt was made to compute the change in stiffness factor (EI) based on the strain data collected from each test. To accomplish this, a simple equation (Equation II-4.2) was developed through basic mechanics principles. Note that the modulus of elasticity (E) on the exterior and interior beam was assumed constant. Using this equation, the change in stiffness before and after the installation of CFRP plates was determined to be 0.47%, 0.81% on Beam 3 and Beam 4, respectively. From the comparison with the preliminary analysis shown in Fig. II-35, it was found that the change in stiffness based on the measured strain is lower than the preliminary analysis results.

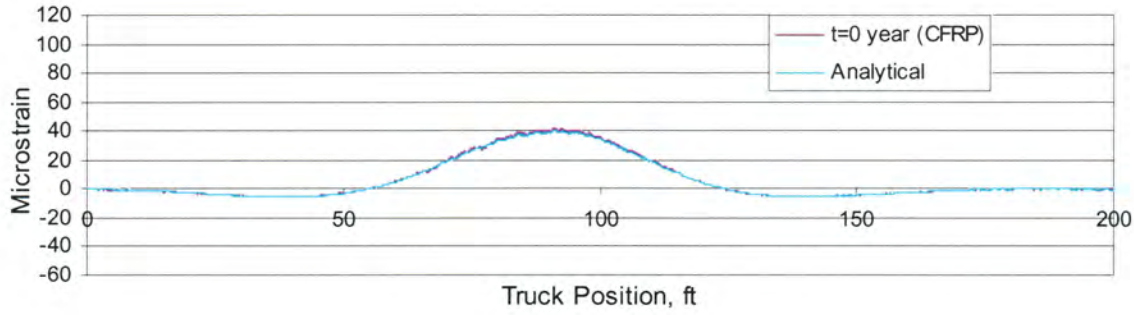

(a) Path Y1

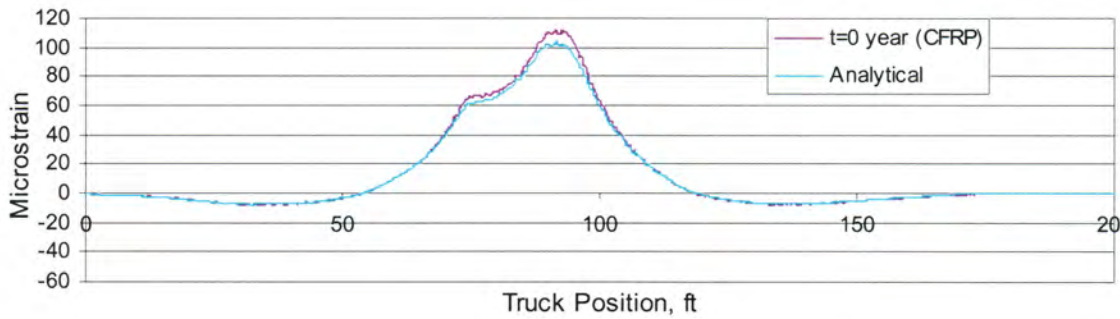

(b) Path Y2

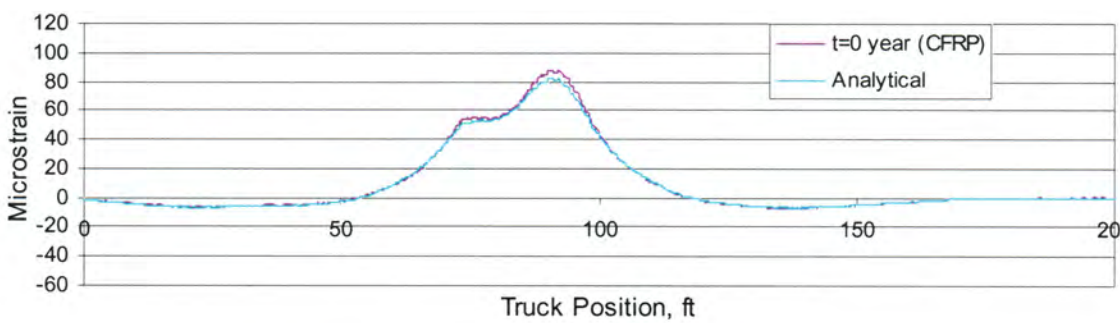

(c) Path Y3

Figure II-33. After strengthening: strain in Beam 3 at Section D.

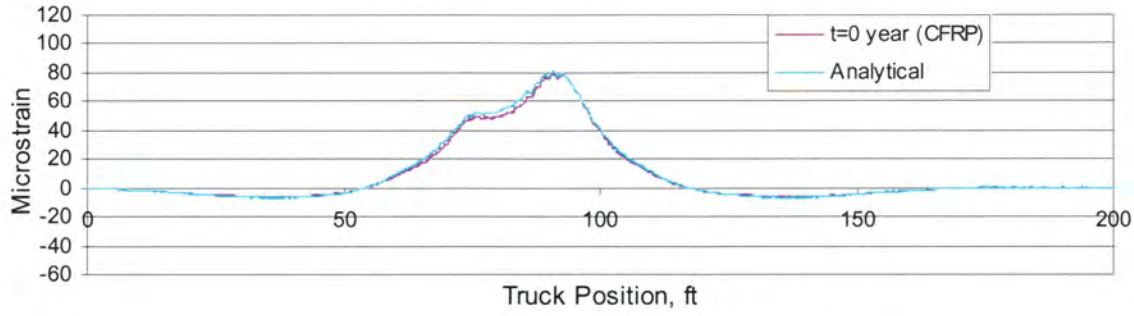

(a) Path Y1

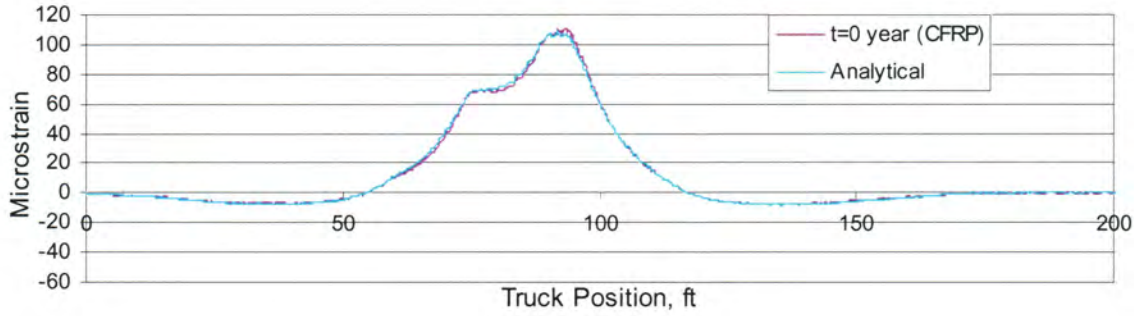

(b) Path Y2

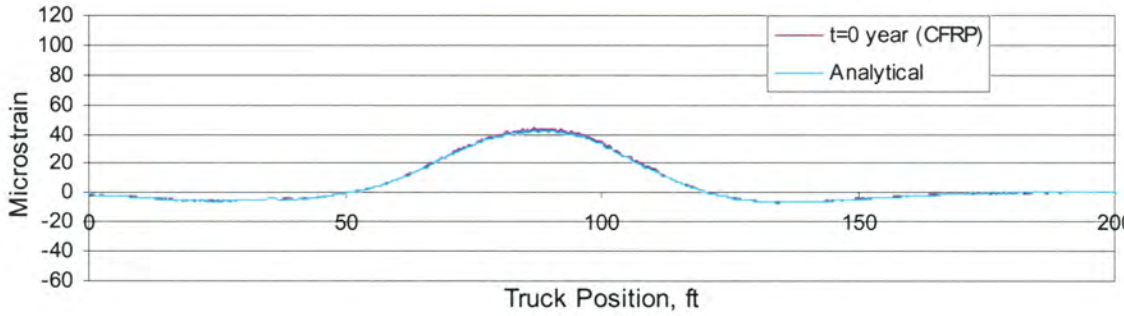

(c) Path Y3

Figure II-34. After strengthening: strain in Beam 4 at Section D.

$$(EI)_i = \frac{M_i y_i}{\varepsilon_i} \qquad \text{(II-4.2)}$$

where

M_i = $M * (DF)_i$

M = maximum moment at Section D induced by load truck (wheel line load).

$$(DF)_i = \text{distribution factor} = \frac{\varepsilon_i S_i E_i}{\sum(E_i \varepsilon_i S_i)} = \frac{\varepsilon_i S_i}{\sum(\varepsilon_i S_i)}$$

ε_i = bottom flange strain of i th beam induced by load truck.

S_i = section modulus of i th beam.

E_i = modulus of elasticity of i th beam.

y_i = distance from composite neutral axis (NA) to strain gage on i th beam.

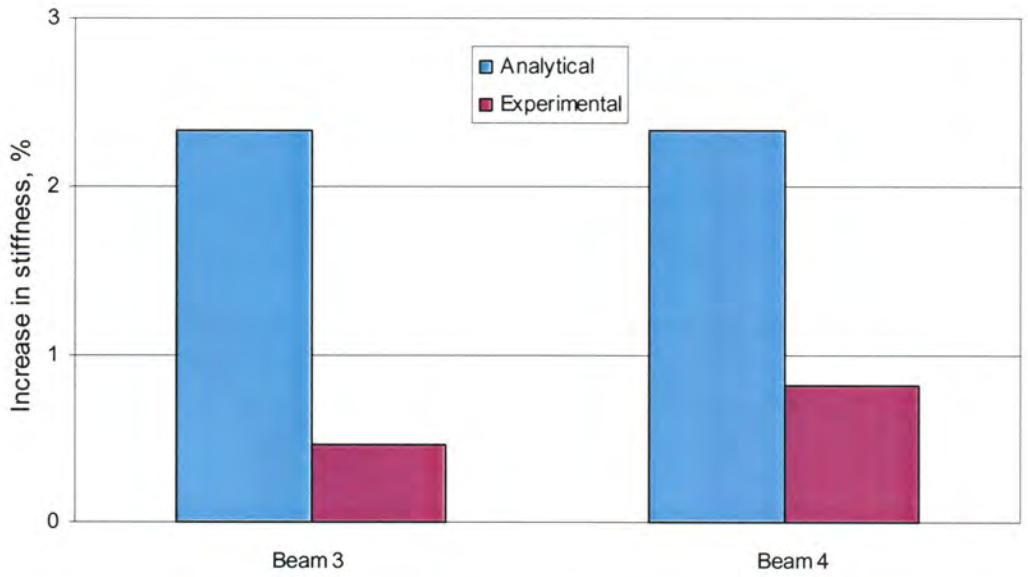

Figure II-35. Comparison of change in stiffness at Section D.

5. SUMMARY AND CONCLUSIONS

5.1. SUMMARY

Primary objective of this project was to investigate and evaluate the effectiveness of CFRP plates to strengthen an existing, structurally deficient steel girder bridge. The bridge strengthened with CFRP plates was a 150 ft x 30 ft three-span continuous I-beam bridge in Pottawattamie County, Iowa, on State Highway IA 92. The research program consisted of several tasks with the main emphasis on the design and installation of the strengthening system and associated field-testing. Before the CFRP plates were installed, a diagnostic load test was conducted on the bridge to establish a baseline static behavior of the unstrengthened system. The strengthening system consisted of preparation of the bonding surface and installation of the CFRP plates. The design of the CFRP plates was based on the Iowa legal load utilizing the Load Factor Design approach. The implemented design consisted of from one to three layers of CFRP plates bonded to the overstressed tension regions with a high strength epoxy adhesive to improve the live load carrying capacity. The CFRP plate strengthening system consisted of three primary components: CFRP plates, Primer, and Structural epoxy. The installation of strengthening system was followed by a second diagnostic load test to assess the short-term effectiveness of the strengthening scheme.

5.1. CONCLUSIONS

Based on the field test and analytical results, the following conclusions were made and summarized below:

- The analytical study indicated that with the relatively small change in stiffness in the strengthened member, a considerable increase (approximately 10% increase per layer up to three layers) in the moment capacity on the strengthened beams was attainable and thereby, improving the overall live load carrying capacity of the bridge.
- The bond performance between the beam and CFRP plates was good and, therefore, it appeared that no significant debonding occurred shortly after the installation.
- The handling and installation of the CFRP plates was relatively labor intensive and required some training. At least a three-man crew was needed to install the system (a day per layer).

6. RECOMMENDATIONS

The use of external bonded CFRP plates appears to be a feasible, practical alternative to traditional methods for strengthening an existing bridge. However, the use of CFRP plates bonded to the steel girder bridge is relatively a new technology that has not been broadly accepted by specification or code authorities. Therefore, it is recommended to complete more studies on the characteristic of this strengthening system such as its fire resistance, long-term creep characteristics, and degradation of bond forces with time. In addition, more extensive studies to fully understand its failure mechanisms and the development of design standards are needed for the future use of other engineers. It is further recommended, for this project, that any signs of delamination or bond failure at the bond line on the strengthened beams be closely observed and, if detected, appropriate actions be taken since these types of failure would lead to a significant reduction in strength.

7. REFERENCES

1. Tang, B., and W. Pdolny, "A successful Beginning for Fiber Reinforced Polymer (FRP) Composite Materials in Bridge Applications." *FHWA Proceedings*, Orlando, FL, December 1998.

2. Al-Saidy, A.H., "Structural Behavior of Composite Steel Beams Strengthened/Repaired with Carbon Fiber Reinforced Polymer plates." Dissertation, Iowa State University, Ames, IA, 2001.

3. Mertz, D.R., and J.W. Gillespie Jr., "Rehabilitation of steel bridge girders through the application of advanced composite materials." NCHRP-IDEA final report, Transportation Research Board, Washington, D.C., 1996.

4. Tavakkolizadeh, M., and H. Saadatmanesh, "Strengthening of Steel-Concrete Composite Girders Using Carbon Fiber Reinforced Polymers Sheets." *Journal of Structural Engineering*, Vol. 129, No. 1, January 1, 2003.

5. Miller, T.C., "The Rehabilitation of Steel Bridge Girders Using Advanced Composite Materials." Mater's Thesis, University of Delaware, Newark, DE, 2000.

6. American Association of State Highway Officials. *Standard Specifications for Highway Bridges*, 16th Edition, Washington, D.C., 1996.

PART III. EVALUATION OF CORROSION RESISTANT STEEL REINFORCING IN THE DECK SLAB OF A THREE SPAN PRESTRESSED GIRDER BRIDGE (FIELD MONITORING)

1. INTRODUCTION

1.1. BACKGROUND

Deterioration due to corrosion of reinforcing steel is one of the most costly and prevalent challenges for bridge structures. This problem has increased significantly in the last three decades and is likely to continue getting worse. Although corrosion of the reinforcing steel is not the only cause of all structural deficiencies, its contribution is so significant that it has become one of the biggest major concerns and has reached alarming proportions in various parts of the world. It was recognized in the mid 1970s that even a small amount of chloride from deicing salts could cause serious disruptive effects on steel members in concrete that, in turn, eventually would result in structural deficiency. However, the use of deicing salts on the road is not likely to decrease.

Bridge engineers have spent much time, money, and effort on finding an innovative technology to mitigate or even eliminate the corrosion problem from the bridges. Since inspection of steel reinforcement embedded in a concrete structure cannot be done easily, the presence of corrosion cannot usually be detected until the problem becomes significant. Although early detection of corrosion within reinforced concrete structures would provide engineers with an opportunity to remedy the problem, this alone will not abate the nature of the problem. Regardless of what can be done, the reinforcing steel, itself, will be the last line of defense against corrosion.

This report presents a portion of the project that investigates corrosion of reinforcement steel in the deck slab of two prestressed concrete girder bridges. A relatively new form of corrosion resistant material, Micro-composite Multi-structural Formable Steel (MMFX) reinforcing rebar, was utilized, and the performance was compared with conventional epoxy coated steel. The other part of this project, a laboratory evaluation of the corrosion performance of various reinforcing steels including MMFX, is being conducted at Iowa State University. The final results of that portion of this study will be available in 2005.

1.2. LITERATURE REVIEW

1.2.1. Corrosion Process

Corrosion rate is a function of the availability of oxygen and moisture, and the type and variability of the environment. The actual process of corrosion is electrochemical, which is similar to a battery. Corrosion leads to a flow of electrons from an anode site (where corrosion occurs) to a

cathode site (where no corrosion occurs) on a corrodible surface. Two essential elements are needed to allow corrosion reactions to take place, oxygen and moisture. Corrosion will not occur in the absence of either. Ferrous ions and liberating electrons are formed when irons at the anode dissolves in pore water [1]. They travel through the steel reinforcement to the cathode and react with water and oxygen to form hydroxyl ions, after which the ferrous ions react further with oxygen and water to form solid corrosion products known as rust. Corrosion is the result of the electrochemical process that takes place in two sub-steps [2] as illustrated in Fig. III-1.

$Fe \rightarrow Fe2^{+} + 2e^{-}$ (Anodic Reaction)

$2e^{-} + H_2O + \frac{1}{2} O_2 \rightarrow 2OH^{-}$ (Cathodic Reaction)

$Fe(OH)_2 + X \bullet O_2 + Y \bullet H_2O \rightarrow$ Rust

(a) Reactions

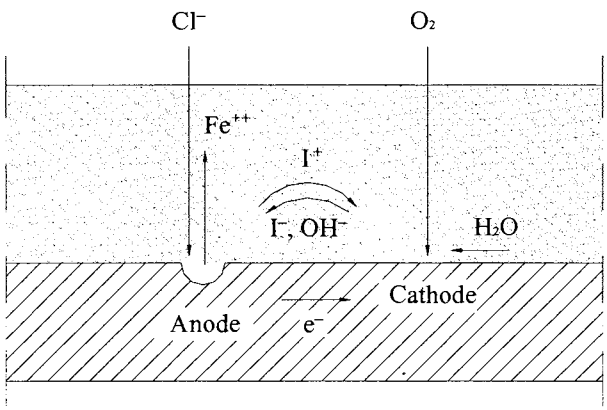

(b) Corrosion process

Figure III-1. Schematic of corrosion process.

1.2.2.Corrosion in Reinforced Concrete

Since the period between the late 19th and early 20th Century, the use of reinforcing steel in infrastructure has exploded, and the accompanying corrosion problem has resulted in billions of dollars in maintenance and replacement costs. Whereas concrete is often perceived as a simple material, it is actually a complex composite material that has a microstructure whose properties change over time. While steel reinforcement is widely used in concrete structure as a cost effective construction material, steel degradation due to corrosion has become a major concern. Among the many deterioration mechanisms possible in reinforced concrete (such as alkali-silica reactivity, freeze-thaw, plastic shrinkage, thermal movement, settlement, unusual chemical attack, etc.), this

section will concentrate on corrosion of atmospherically exposed reinforced concrete structures and elements.

It is well known that concrete has an abundant amount of calcium hydroxide and relatively small amounts of alkali elements such as sodium and potassium. This presence of high calcium hydroxide and low alkali elements gives concrete a very high alkalinity. According to the study conducted by Hausmann [3], concrete has pH values typically in the range of 12 to 13, which gives enough alkalinity to provide steel with a protective environment by forming a thin film of passivating iron oxide on the surface of the steel member (transformation of surface layer of the embedded steel to a tightly adhering film). Corrosion of steel in concrete is caused by the breakdown of the natural passivity due to either carbonation, or chloride attack [4]. If the condition of reinforcing steel in the concrete is ideal, the steel tends to passivate and display negligible corrosion rates. In other words, as long as this passivating film is not disturbed, it will maintain the steel's passive state and, thus, protect from corrosion. In reality, however, corrosion will eventually be initiated as a consequence of the breakdown of the passivating film unless the passivation layer on the surface of the reinforcement is regenerated. The two most common causes of steel corrosion are chloride induced corrosion and carbonation. The chloride induced rebar corrosion can be referred to as a localized breakdown of the passive film on the steel caused by a presence of chloride ions. For example, when deicing salts are used on a reinforced concrete deck, chloride ions from the deicing salts penetrate into the concrete through cracks or pores in the hydrated cement paste. The chloride ions will eventually contact the steel and accumulate to a certain concentration level that, in turn, leads to disruption of the protective film and initiates corrosion. Corrosion can be also initiated even in the absence of chloride ions (i.e., through carbonation). Carbonation can be referred to as a general breakdown of passivity caused by the surrounding acidic environment that leads to a process where carbon dioxide from the air mixes with water in the concrete pores and removes the passivating layer. This results in a decrease of the alkalinity (pH as low as 8.5), thereby allowing corrosion to begin. Relatively rapid deterioration of reinforcing steel in the bridge deck may occur due to corrosion cells created by potential differences between steel contaminated with chloride and steel uncontaminated.

Corrosion of reinforcing steel results in an expansion of voluminous corrosion products that become five to ten times the original volume of the consumed steel. This increase will generate tremendous internal pressures on the surrounding concrete and the protective concrete cover, as a consequence, will be compromised. This would eventually result in cracking and spalling of the

concrete surface. Corrosion damage will eventually affect the load bearing capacity of a structure and, thereby, its remaining service life will be decreased.

1.2.3. Comparison Study on MMFX and Other Conventional Reinforcing Steels

MMFX reinforcing steel developed by MMFX Steel Corporation of America [5] is publicized as a proprietary chemical composition material and known to have a unique microstructure with enhanced corrosion resistance characteristics and higher mechanical properties (yield and tensile strength) than conventional ASTM A 615 steel. It is designed to delay corrosion initiation and slow corrosion after initiation.

With no previously published study available on MMFX steel performance, a project [6] was conducted by the University of Kansas Center for Research to evaluate the performance of MMFX steel with a major emphasis drawn into the comparison of corrosion resistance of MFFX steel, conventional steel, and epoxy coated steel. This study was conducted in cooperation with the United States (US) DOT FHWA, the Kansas DOT, the South Dakota (SD) DOT, and the National Science Foundation. The rapid macrocell test was utilized as the principal evaluation test. The complete evaluation involves the corrosion testing, the measurement of bar deformation, the analysis of material composition, and the impact of bar properties on the structural performance of bridge decks. Also, the results of the corrosion evaluation are supplemented with the construction and maintenance experience in South Dakota and other states in evaluating the impact on the life expectancy and cost effectiveness of concrete decks.

From physical and mechanical tests, several drawbacks were encountered in the implementation phase where MMFX steel was used in trial designs for three bridge decks in South Dakota. It was found from the design phase that MMFX provides few satisfactory options for replacing conventional reinforcing steel under current AASHTO design procedures; it exceeds maximum allowable steel and concrete stresses, violates crack control and fatigue provisions, and exceeds the maximum allowable percentage of reinforcement. From laboratory corrosion testing, the epoxy coated steel was found to be more effective in corrosion performance than the MMFX steel. The MMFX steel appeared to corrode when exposed to the environment but not in contact with concrete or submerged in water. It was also found that the mechanical properties provided by manufacturer were somewhat higher than what was resulted from a series of tests conducted by the Kansas DOT. These discrepancies are presented in Table III-1.

Overall, the report concluded that the use of MMFX reinforcing steel in bridge decks did not appear to be cost effective compared to the use of epoxy coated steel.

Table III-1. Properties of MMFX steel tested.

Given by	Yield Strength, ksi	Tensile Strength, ksi
MMFX Steel Corp. of America	119-133	180-186
Kansas DOT	110-120	160-175

1.3. OBJECTIVE

The primary objective of the project described in the following chapters was to investigate and evaluate the field performance of innovative and conventional reinforcing steel in the deck slab of two newly constructed prestressed concrete girder bridges.

1.4. SCOPE

The research program consisted of several tasks with the main emphasis drawn to the field monitoring. To identify any sign of initiation and ongoing corrosion in the bridge deck, embeddable sensors were, during construction, installed on selected reinforcing bars in two parallel bridges. Data were recorded occasionally to assess and compare the performance, in terms of corrosion resistance, of two different types of reinforcing steel (i.e., MMFX and conventional epoxy coated steel).

A detailed description of the subject bridges and the installation of monitoring sensors are given in Chapter 2. The field monitoring results are presented and discussed in Chapter 3, and a general summary is presented in Chapter 4.

2. BRIDGE AND CORROSION MONITORING SYSTEM DESCRIPTION

This chapter describes the physical characteristics of the two newly constructed bridges being evaluated in this study. The layout and installation of corrosion sensors and the monitoring protocols are also described.

2.1. CONSTRUCTION AND DESCRIPTION OF BRIDGE

The subject bridges are new twin 83.5 m x 12 m, three-span pre-stressed concrete girder bridges constructed in 2002. The bridges are located in northeast Iowa on relocated U.S. 20 over South Beaver Creek in Grundy County, Iowa. The bridges have a total length of 83.5 m consisting of two 24.75 m end spans and a 34 m center span. The bridge deck is a nominal 200-mm thick cast-in-place, reinforced concrete slab that includes a 13-mm integral wearing surface. The roadway width is 12 m allowing two traffic lanes with a narrow shoulder on each side. The decks of the two bridges were constructed with two different types of reinforcing steel; MMFX steel in the eastbound bridge (referred to as MMFX bridge) and Epoxy coated steel in the westbound bridge (referred to as Epoxy bridge). There was essentially no difference in how these two bridges were constructed. The top transverse reinforcing steel was placed parallel to and 65 mm clear below top of slab while the bottom transverse reinforcing steel was placed parallel to and 25 mm clear above bottom of slab. Approximately 50 mm of clear distance from the face of concrete to near reinforcing bar was used. The deck is supported by six pre-stressed concrete beams spaced at 2,200 mm on center. See Fig. III-2 for a general framing plan and typical cross-section of the subject bridges.

The concrete deck was cast for both bridge decks in May, 2002. All slab and diaphragm reinforcing steels were tied in place and adequately supported before concrete was poured. The pier and abutment diaphragm concrete was placed monolithically with the floor slab. Moderate curbs were constructed integral with the deck and concrete guardrails connected to the curbs. The bridges were open to traffic in August 2003.

Typical photographs of subject bridges taken during construction are shown in Figs. III-3 through 6. Also, photographs of the completed bridges are presented in Fig. III-7.

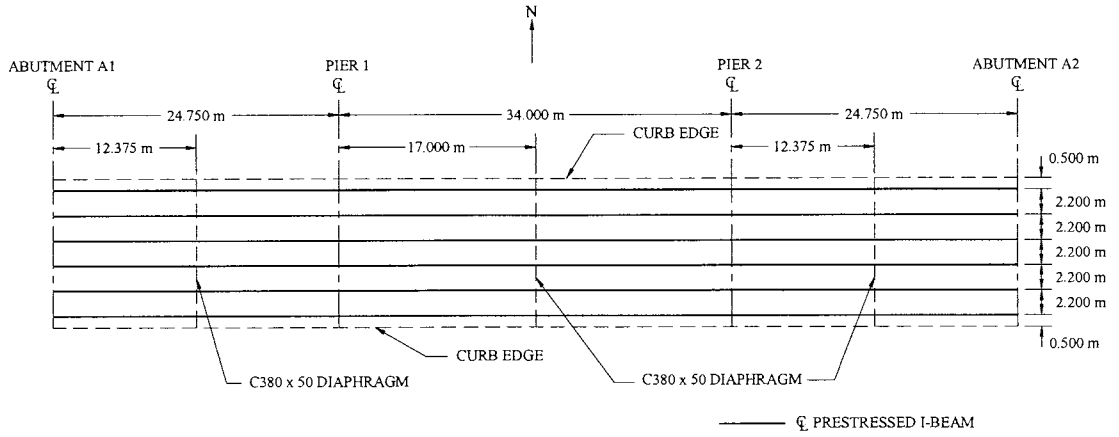

(a) General framing plan

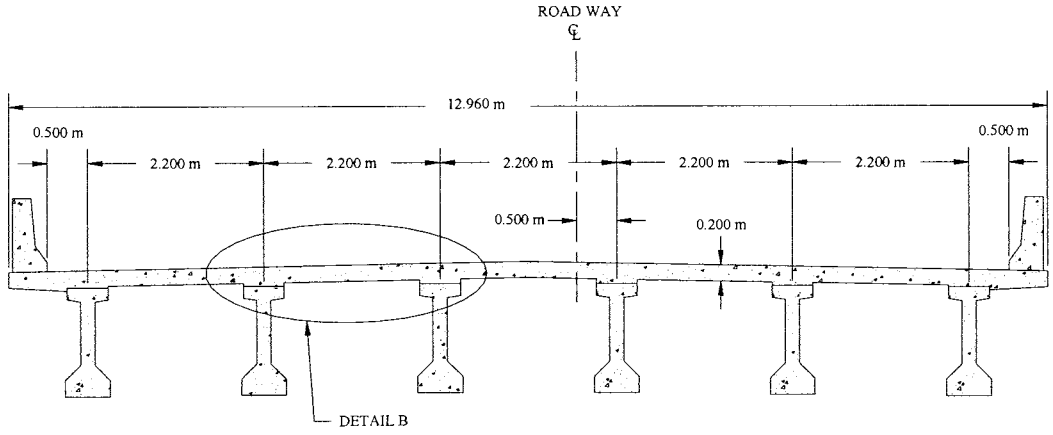

(b) Typical cross-section

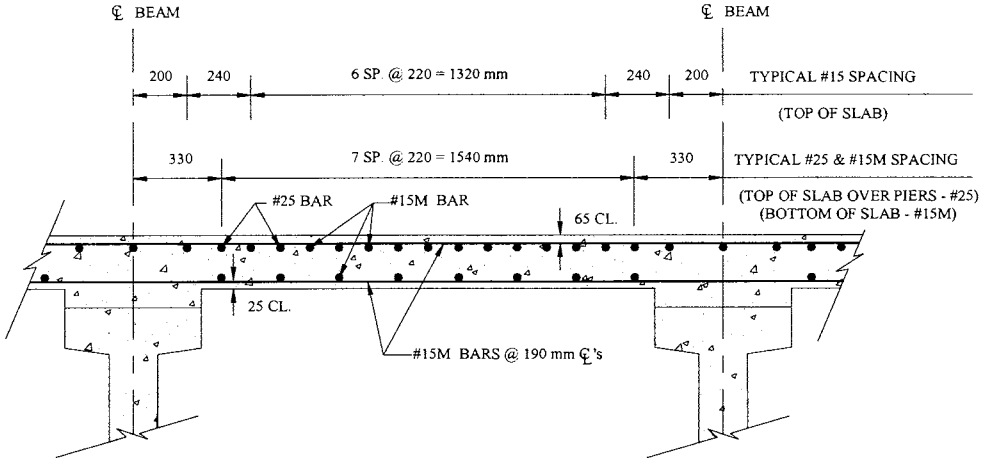

(c) Detail B

Figure III-2. Bridge framing plan and typical cross-section.

(a) Typical beam layout

(b) Side view

Figure III-3. Photographs of typical prestressed I-beams.

(c) Typical beam connection at pier

Figure III-3. Photographs of typical prestressed I-beams - continued.

Figure III-4. Typical scaffolding.

(a) MMFX bridge (looking northwest)

(b) MMFX bridge (looking west)

Figure III-5. Concrete placement for bridge deck.

(c) Epoxy bridge (looking southwest)

(d) Epoxy bridge (looking to the West)

Figure III-5. Concrete placement for bridge deck - continued.

Figure III-6. Concrete placement for bridge deck completed.

(a) Side view (MMFX bridge)

Figure III-7. Photographs of the completed bridges.

(b) Side view (Epoxy bridge)

(c) End view

Figure III-7. Photographs of the completed bridge - continued.

(d) Bottom view (abutment)

(e) Bottom view (center span and west pier)

Figure III-7. Photographs of the completed bridge - continued.

2.2. CORROSION MONITORING SYSTEM

Corrosion detecting devices installed on both bridge decks consisted of V2000 monitoring electrodes (see Fig. III-8). These sensors consist of a solid silver-silver chloride wire electrode wrapped in a permeable, non-conducting PVC covering. These are used to monitor reinforcing steel in concrete for the onset of corrosion, cessation of corrosion, and intensity of corrosion growth.

The use of this embeddable sensor offers an ability to monitor an interior state of a structure by measuring parameters that can be used as reliable indicators of the likelihood of corrosion in the surrounding area. Although the sensor does not address the specific electrochemical mechanisms, it provides a reliable and cost-effective monitoring system to measure the basic electrochemical processes.

Figure III-8. CMS V2000 silver/silver electrode.

Both bridges were instrumented with V2000 electrode sensors permanently embedded in the concrete deck. A plan view of the bridge with the sensor locations can be found in Fig. III-9 with "Detail C" in Fig. III-10. A total of twenty No. 25 (ASTM) top bars (10 on each bridge – M1 through M10 on MMFX bridge, and E1 through E10 on Epoxy bridge) in the negative bending moment region near the eastern drainage points were instrumented. Electrode sensors were wound around the

length of approximately 4.6 m of each bar. Each electrode was connected to a red lead wire with a protected butt splice (see Fig. III-11). A black wire is attached directly to the bar using a stainless steel clamp. These lead wires (see Fig. III-12) were run out of the deck and are used to measure internal voltage and electrical current to assess corrosion development.

On the Epoxy Bridge, two additional short sections of MMFX bars were instrumented with electrodes and placed between other epoxy coated bars (i.e., one on the north side - referred to as 'NO', and one on the south side - referred to as 'SO') to compare with the epoxy bars within the same environment. Figs. III-13 and 14 show typical photographs of the instrumentation layout on both MMFX and Epoxy bridges.

2.2.1. Monitoring Concept

The electrical process induced by steel cathode corrosion is an electrochemical process. Electric potential differences arise when an electrochemical reaction (corrosion) takes place. With the V2000 electrode, the potential between the electrode sensor and the bar is measured. The electrode sensor serves as a cathode and the rebar as an anode, thereby creating a "battery". The electrochemical process, on the other hand, is separate and distinct from the battery formed by the V2000 electrode cable (silver-silver chloride), steel, and alkaline concrete. This electrochemical reaction occurs when a local pH value at the concrete-steel interface drops below 9 due to an incursion of chlorine atoms. During this process, electrons are released as a product of the chemical reaction. Therefore, the corrosion site acts as another independent "chemical battery". These two batteries then become additive to one another and the internal voltage increases. By measuring DC voltage (in volts, V or millivolts, mV) and DC current (in milliamps, mA or microamps, μA) with a voltmeter (see Fig. III-15), it can be determined if corrosion activity on each bar is occurring, and if so, how severe it is.

The actual output value depends mostly on the conditions of the concrete after placement. It is normal to expect high voltage levels (it could be over 1000 mV) shortly after concrete placement since considerable moisture is present. While it is fresh and uncured, it is highly active and generates high output. This initial "spike" typically subsides back to within the "normal" range of less than 400 mV as the concrete cures.

In general, electrical current readings below 0.100 mA (1000 μA) can be considered a weak site of corrosion. When corrosion occurs, however, a natural DC current starts to flow from one area to another and this electrical current reading increases significantly; if it exceeds 1000 μA, corrosion activity is considered quite active.

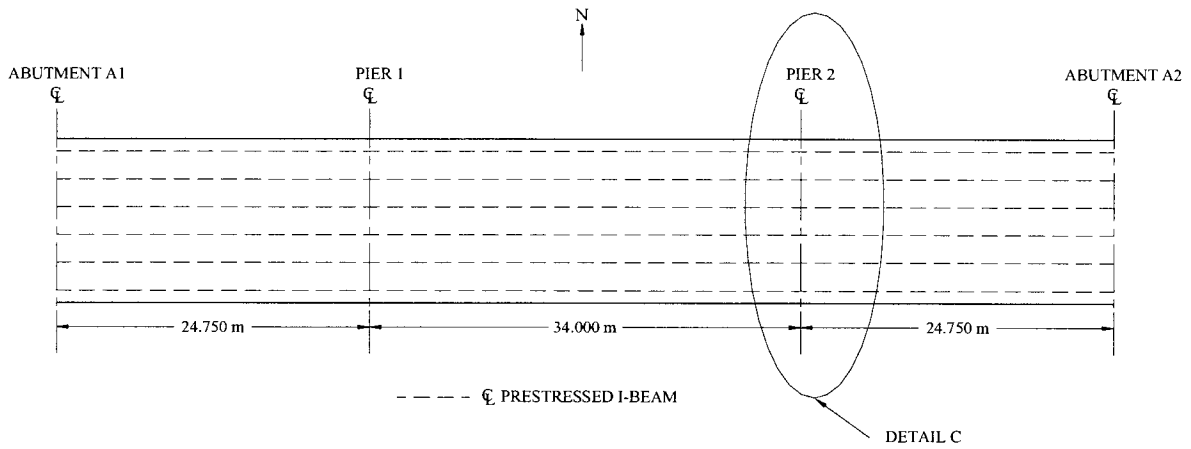

Figure III-9. Plan view with sensor location.

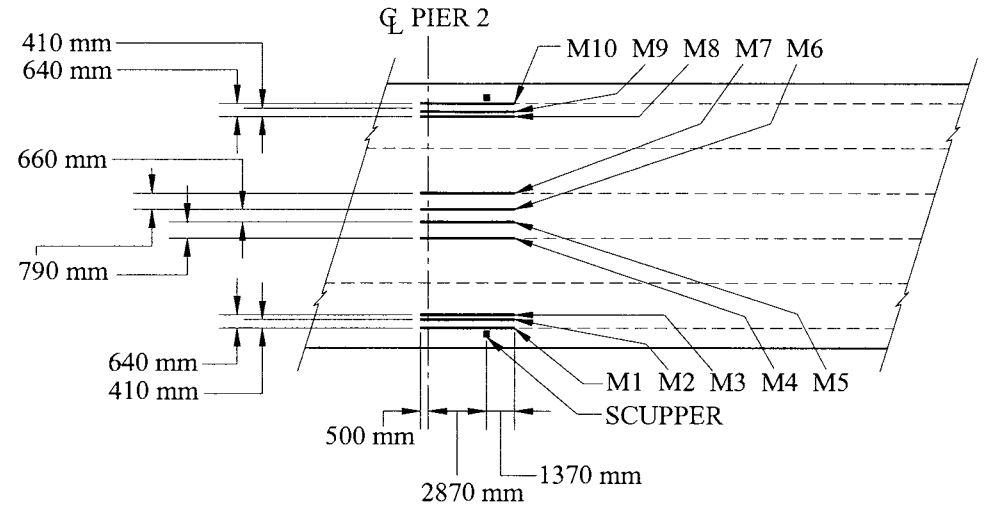

(a) MMFX bridge

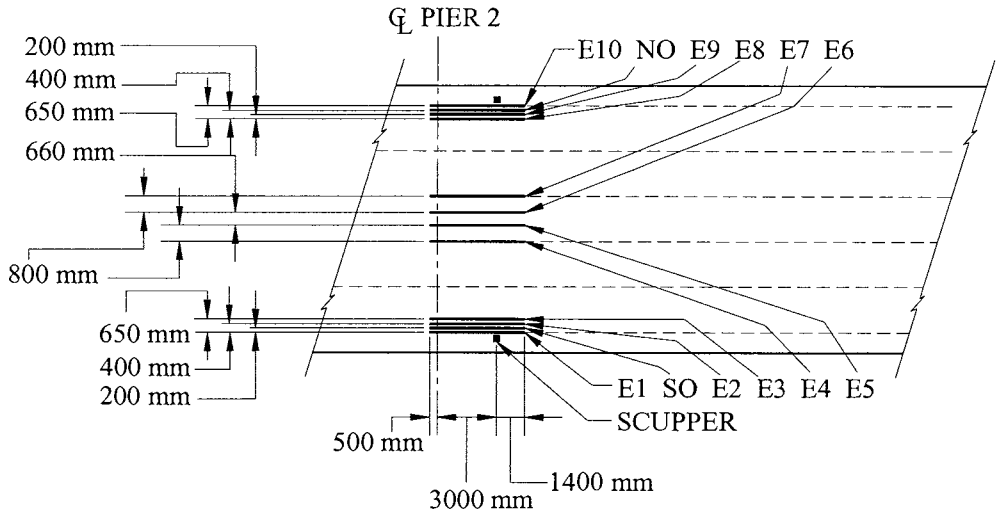

(b) Epoxy bridge

Figure III-10. Detail C (general instrumentation of V2000 sensors).

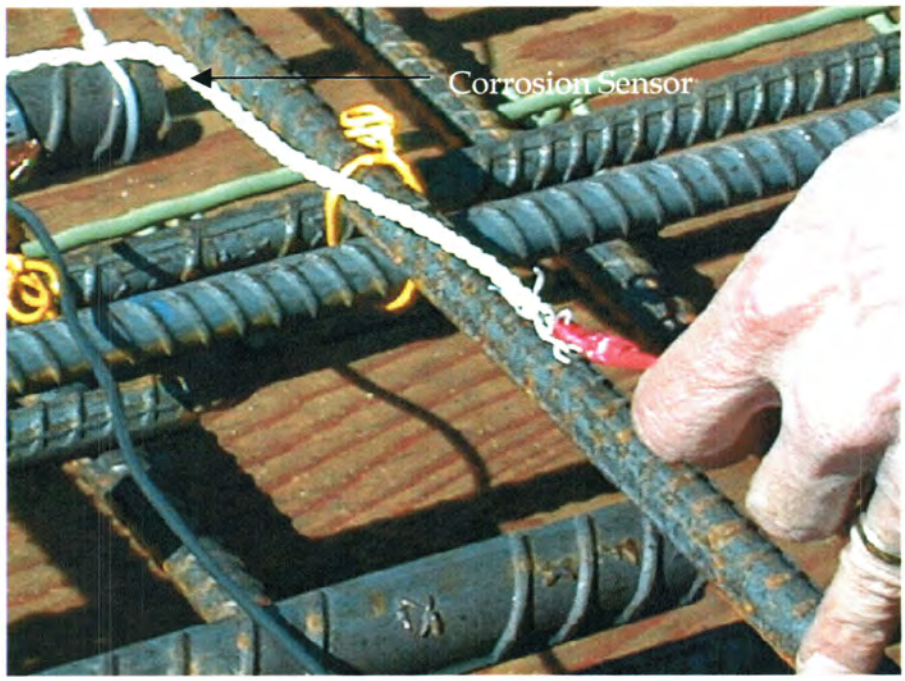

(a) Butt splice of electrode corrosion sensor and lead wire

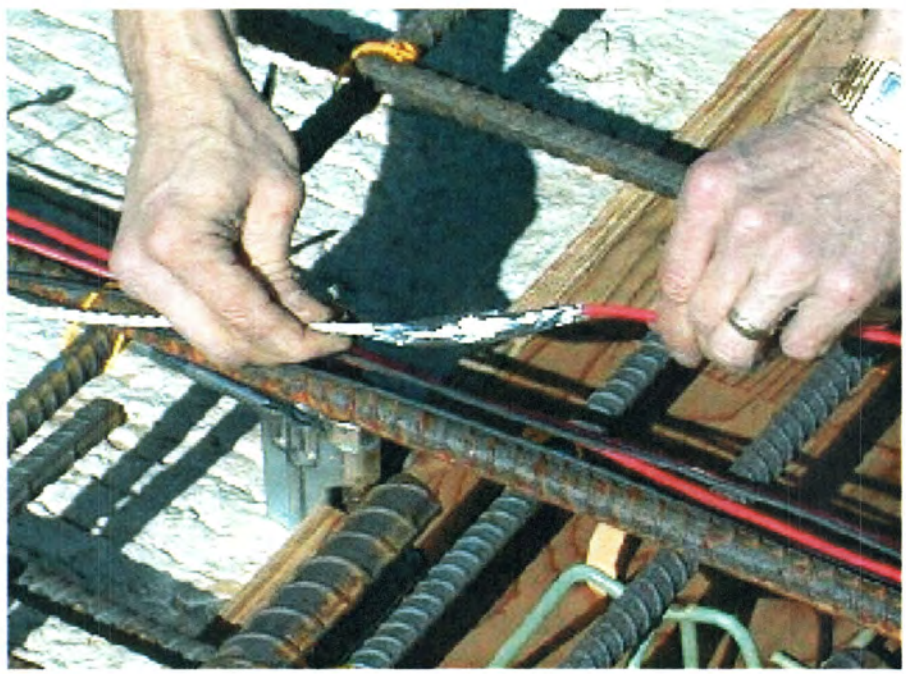

(b) Butt splice protected with butyl rubber underneath aluminum foil tape

Figure III-11. Connecting V2000 sensor with lead wire.

Figure III-12. Extending lead wires for data measurement.

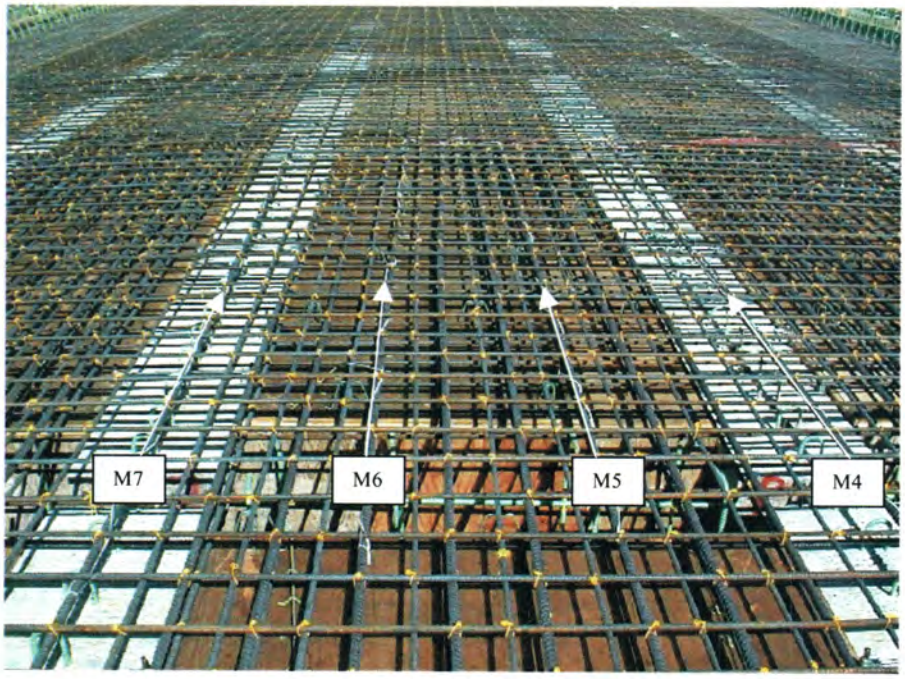

Figure III-13. Typical photograph of the instrumentation layout on MMFX bridge.

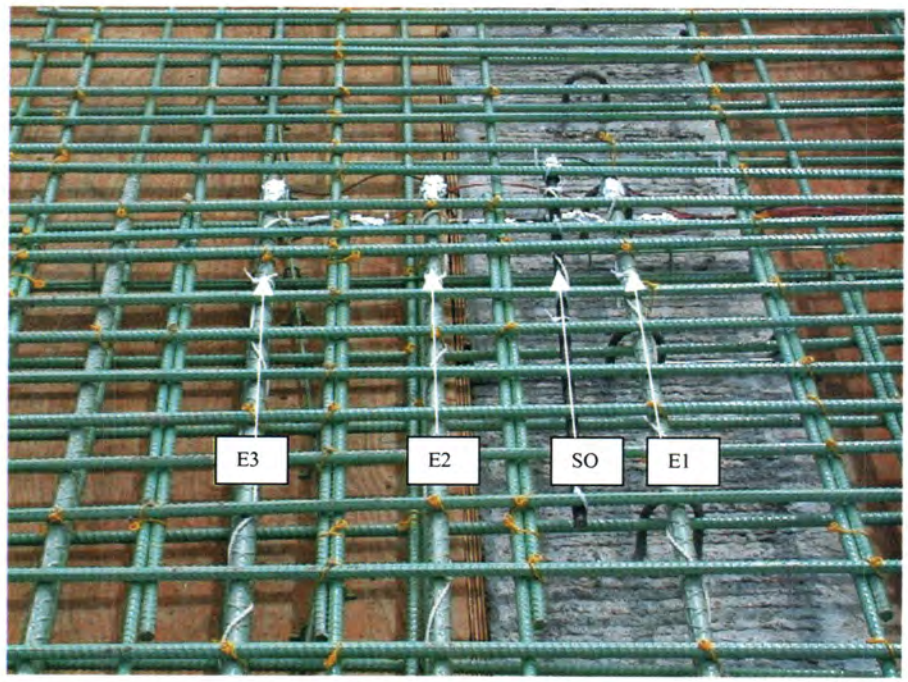

(a) 'SO' MMFX bar and Epoxy bars E1-E3 (looking east)

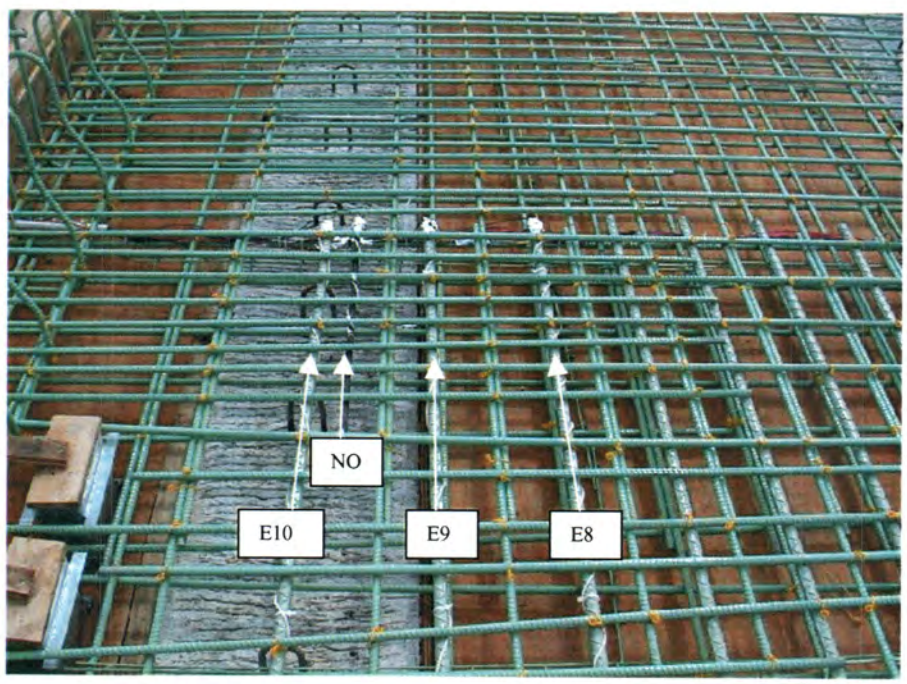

(b) 'NO' MMFX bar and Epoxy bars E8 – E10 (looking east)

Figure III-14. Typical photographs of the instrumentation layout on Epoxy bridge.

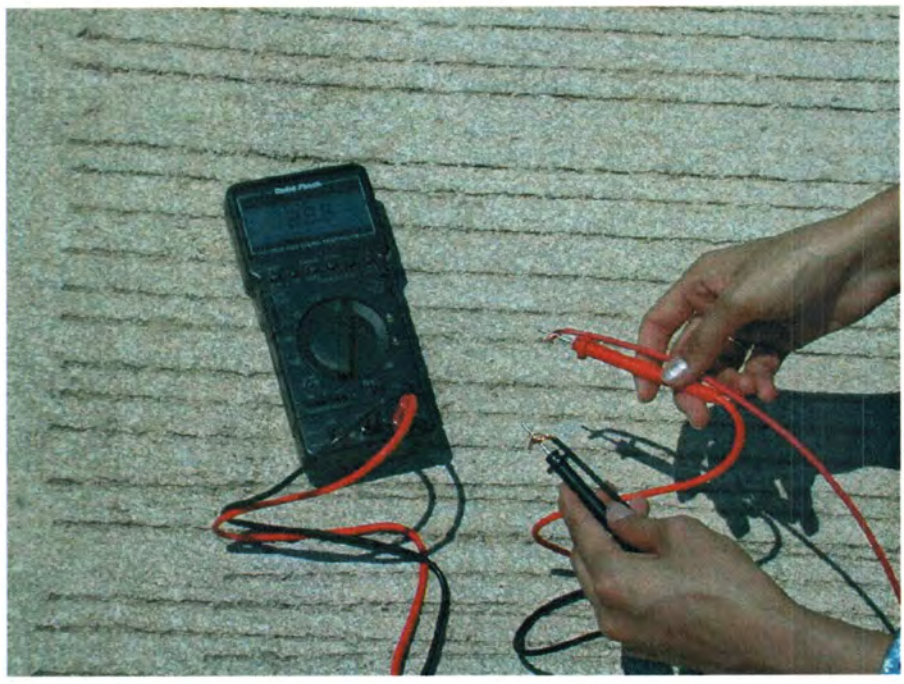

Figure III-15. Data measuring with voltmeter.

3. FIELD MONITORING AND DISCUSSION

Visual inspections of both bridges have regularly been conducted to identify any sign of potential cause of corrosion. To date (October, 2003), no obvious external signs of damage were observed: no signs of crack, spall, delamination, etc.

Figures III-16 and 17 show the internal voltage and electrical current readings for all instrumented reinforcing steels in both bridge decks to date. All MMFX bridge data appear to be as one would expect; although the data increased above 400 mV (see Fig III-16a) at the initial stage, they returned to normal levels after concrete cure (i.e., the initial "spike" has ceased). Note that even at this initial stage, the electrical current remained below 1000 μA (indication of weak site of corrosion) as shown in Fig. III-17a. Since approximately three months after concrete placement, all voltage levels for the MMFX bridge have dropped steadily and remained within "normal" range and stayed less than 100 mV. At this point, it appears that there is no ongoing corrosion activity.

The epoxy coated bars, on the other hand, behaved somewhat unexpectedly. Readings on the Epoxy bridge were higher (about two times higher than the readings on the MMFX bridge) than originally expected. During the initial stage, shortly after concrete placement, some of readings increased over 1200 mV (see Fig. III-16b). Although these high data readings dropped below 400 mV, some of readings are still above 300 mV. Theoretically, there should be nearly zero readings if the bar is coated perfectly; steel will be perfectly protected without any "contact" between the coated steel and the concrete. As shown in Figs III-16b and 17b, however, it is clear that, with the exception of E9, the "contact" has been made on virtually all specimens being monitored. This is an indication that there is at least one or more defect (i.e., coatings may have been nicked and/or scratched during the process of layout) in the epoxy coating on most bars.

Note that some data show negative readings (M8 and SO). This phenomenon is likely attributed to a possibility of lead wires either connected in reverse or damaged during concrete placement process.

Overall, data up to date indicate that readings are lower on the MMFX bridge than on the Epoxy bridge. Some of the bars (E2, E3, and E4) need to be closely watched in the future since they showed relatively high data readings. It should be noted, however, that no significant active corrosion

is observed in either bridge decks at this point; electrical current readings are currently close to zero as shown in Fig III-17. Although not completed, through monitoring and evaluation with more data collected, this on-going investigation of corrosion monitoring system will allows engineers to better understand the performance of these reinforcing steels under service.

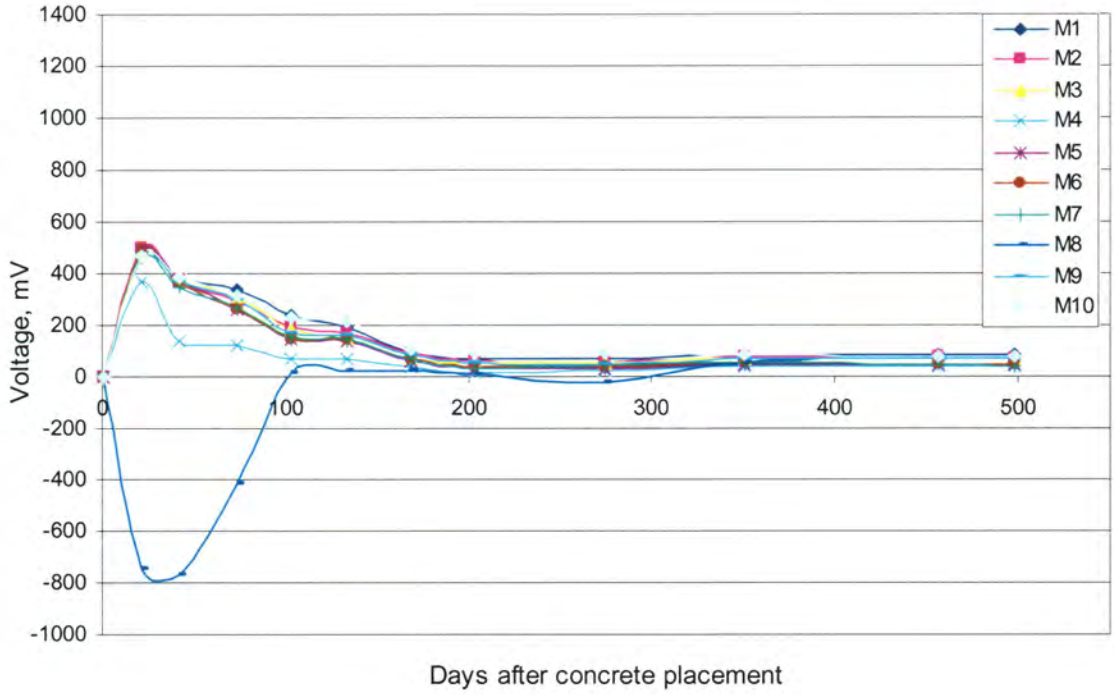

(a) MMFX bridge

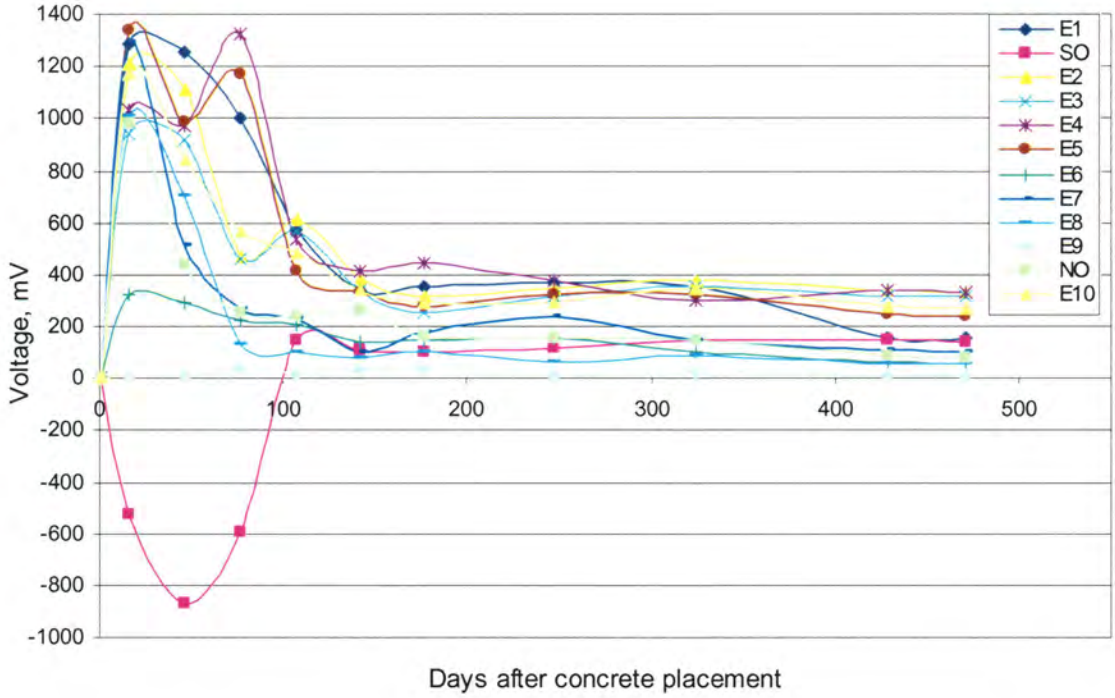

(b) Epoxy bridge

Figure III-16. Voltage readings from V2000 sensors on instrumented reinforcing bars.

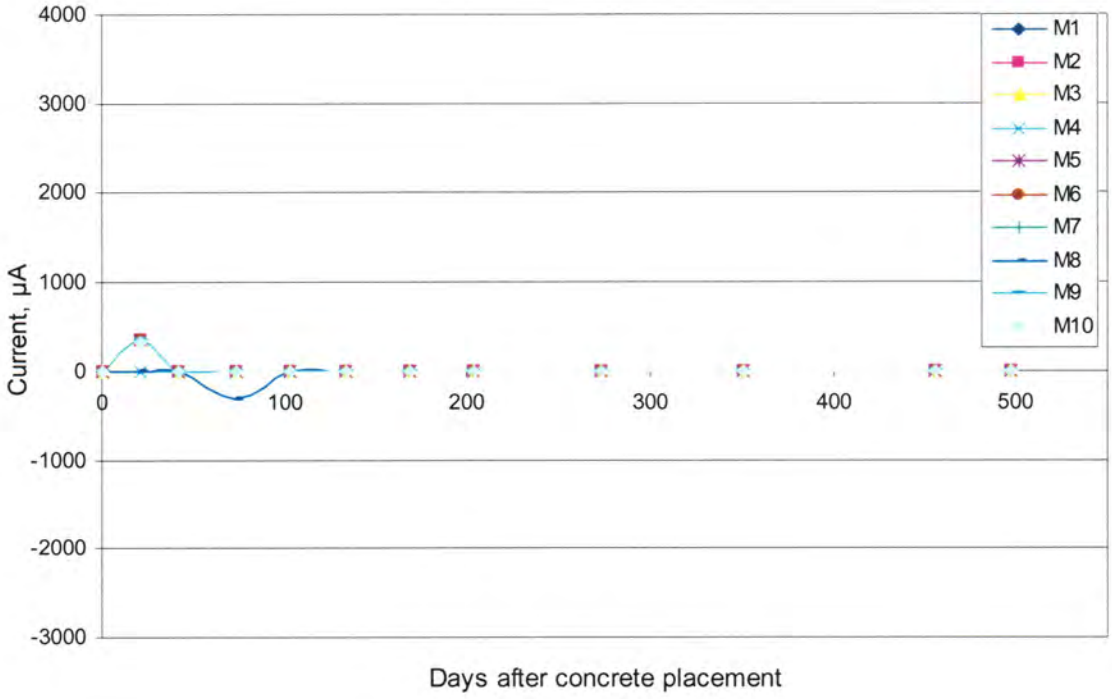

(a) MMFX bridge

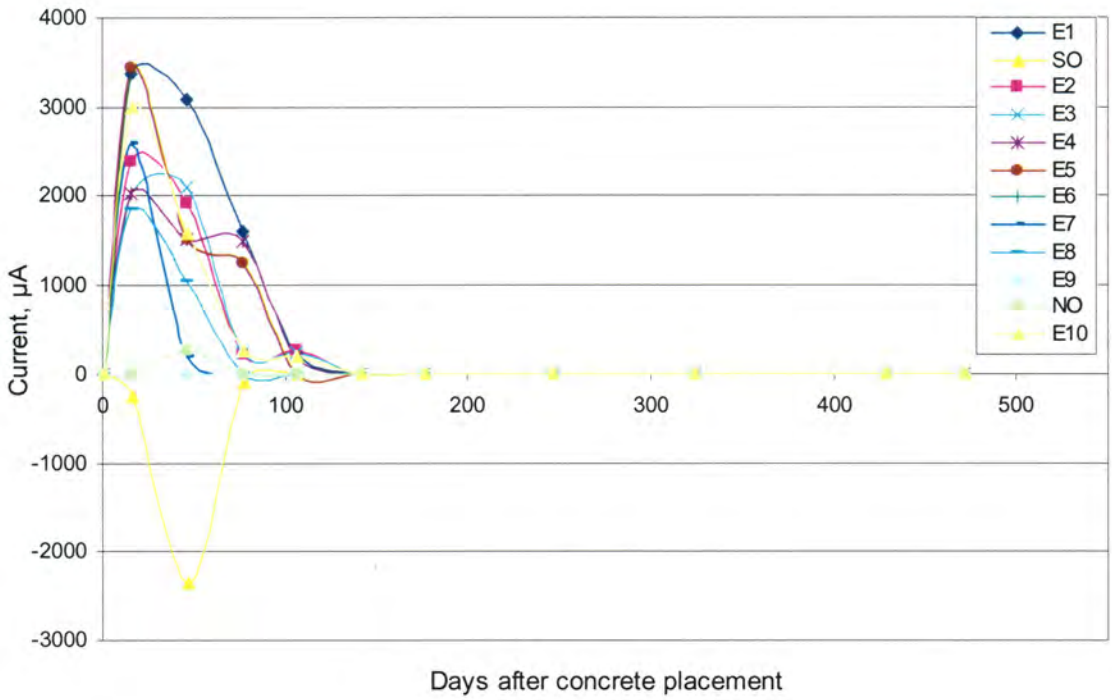

(b) Epoxy bridge

Figure III-17. Electrical current readings from V2000 sensors on instrumented reinforcing bars.

4. SUMMARY

Part III presented a portion of an on-going project that investigated corrosion of reinforcement steel in the deck slab of two prestressed concrete girder bridges. A relatively new form of corrosion resistant material, Micro-composite Multi-structural Formable Steel reinforcing rebar, was utilized, and its performance was evaluated and compared with conventional epoxy coated steel. The bridges evaluated were new twin 83.5 m x 12.0 m pre-stressed concrete girder bridges, on relocated Highway U.S.20 located in Grundy County, IA. The decks of the two bridges were constructed with two different types of steel; MMFX steel in the eastbound bridge and Epoxy coated steel in the westbound bridge. The concrete deck was cast for both bridge decks in May, 2002 and the bridges were open to traffic in August, 2003.

The research program consisted of several tasks with the main emphasis drawn to the field monitoring. To identify any sign of initiation and ongoing corrosion in the bridge deck, embeddable corrosion sensors (V2000 monitoring electrodes) were, during construction, installed on selected reinforcing bars in the negative bending moment region near the drainage points. On the Epoxy Bridge, two additional short sections of MMFX bars were instrumented with electrodes and placed between other epoxy coated bars to compare with the epoxy coated bars within the same environment. Using a voltmeter, data were recorded, by measuring DC voltage and DC current, periodically to assess and compare the performance, in terms of corrosion resistance, of two different types of reinforcing steel.

To date (October, 2003), data indicated that readings were generally lower on the MMFX bridge than on the Epoxy bridge. Also, no significant active corrosion was observed in either bridge deck at this point; electrical current readings are currently close to zero.

5. REFERENCES

1. Broomfield, J.P., "Field measurement of the Corrosion Rate of Steel in Concrete using a Microprocessor Controlled Unit with a Monitored Guard Ring for signal Confinement." American Society for Testing and Materials (ASTM) Special Technical Publication 1276 on Corrosion Activity of Steel Reinforced Concrete Structures, pp 91-106., ASTM, West Conshohocken, PA, 1996.

2. Raupach, M., "Corrosion of Steel in the Area of Cracks in Concrete." *Fourth International Symposium on Corrosion of reinforcement in concrete construction*, Robinson College, Cambridge, UK, July, 1996.

3. Hausmann, D.A., "Electrochemical Behavior of Steel in Concrete." *Journal of American Concrete Institute*, Vol. 61, No. 2, pp. 171-188. 1964.

4. Bentur, A., S. Diamond and N.S. Berke, "Steel Corrosion in Concrete". Chapman & Hall, London, UK, 1997.

5. MMFX Steel Corporation of America, http://www.mmfxsteel.com/, 2003

6. University of Kansas Center for Research, Inc., "Mechanical and Corrosion Properties of a High-Strength, High Chromium Reinforcing Steel for Concrete." Study SD2001-05, Final Report, 2001.

GENERAL SUMMARY

Among the many projects funded through the IBRC Program, this thesis summarized three projects (Part I, Part II, and Part III) that utilized innovative materials to strengthen existing deficient bridges and in the construction of a new bridge. The projects presented in this thesis focused on the demonstration of the use of new, cost-effective, innovative materials and the associated performance evaluation.

In the first two parts (Part I and Part II), the use of carbon fiber reinforced polymer (CFRP) materials to strengthen existing, structurally deficient steel girder bridge was summarized. Among various strengthening materials, CFRP composite materials were selected due to their outstanding mechanical characteristics and non-corrosive nature. Two bridges were strengthened using these materials in an effort to improve the live load carrying capacity of the bridges. The two primary objectives of these projects were to investigate the effectiveness of CFRP composite materials to strengthen existing, structurally deficient steel girder bridges and to identify changes in structural behavior due to addition of strengthening system. In one case (Part I), a bridge was strengthened using CFRP bars that were post-tensioned in the positive moment region to generate the stresses that counteract stresses produced by dead and live loads and thereby improving the overall live load carrying capacity of the bridge. The bridge selected for strengthening with the CFRP P-T bars was a three-span continuous steel stringer bridge in Guthrie County, Iowa on State Highway IA 141 approximately 1.6 miles west of Bayard, Iowa. The installation of the P-T system required no special equipment or training other than access equipment, an acetylene torch to remove a portion of several diaphragms, and a hydraulic jack for the application of the P-T force to the CFRP bars. A three-man crew was able to install the system in just over one day. Before the P-T system was installed, a diagnostic load test was conducted on the subject bridge to establish a baseline behavior of the unstrengthened bridge. During the process of installing the P-T hardware and stressing the system, both the bridge and the P-T system were monitored. The installation of the hardware was followed by a follow-up diagnostic load test to assess the immediate effectiveness of the P-T strengthening system. Additional load tests were performed over a two-year period to identify any changes in the strengthening system with time. After the last follow-up test (two years of service) was completed, the P-T force was removed from the bridge (and re-applied) to investigate any losses that may have occurred over the two-year period. By comparing the results from each field load testing in terms of strain, it was found that the addition of the P-T strengthening system had a negligible impact on

changing the stiffness of the bridge, and that the live load distribution characteristics were virtually the same before and after the installation of the P-T strengthening system. From analysis performed to illustrate the effect of the P-T system, it was found that the P-T strengthening system reduced dead and live load induced moments by approximately 3 to 5%, thus allowing the bridge to carry additional live load.

In the other case (Part II), a bridge was strengthened by installing CFRP plates to the bottom flange of girders in the positive moment region. The bridge strengthened with CFRP plates was a 150 ft x 30 ft three-span continuous I-beam bridge in Pottawattamie County, Iowa, on State Highway IA 92. The strengthening system consisted of preparation of the bonding surface and installation of the CFRP plates. The design of the CFRP plates was based on the Iowa legal load utilizing the Load Factor Design approach. The implemented design consisted of from one to three layers of CFRP plates bonded to the overstressed tension regions with a high strength epoxy adhesive. The handling and installation of the CFRP plates was relatively labor intensive and required some training. At least a three-man crew was needed to install the system (a day per layer). From the preliminary study conducted to predict the change in moment capacity and stiffness due to adding the CFRP plates to the bottom of the bottom flange, it was found that with the relatively small change in stiffness in the strengthened member, a considerable increase (approximately 10% increase per layer up to three layers) in the moment capacity on the strengthened beams was attainable and thereby, improving the overall live load carrying capacity of the bridge. By comparing the field data with analytical prediction, it was also found that the bonding performance between the beam and CFRP plates was good and, therefore, it appeared that no significant debonding occurred shortly after the installation.

In Part III, a portion of a project that investigates the use of corrosion resistant reinforcing steel was presented. A relatively new form of corrosion resistant material, MMFX reinforcing steel, was utilized, and its performance was evaluated and compared with conventional epoxy coated steel. The bridges evaluated were new twin 83.5 m x 12.0 m pre-stressed concrete girder bridges, on relocated Highway U.S.20 located in Grundy County, IA. The decks of the two bridges were constructed with two different types of steel; MMFX steel in the eastbound bridge and Epoxy coated steel in the westbound bridge. The concrete deck was cast for both bridge decks in May, 2002 and the bridges were open to traffic in August, 2003. The research program consisted of several tasks with the main emphasis drawn to the field monitoring. To identify any sign of initiation and ongoing corrosion in the bridge deck, embeddable corrosion sensors (V2000 monitoring electrodes) were, during

construction, installed on selected reinforcing bars in the negative bending moment region near the drainage points. Using a voltmeter, data were recorded, by measuring DC voltage and DC current, periodically to assess and compare the performance, in terms of corrosion resistance, of the two different types of reinforcing steel. To date (October, 2003), the data indicated that no significant active corrosion is occurring in either bridge deck.

APPENDIX

(Post-tensioning events)

Table A-1. P-T West End Span

Event	Beam Number	Beam	CFRP Bar	Force applied (kips)
1	4	Exterior	Bottom	0
2	4	Exterior	Bottom	6
3	4	Exterior	Top	0
4	4	Exterior	Top	6
5	4	Interior	Bottom	0
6	4	Interior	Bottom	6
7	4	Interior	Top	0
8	4	Interior	Top	6
9	4	Interior	Top	12
10	4	Interior	Bottom	6
11	4	Interior	Bottom	12
12	4	Exterior	Bottom	6
13	4	Exterior	Bottom	12
14	4	Exterior	Top	6
15	4	Exterior	Top	12
16	4		Beam 4 completed	
17	1	Interior	Bottom	0
18	1	Interior	Bottom	6
19	1	Interior	Top	0
20	1	Interior	Top	6
21	1	Exterior	Bottom	0
22	1	Exterior	Bottom	6
23	1	Exterior	Top	0
24	1	Exterior	Top	6
25	1	Exterior	Top	12
26	1	Exterior	Bottom	6
27	1	Exterior	Bottom	12
28	1	Interior	Bottom	6
29	1	Interior	Bottom	12
30	1	Interior	Top	6
31	1	Interior	Top	12
32	1		Beam 1 completed	

Table A-2. P-T Center Span

Event	Beam Number	Beam	CFRP Bar	Force applied (kips)
33	4	Exterior	Bottom	0
34	4	Exterior	Bottom	6
35	4	Exterior	Top	0
36	4	Exterior	Top	6
37	4	Interior	Bottom	0
38	4	Interior	Bottom	6
39	4	Interior	Top	0
40	4	Interior	Top	6
41	4	Interior	Top	12
42	4	Interior	Bottom	6
43	4	Interior	Bottom	12
44	4	Exterior	Bottom	6
45	4	Exterior	Bottom	12
46	4	Exterior	Top	6
47	4	Exterior	Top	12
48	4		Beam 4 completed	
49	1	Interior	Bottom	0
50	1	Interior	Bottom	6
51	1	Interior	Top	0
52	1	Interior	Top	6
53	1	Exterior	Bottom	0
54	1	Exterior	Bottom	6
55	1	Exterior	Top	0
56	1	Exterior	Top	6
57	1	Exterior	Top	12
58	1	Exterior	Bottom	6
59	1	Exterior	Bottom	12
60	1	Interior	Bottom	6
61	1	Interior	Bottom	12
62	1	Interior	Top	6
63	1	Interior	Top	12
64	1		Beam 1 completed	

Table A-3. P-T East End Span

Event	Beam Number	Beam	CFRP Bar	Force applied (kips)
65	4	Exterior	Bottom	0
66	4	Exterior	Bottom	6
67	4	Exterior	Top	0
68	4	Exterior	Top	6
69	4	Interior	Bottom	0
70	4	Interior	Bottom	6
71	4	Interior	Top	0
72	4	Interior	Top	6
73	4	Interior	Top	12
74	4	Interior	Bottom	6
75	4	Interior	Bottom	12
76	4	Exterior	Bottom	6
77	4	Exterior	Bottom	12
78	4	Exterior	Top	6
79	4	Exterior	Top	12
80	4		Beam 4 completed	
81	1	Interior	Bottom	0
82	1	Interior	Bottom	6
83	1	Interior	Top	0
84	1	Interior	Top	6
85	1	Exterior	Bottom	0
86	1	Exterior	Bottom	6
87	1	Exterior	Top	0
88	1	Exterior	Top	6
89	1	Exterior	Top	12
90	1	Exterior	Bottom	6
91	1	Exterior	Bottom	12
92	1	Interior	Bottom	6
93	1	Interior	Bottom	12
94	1	Interior	Top	6
95	1	Interior	Top	12
96	1		Beam 1 completed	